9-12-2014

Design and Development of Advanced Adaptive Polymer Lenses

Freddie Santiago

Freddie Santiago

Candidate

Electrical and Computer Engineering

Department

This dissertation is approved, and it is acceptable in quality and form for publication:

Approved by the Dissertation Committee:

Sanjay Krishna, Ph.D.,UNM, ECE , Chairperson

Jean-Claude Diels, Ph.D., UNM, P&A

Ralph Dawson, Ph.D., UNM, ECE

Brett Bagwell, Ph.D., SNL

Design and Development of Advanced Adaptive Polymer Lenses

by

Freddie Santiago .˙.

M.S., Physics, University of Puerto Rico, Mayaguez, 2006
B.S., Physics, University of Puerto Rico, Mayaguez, 2002

DISSERTATION

Submitted in Partial Fulfillment of the
Requirements for the Degree of

Doctor of Philosophy
Engineering

The University of New Mexico

Albuquerque, New Mexico

July, 2014

Dedication

To my parents, my brother and my family.

Para mis padres, mi hermano y mi familia.

Acknowledgments

First I would like thank my parents and brother for all the sacrifices they have made, their encouragement and motivation so that I could reach my goals, love you.

To my grandparents, aunts, uncles, cousins and friends who in one way or another always pushed me and motivated me, love you all. To Meghan who put up with my stress and long nights, and was always there for whatever I needed, love you.

There are too many to name them all, but I want to thank,

- friends and professors from Puerto Rico thank you for your support and teachings
- friends, professors and administrative personal at UNM CHTM, ECE and P&A
- friends and mentors from Los Alamos National Laboratories
- friends and mentors from Naval Research Laboratories
- friends and mentors from Sandia National Laboratories and the many collaborators and contractors whom have helped along the way

I would like to thank my committee members, Professor Sanjay Krishna, Professor Ralph Dawson, Professor Jean-Claude Diels, Dr. Brett Bagwell and Dr. Sergio Restaino for their time, support, motivation and most importantly their teachings.

Thank you all.

Design and Development of Advanced Adaptive Polymer Lenses

by

Freddie Santiago ∴

M.S., Physics, University of Puerto Rico, Mayaguez, 2006
B.S., Physics, University of Puerto Rico, Mayaguez, 2002

Ph.D., Engineering, University of New Mexico, 2014

Abstract

The dissertation presented here describes advancements made in adaptive polymer lens design and implementation. Singlets and doublets lenses were constructed for visible, short- wavelength infrared (SWIR), and middle-wavelength infrared (MWIR) applications. The lenses are implemented in a variety of tactical imaging systems to demonstrate their performance. A process was developed that defines the allowable fabrication variables, first for APL singlets and then for APL doublets. A first-order finite element model is described that enables going from an optical design to APL fabrication. This model was then extended to the design of fluidic doublets, which are equivalent to their two-element glass counter-parts. Two constant volume fluidic chambers were enclosed by three flexible membranes resulting in a variable focal length doublet. Chromatic focal shift was then used to compare numerical modeling to experimentally measured results.

These same tools, methodology, and process were lastly used in the definition and fabrication of the SWIR and MWIR adaptive polymer lens for tactical systems.

Imaging and illumination systems are presented, based on these lensesnotably an adaptive zoom imaging system, in the MWIR. This is the first known instance of such a system in this band.

Contents

List of Figures

List of Tables

Chapter 1

Introduction

The field of optics is challenged but also inspired by nature every day in the development of cameras, detectors, and imaging to name a few. One of the most sophisticated system is the human eye, and since the 1800s a lot of effort has been made attempting to replicate it. The eye is capable of rapidly changing its optical properties in order to adapt to changing environments and conditions. One of the most basic properties of the eye is the ability to change its focal length in a relatively fast manner.

Variable radius of curvature (ROC) is one of the most common techniques implemented in order to emulate this property of the eye. Since the 1800s scientists have developed experiments that encase clear fluids in shells and deform or alters the shape of these shells in order to produce a change in ROC therefore a change in its focal length.

The first patent, in 1866, was filed by D.A. Woodward (US Patent 60,109), wherein he described how to make a fluidic lens by filling the area between two or more bowed glass plates. He also described using different index fluids in multiple chambers to achieve chromatic correction (i.e. a fluidic achromat). The first

variable focus fluidic lens appears to be by Robert L. Gordon, who in 1918 patented eyeglasses that could vary their focal length to accommodate the needs of different individuals or different viewing distances (US Patent 1,269,422). In 1940, Robert Graham, wrote *A Variable Focus Lens and Its Uses* (JOSA 30, p 560(Nov 1940)) and discussed a novel solution to a common problem that existed in previous variable focal-length lenses. Specifically, he suggested varying the radius of curvature of cylindrical surfaces (rather than spherical) to reduce aberrations. He then used two orthogonal cylindrical lenses to create a spherical lens. This, he concluded, could be used to quickly and more accurately test the refractive errors in an individuals vision (i.e. phoropter). He also was the first to suggest their potential use in cameras, a field which continues to gain interest to this day.

Infrared applications for variable focal lengths lens have been limited due to the absorption of materials at longer wavelengths. Work had been demonstrated in the near infrared and suggestions made for longer wavelengths, this either by using fluidic lenses(with no flexible polymer membrane) or liquid crystal based lenses[21][8]. Size and weight reduction as well as rapid variable field of view are some of the advantages that this type of technology can be used to improve infrared systems.

More recent commercial attempts have returned to mechanical deformation of a compliant surface. Lenses from Holochip and Optotune have significantly larger apertures (10-20mm). The greatest challenge associated with moving to larger, and more useful, apertures is the introduction of aberrations due to gravity (e.g., coma).

Non-commercial efforts by DARPA, Sandia National Labs (SNL), and the Naval Research Labs (NRL) continues to push this technology. NRL, in particular, has a long history in variable focal length devices, starting with Guy Beadie, Marie Sandrock, etc. [4]

In total, there have been hundreds of articles and dozens of patents describing

methods for achieving the perfect variable lens. Variable focal length lenses are being proposed for autofocus in cell phone cameras, depth correction in endoscopes and push-button zoom in military rifle scopes. As active devices continue to improve in dynamic range, power consumption, and wavefront quality, they will find their way into a variety of commercial and military applications.

SNL has identified the need for increased aperture (larger than $10mm$), large dynamic range, and high optical quality adaptive polymer lenses (APL). This for incorporation in applications such as surveillance systems, correction of atmospheric turbulence effects in adaptive optics systems, variable optical magnification for rifle scopes and other direct view optical systems as well as infrared systems which require rapid non-conventional zoom. In recent years, companies such as Holochip, Varioptic and Optotune have been pursuing the commercialization of these large aperture lenses but none have been able to address key challenges such as wavefront quality, dynamic range and operation at longer wavelengths, that will make these lenses viable for field applications. For example, commercial tunable lenses have a clear aperture in the order of $10 - 20mm$ and a focusing range of $-40mm$ to $40mm$, but the lenses suffer from high amounts of aberrations and are limited by customization for specific systems. Other lenses are limited by clear aperture in addition to aberrations. Varioptic lenses present the best optical quality and dynamic range but the maximum clear aperture is on the order of 5 mm, greatly limiting its applications.

Large aperture fluidic lenses present a challenge due to the aberrations introduced in these lenses mostly due to gravity and the fabrication process. Gravity effects manifest as a high coma component, an effect that can be minimized but not eliminated, Figure 1.1. In addition to gravity induced coma, two of the most impactful and limiting properties are chromatic aberration and thermally induced focal length change this due to the materials. From the fabrication process, the dominant aberrations is astigmatism, and this is mostly due to the boundary conditions

established by the support structures.

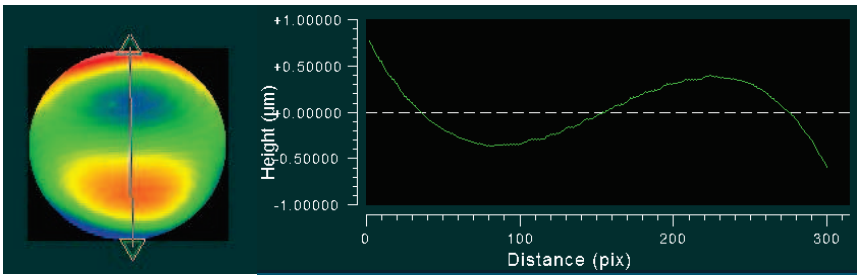

Figure 1.1: (Left) False color representation of coma effect on a adaptive polymer lens due to gravity measured with an optical interferometer. (Right) Cross section of the lens surface.

One of the main objectives of this dissertation is to develop an adaptive polymer lens doublet (APL). In order to achieve this, work was performed to understand and control the design and fabrication variables of singlet APLs and with the knowledge acquired develop the APL doublet (APLD). The lenses main application is for variable magnification direct view optics(DVO) systems, optics that rely on the eye as the detector, and for camera base system at longer wavelengths such as short-wavelength infrared (SWIR) and mid-wavelength (MWIR). This requires an understanding and control of aberrations as well as identifying a process which can be used to related design variables to fabrications variables.

1.1 Background

Typical zoom lens systems rely on mechanical or digital zoom, to vary the image magnification. Mechanical zoom is achieved when elements are moved along the optical axis of an imaging system to change magnification, this is most commonly used in cameras, surveillance systems, telescope and rifle scopes or DVOs. These systems are fairly complex due to the number of mechanical parts required to translate the

optical elements. They are also limited due to weight and size, which is related to the magnification power presenting a limitation for compact systems. Digital zoom simply remaps the pixels into a larger image, making it appear larger, but without any change in resolution, resulting in no increase of information. Figure1.2 shows the difference between digital and optical zoom.

Non-conventional zoom or non-mechanical zoom relies on active elements in order to vary magnification and optical resolution[16][30]. An active element is an optic in which its optical power is altered by a change in radius of curvature. Examples of active elements are deformable mirrors, adaptive lenses and liquid crystals.

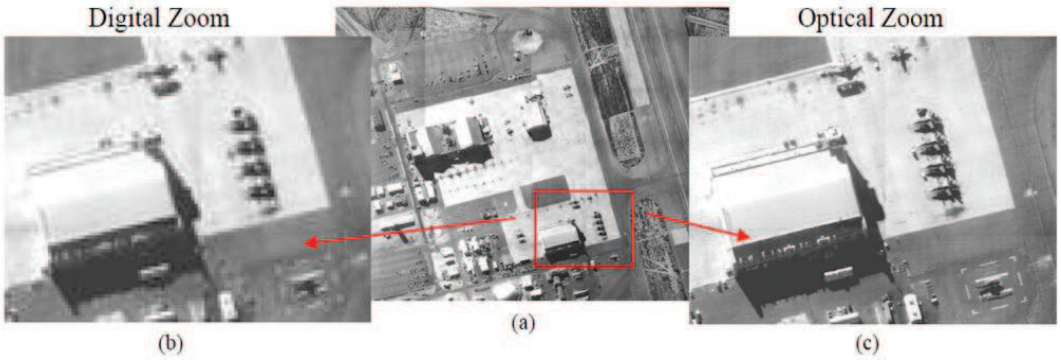

Figure 1.2: (a) Airfield image.(b)Digital zoom, no resolution improvements, pixelated image.(c) Optical zoom showing and increase in magnification and resolution

The focus of the work for this dissertation is on APLs. Some of the applications of interest to SNL for adaptive polymers lenses are for surveillance, light weight zoom systems for ground or unmanned aerial vehicles (UAVs), tactical zoom systems such as rifle scopes, and correction of aberrations in adaptive optics systems for horizontal beam propagation and imaging. Current work is focused on rapid adaptive zoom rifle scopes (RAZAR) systems for military applications. The main idea is to incorporate two or more APLs in a rifle scope and allow the user to toggle between magnification, or zoom, states by the simple push of a button. Current rifle scopes accomplish this by turning a dial by hand, which will move glass lenses inside the housing; this takes

time and the hand of the operator from the weapon, which in tactical environments can be dangerous, time consuming, and potentially deadly. Since classical rifle scopes draw no power, thermal effects are minimal and these instruments have been field-tested, making this the most complicated platform that APLs can be incorporated into. Advantages of APL rifle scopes are, the rapid change in zoom or field of view (i.e. tenths of a second actuation between a 1-2-3X system), length and weight reduction in comparison with classical scopes, and larger dynamic range without physically moving optical elements.

In order to create an APL based system for a rifle scope, the optical quality, performance, and capabilities of singlets or doublet APLs have to be comparable to glass lens. Also, issues such as chromatic aberration and thermal effects need to be addressed, in order to minimize the burden at the system level. All of the above challenges have to be managed over the entire dynamic range of the APL. This implies that all the variables of the APL need to be known, optimized and controlled. The bulk of the work for this dissertation is making singlet APLs comparable to glass singlets by minimizing aberrations and improve optical performance. The acquire knowledge will be use to expand the scope of the work to APLs in the infrared spectrum.

1.2 Aberrations

A wavefront is a locus of point which have the same phase. Deviations from a perfect wavefront, know as aberrations, are due to the optical or component fabrication, misalignment or diffractive properties of it. Optical aberrations were first described by Seidel in the mid 19th century and to this day are used by optical designers. Another means of describing the aberrations is by the use of Zernike polynomials introduced in the early 20th century. Aberrations can be categorized in two main

types: monochromatic(which can be describe by Seidel and Zernike) and chromatic aberrations which are a result of the wavelength dependent of the index of refraction, n.

For the purpose of this work, most of the focus for the optical aberrations will be based on those created by the fabrication process. For example for monochromatic aberrations, a particular attention on astigmatism, coma which is mostly due to gravity, but dependent on the membrane fabrication, and higher-order aberrations mostly resulting from imperfections. These effects will be quantified using a Zygo interferometer, which measures the deviation from a perfect wavefront in units of optical path difference, more commonly specified using the wavelength used in the measurement, referred to as *waves*.

The second aberration which will be an objective in this dissertation is due to the dependence of wavelength with index of refraction, chromatic aberration.

1.2.1 Chromatic Aberration

Chromatic aberration results from the dispersion properties of materials used in optical systems. It manifests axially, where different wavelength focus at different planes from the lens, and as laterally, where the magnification and image height varies with wavelength [7]. This aberration is present on glass singlets lenses but it is easily corrected and mitigated by the use of achromatic lenses, typically doublets. In glass lenses, chromatic aberration is typically corrected by using two or more elements of different dispersion material, eliminating or balancing dispersion. Materials have a dispersive indices or Abbe number (V-number), which determine how dispersive it is, the lower the V-number, the higher the dispersion and vice-versa, as seen in Figure 1.3. The effect on an imaging system can be impactful as seen in Figure 1.4.

Chromatic aberration balancing (with other static elements) only works up to

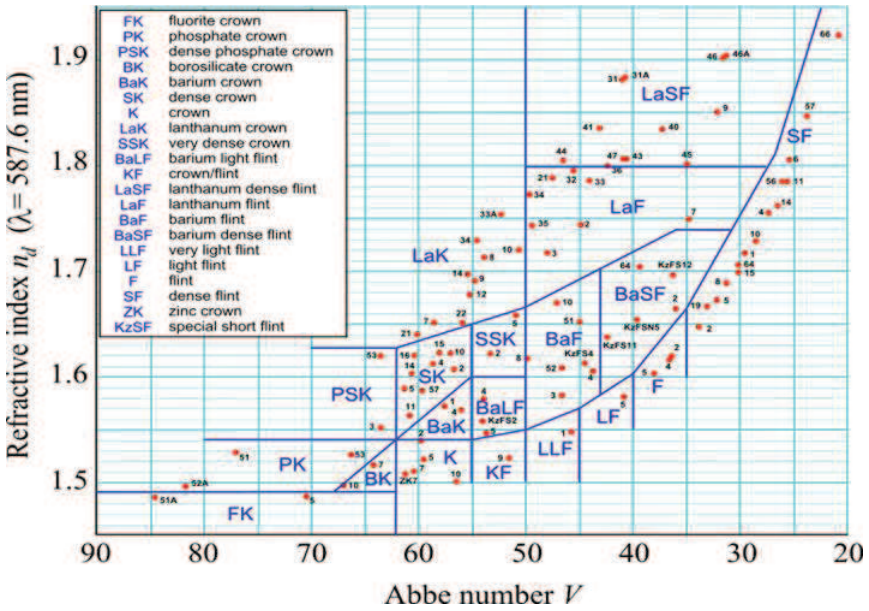

Figure 1.3: Glass Abbe diagram: plots Abbe number against refractive index

a point because APL change their shape from state-to-state, so do their chromatic aberrations. Static balancing only works perfectly at one ROC. That's why achromatic APLs are needed. But this approach presents a complexity and challenge from

Figure 1.4: (Top) Corrected image (Bottom) Chromatic aberrated image

the optical design perspective [26]. As mentioned above, the idea of achromatization of APLs has been suggested since the $1800s$[31] but the attempt has been limited to just to an idea, concept or model but never fabricated [31][5][13]. One of the biggest challenges of these types of lenses is from the material side; there are a limited amount of fluids with the required optical properties such as refractive index and V-number. A large challenge is to maintain the achromatization over the full dynamic range of the lens. Achromatization of the adaptive polymers lens will be one of the main areas of research in this dissertation work.

1.2.2 Temperature Dependence

Temperature variations affect two main properties of a lens: its physical dimensions and its index of refraction. For example, in a glass lens, as the temperature increases all the physical dimensions of the lens increases which changes the lens effective focal length due to the coefficient of thermal expansion (CTE) of the lens material. Secondly, the index of refraction is a function of temperature. Which for many glass materials, the index of refraction increases as temperature increases therefore reducing the lens focal length (but not necessarily as it is with fluidic lenses). This particular effect is referred to as the temperature coefficient of refractive index, dn/dT[10]. Thermal effects on APLs are orders of magnitude higher than it is for a typical glass lens. This is the biggest and most limiting challenge for the use of adaptive polymers in optical systems.

Coefficient of Thermal Expansion (CTE)

The APLs, singlet, are manufactured of 3 main components; support rings (typically 2 or more), polydimethylsiloxane (PDMS) membranes (quantity 1 or more) and an optically transparent fluid. The rings provide support and a surface to adhere the

PDMS membranes. The PDMS membranes are made of Dow Corning Sylgard 184 and function as an enclosure of the optical fluid. As a result of the different materials, the APL singlet results with multiple CTEs. For the rings, if made of glass, the CTE is 3 ppm/C°, for the membranes the CTE is 930 ppm/C° and the fluid varies from 530 to 950 ppm/C°. For comparison, a typical glass lens contains a single CTE which ranges from 0.55 to 10 ppm/C° depending on the material.

Temperature coefficient of refractive index, dn/dT

For an APL, the effect of the temperature coefficient of refractive index on focal length, is a function of temperature and actuation state of the lens. The effect of dn/dT for a polymer lens is different than as in a glass lens, since it is dependent on the curvature of the lens. The impact of dn/dT increases as the focal length of the polymer lens decreases. This dependence of dn/dT on curvature, or focal length, and the larger magnitude of its value in fluids, in comparison to optical glass materials, make this the most challenging effect to compensate or correct for. A change in temperature results in a focus shift of the lens, which at the system level manifests itself as image degradation. There are several methods to athermalize an optical system, by mechanically passive or active and optically passive. The former two introduce complexity in the system and have been demonstrated for glass systems [25] and for APLs at the singlet and system level [3]. As mentioned above, this mechanical compensation adds complexity and also relies on constant power consumption. These solutions may not be practical due to cost constraints, packaging, or customer desire, making the optically passive approach the most desirable but also challenging due to the wide change in focal length of fluid based lenses.

1.3 Scope of Work

There are various ways to manufacture an APL, some of the most common are:

- Two fluids between glass plates: electrowetting concept used by Varioptics, Figure 1.5. Limited by aperture size in the order of $5mm$ or less.
- Single fluid chamber open: One side has a glass plate and other side flexible membrane (mostly PDMS) or chamber made of flexible membranes. Or another in which there is a reservoir of fluid attached to the lens and fluid is pump in and out in order to physically change the surfaces of the lens, therefore changing its optical power, Figure 1.6. Limited by complexity of the reservoir and complexity in integration on systems.
- Single fluid chamber close: Fluidic chamber enclosed by two flexible membranes or a single membrane glass plate in which an applied pressure to the surface/s changes it curvature. Concept most used today by companies such as Holochip, Optotune and National Labs such as SNL-NRL. Limited by manufacturing quality and dynamic range. Figure 1.7

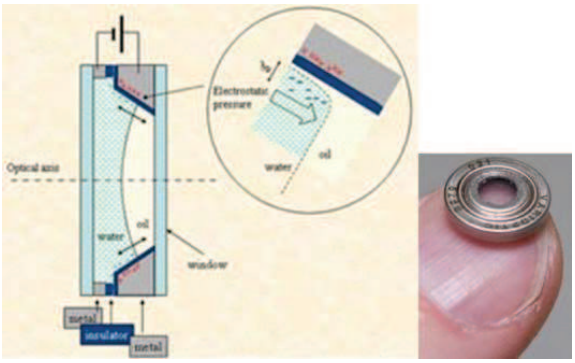

Figure 1.5: Varioptics lens: concept and picture

Of the 3 main types of APLs, the latter one presents the most potential for defense, tactical, and military applications. Reasons such as capabilities of potential

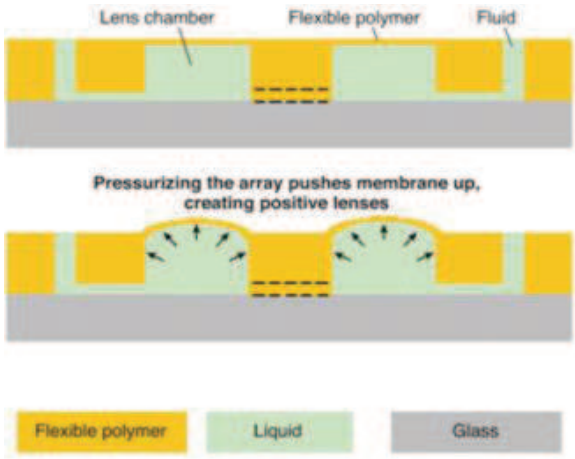

Figure 1.6: Fluidic reservoir lens

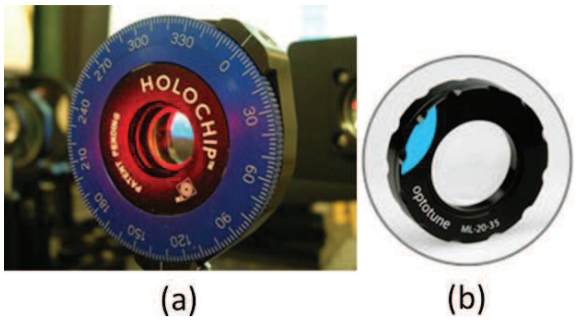

Figure 1.7: Holochip(a) and Optotune(b) lenses

improvement in manufacturing quality, clear aperture size control, mechanical simplicity, make this type of lens the focus of my efforts. Over the past three years, SNL has been developing APLs with support of Picatinny Arsenal, under the Picatinny Adaptive Lens (PAL) project, which follow the single fluid chamber fabrication process, Figure 1.8. SNL APL follow a iterative process between manufacturing, materials research, optical quality, performance testing, and a finite element model in order to continuously improve the lens adaptive/active performance.

Each APL is composed of 3 rings, 2 membranes, and an optical fluid. The process starts by manufacturing optically flat membranes of PDMS of a desire thickness.

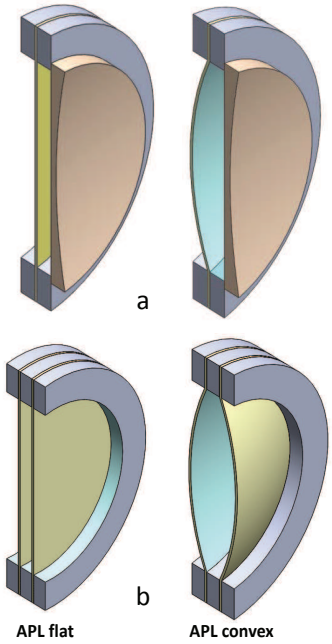

Figure 1.8: Single (a) and double (b) membrane APL singlet, on a flat and convex configuration

Glass rings are cut from borosilicate glass plates with desired dimensions of an outside diameter (OD) of 31.75mm, inner diameter (ID) of 23.77mm and a thickness of about 2.7mm or as determined by the optical design. All surfaces of the membrane and the glass ring's that will be in contact with the membrane are treated with an atmospheric corona[12], followed by bringing the parts into contact. The first bond is filled with an optical fluid and the process is repeated in order to create the enclosed fluid chamber.

For an example of a two membrane adaptive lens, the resting optical prescription of the lens can be approximated by the following procedure. For a positive equiconvex lens the volume of the spherical cap is added twice, for a negative biconcave lens the volume is subtracted twice to the volume of the cylinder. These APLs have been manufactured following the conventional approach of typical single element glass lenses, or singlets, but with the caveat that both surfaces of the APLs are manufac-

tured and assumed to be either equally concave or convex depending on the desired optical prescription. As with glass singlets, APLs suffer from basic aberrations such as spherical, chromatic, astigmatism and coma, with the latter mostly influenced by gravity effects on the fluid. Some of these aberrations, such as astigmatism, are induced by the manufacturing process, which will be also addressed. Once the APL is finished in order to actuate it, one or two cylindrical plungers are used to compress the membranes and therefore the fluid inside; this creates a bulge on the membranes which impart a radius of curvature change to the lenses which can be changed by varying the position of the plungers, Figure 1.9.

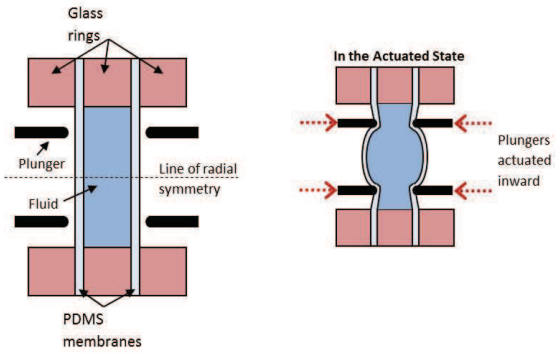

Figure 1.9: Cross section of APL, before plunger make contact with membrane and once lens is actuated

Different modalities of actuation can be implemented; for example,

- Two symmetrically moving plungers which compress the APL
- A static plunger with lens in contact and a moving plunger which compresses the APL
- A static plunger with a lens on a moving platform that compress the APL against the static side

The modality selected is dependent on the optical system design.

From the process describe above, the following variables were identified:

- Membrane thickness before and after pre-tension
- Pre-tension imparted on the membranes
- Physical dimensions and surfaces uniformity of the glass rings
- Atmospheric corona bonding
- Volume calculations and control
- Actuation modalities

All of the variables mentioned above contribute to the overall optical performance and quality and are the potential source of failure mechanisms of the APL. The first part of this dissertation work will be composed of understanding the impact, weight factor, quantification, and controlling of these variables under various actuation modalities. The second part encompass the development, model, fabrication and testing of an APLD. The third part demonstrates work performed and the use of APL for applications in the visible (VIS), SWIR and MWIR applications.

1.4 Contributions

The following is a list of the contributions or accomplishment resulting from the work performed under this dissertation.

1. First APL for tactical military direct view optics (DVO) applications: APLs were developed an incorporated in a DVO system for small arms systems, Figure 1.10

Figure 1.10: APL based DVO live fire evaluation.

2. First APL doublet under constant volume condition for imaging applications, Figure 1.11.

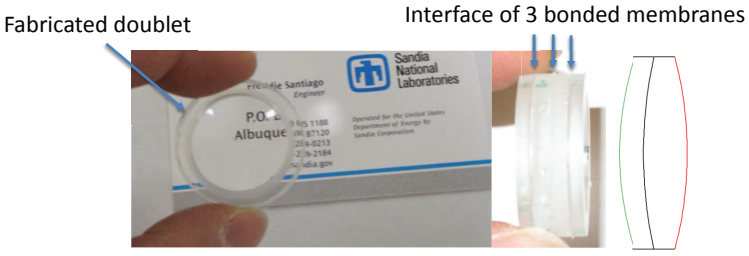

Figure 1.11: Fabricated APLD under constant volume condition.

3. First APL for SWIR tactical applications: push button variable magnification and divergence control, Figure 1.12.

4. First APL for MWIR tactical applications: push button variable magnification, Figure 1.13.

Publications:

- F.Santiago, B. Bagwell, T. Martinez, S. Restaino and S. Krishna Large aperture adaptive doublet polymer lens for imaging applications (Submitted May 2014: JOSA)

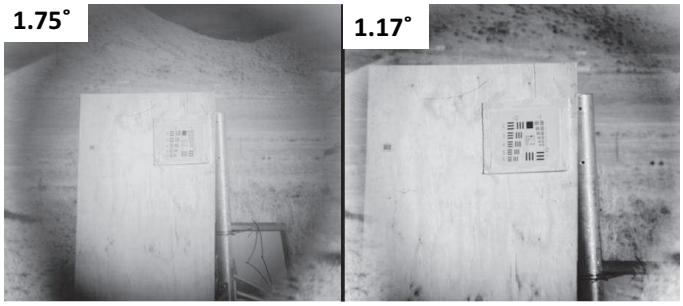

Figure 1.12: APL SWIR images at two FOV.

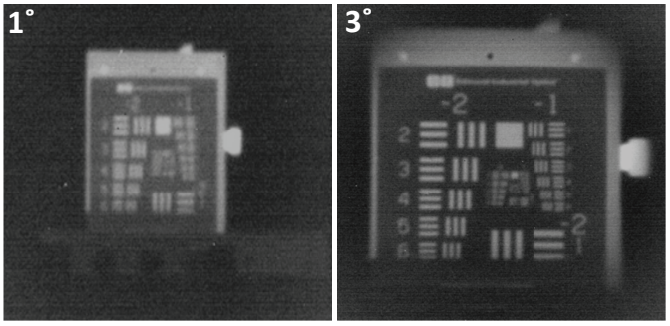

Figure 1.13: APL MWIR images at two FOV.

- F.Santiago, V. Pinon II, B. Bagwell and S. Krishna Adaptive polymer lens for rapid zoom shortwave infrared (SWIR) imaging applications (Submitted June 2014 OE Letter 2014)
- F.Santiago, V. Pinon II, B. Bagwell and S. Krishna Adaptive polymer lens for Mid-wavelength infrared tactical applications (Submitted June 2014: Optics Letters 2014)
- R&D100 nominee: RAZAR, Rapid Adaptive Zoom Rifle Scope. RD100, 2014.
- M. I. White, F. Santiago, B. Bagwell, E. R. Beckel, J. P. Bruhn, B. J. Anderson,J. R. Brown, , and J. M. Hochrein. Characterization of gas permeation through optical membrane for variable focal length rifle scope lenses. 41st Polymac, Sandia National Laboratories, April 2012.

- B. J. Anderson, J. P. Bruhn, M. I. White, J. R. Brown, J. M. Hochrein, E. R. Beckel, F. Santiago, and Brett Bagwell. Development and characterization of low permeation optical membranes for variable focal length rifle scope lenses. 41st Polymac Conference, Sandia National Laboratories, April 2012.

- M.S. Baker, B.J. Anderson, G. Soehnel, B. Bagwell, and F. Santiago. Polymer adaptive lens athermalization. Sandia Report SAND10, Sandia National Laboratories, P.O. Box 5800, Albuquerque, NM., 87185, 2011.RD100-1

Chapter 2

Adaptive Polymer Lens Singlet Development

This chapter demonstrates the concept of APL Singlets(APLS) developed at SNL. APLS consist of a single or double elastomeric membrane with an optical fluid enclosed. An elastomeric membrane is a polymer with viscoelasticity having a low Young's modulus(measurement of the stiffness of an elastic isotropic material) and high strain in comparison with other materials. For the single elastomeric membrane, the fluid is enclosed between the membrane and an optical window which index of refraction is close to the fluid index of refraction and window. These two types of lenses function by redistributing the volume enclosed and works as plano convex/concave or equa convex/concave type of lens. Both configuration of the lens can be seen in Figure 2.1.

APLS has been developed since the 1960s and there are commercial entities that sell them. SNL development of APL is based on zoom imaging systems, consisting of replacing glass lenses with APLS. Commercial APLS are mostly based on a single flexible membrane and after extensive characterization performed on the best avail-

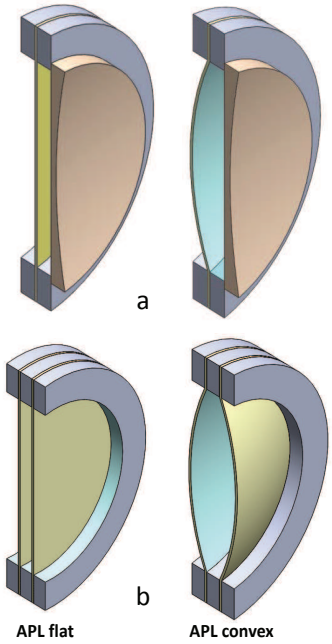

Figure 2.1: Cross sectional representation of the APLs with a single or double membrane.

able APLs in the market SNL decided that none meet the optical and mechanical performance, robustness and characteristic required for the optical zoom application. SNL APLS are required to operate under MIL-STD 810 environments. MI-STD-810 is the United States Military standards, meaning equipment developed for the US military needs to follow this standards over their service life. These APLS also need to sustain high G-forces($\geq$ 1500Gs) due to recoil imparted by weapons systems it would be used on.

In order to solve the problems/complexities introduced in Chapter 1, SNL started the manufacturing of custom APLS focused specifically for direct view optics applications for the military, which require low wavefront errors, while performing in harsh environments and compliance with the MIL-STD. This is a big challenge due to the fact that glass direct view optics that had been used for years does not consume any power and is a established and proven technology.

This chapter presents the failures modes and solutions implemented in order to produce a state of the art APLS with the main focus of its application in military systems. Furthermore, the work performed in this Chapter will be the base for the APL doublet(APLD), design and fabrication. All lessons learned in the APLS development were implemented in the APLD and infrared APL development.

2.1 Background

The APL for this work are composed of an elastomeric membranes, fluid, support rings structure that the membrane is bonded to, the actuation mechanism and electronics. Each of these main components is an important variable which at the same time each introduces complexities. In the end, each one contributes to optical performance and mechanical stability of the APL.

In order to produce a state of the art APL, each one of these variables needs to be identified, controlled and optimized. Once the variables were identified, a solution and control strategy was developed and implemented which would improve performance and allow the repeatable manufacturing of APLs. The following sections encompass the main variables mentioned above, how they where identified, solutions developed, and improved performance results.

A key methodology that was implemented in the process of identifying these variables and solutions for it was the use of a Lean Six-Sigma methodology[11]. Lean Six-Sigma methodology is methodology that combines the concepts of Lean and Six Sigma, to eliminate or reduce waste and improve the performance, capability or output of a process or product.

2.2 Elastomeric polymer membrane

Some of the important properties and characteristics of an ideal elastomeric membrane for APLs are[19]:

- Transmission: membrane should exhibit a high transmission in the spectrum of interest (SNL interest lays on the visible and infrared spectrum)
- Viscoelastic: should be able to stretch and deform without damage and return to original configuration.
- Chemical property: should not react with liquid or damage due to ambient conditions.(SNL)
- Physical-Mechanical properties: should be uniform, nontoxic and compatible with the manufacturing process(SNL)

The most prolific elastomeric polymer, which is currently used by almost all elastomeric polymer lens manufactured, is polydimethylsiloxane, PDMS, due to its physical, chemicals and optical properties. Table 2.1 show some of these properties of PDMS.

n(d)	**Abbe**	dn/dT (10^{-5})	**Density** (g/cm^3)	**Tensile Strength**(MPa)	**Young's Modulus**(kPa)	**CTE**(ppm)
1.43	52	-360	1.03	0.727	1840	310
			0.97∗	2.24∗	360-870∗	

Table 2.1: Line 1: Cured Mechanical and Optical Properties of PDMS measured by SNL. Line 2: other common values presented in literature[19]

PDMS is the main polymer used in the APLs for this dissertation. A study was performed to develop a second elastomeric membrane with similar opto-mechanical properties as PDMS but with a lower gas permeation rate since PDMS is highly permeable to gases[17]. This will be discussed in more detail in Subsection 2.2.3.

2.2.1 Membrane fabrication

SNL APL membranes use thermal induced polymerization. There are 3 main methods of fabricating the membrane. In order to obtain a "uniform" thickness which are by spin-coating [1], using a mold, and using a substrate [2] All of which are exposed to a thermal polymerization typically at $100C^{\circ}$ for 45 minutes or shortened to 10 minutes at $150C^{\circ}$ [19]. The spin-coating is complicated when making large diameter membranes since a large disc in which the membrane solutions lies needs to be rotated at high speeds as well as cured. The mold technique relies on the quality of the mold, any imperfections are transfer to the membrane, these molds can be costly and complicated to use. The substrate also depends on the shape and surface finish of it, both will be address in next sections.

Membranes are prepared by mixing Sylgard 184 base and agent in a ratio 10 : 1. The mixture, which is degassed, poured on the substrate and then bake in an environmental oven that maintains a constant temperature. An-in house process was develop using substrates to cure the PDMS at a particular diameter and desired thickness. Maintaining a uniform thickness is crucial for the optical performance of the APL. Subsection 2.2.2 will concentrate on membrane thickness study. The main advantages of PDMS are its elastic properties, in which elasticity and strength can be tune, it is inexpensive and readily available and it is optically transparent over a wide range of wavelengths.

2.2.2 Membrane Thickness control

One of the most important variables in the APL manufacturing process is the membrane thickness. Variations in membrane thickness results in variations on the APL

[1] one of the most common method used
[2] wafers, glass plate,etc.

desired optical prescription as well as on differences on stress/strain between membranes. This is due to the membrane stiffness which is a combination of the thickness, stress/strain, and diameter. When a membrane with non-uniform thickness is stretched the resultant membrane will contain non-uniform stiffness across its surface and, when compressed or deformed, will be radially non-symmetric, resulting in optical aberrations. Repeatability and control on the manufacturing of the membranes contributes to a reduction in the variations in lens resting radius of curvature(RROC) and aberrations. In order to verify this, a Finite Element Analysis(FEA) model and a series of experiments where developed in which the thickness of the membranes was measured at discrete points and a relationship between the thickness variation and the wavefront established.

Membrane thickness Finite Element Analysis

A Finite Element Model(FEM) was developed using the mechanical properties of PDMS, shown in Table 2.1. This model created a membrane of a particular initial thickness, then stretched a desire amount and the results for strain and stress where qualitatively compared. The model's primary goal was to demonstrate the impact of a non uniform thickness membrane, which would result in non-symmetrical stresses. For the non-uniform thickness variations which are in discrete areas of the membrane, a variance of $\pm 18.5 \mu m$ from that initial $330 \mu m$ thickness was used. This variance was not selected arbitrary; it was obtained by performing thickness measurements on actual membranes made of a particular thickness, using a Wyko interferometer and will be explained in the next section.

A cylindrical fixture boundary condition was used in the thickness face of it or side edge of the membrane, and two different mesh controls were applied to the top and bottom surface as well as to the edge face, respectively. This allows the FEA to improve convergence and reduce computation time[14]. The fixture condition refers

to fixing part of the object in a particular direction while the rest move freely. A similar configuration will be used for verifying membrane deformation under constant pressure which is equivalent to actuating the APL.

Various FEM models were run and Figure 2.2a shows the results for displacement, strain and stress plots for a uniform thickness membrane, notice the symmetry on the false color pattern on the displacement plot, and Figure 2.2b for the non-uniform membrane showing the asymmetry on the displacement plot.

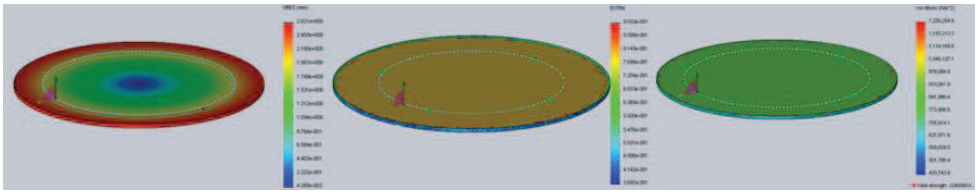

(a)

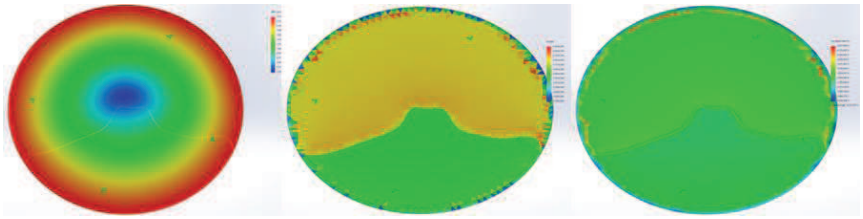

(b)

Figure 2.2: **(a)**(Left)Uniform thickness membrane created in FEM.(Middle)Uniform stress resulting from the applied uniform deformation to the membrane.(Right) Uniform strain resulting from the applied uniform deformation to the membrane.**(b)**(Left)Non-uniform thickness membrane created in FEM.(Middle)Stress resulting from the applied uniform deformation to the membrane.(Right) Strain resulting from the applied uniform deformation to the membrane.

The plots demonstrate that a variation in thickness results in non-uniform strain-stress on the membrane which therefore results in a non-symmetrical displacement when the membrane is stretched causing aberrations. If this membrane is deformed under actuation, it is clear that the deformation would not be symmetrical which in this case translate to aberrations on the lens. Below are experiments which can show

the effects on non-uniform membrane as well as experiments to be able to quantify and solve the problem.

Experiment #1: The first experiment consisted of using a Veeco white light interferometer to measure the thickness of 10 membranes. This is an extremely time consuming process because the setup that is needed to measure the thickness and the field of view(FOV) of this instrument is extremely small meaning a point measurements per step. Also there is no way this type of measurement can be implemented in situ on the fabrication fixtures.

The concept behind this experiment was to verify how repeatable and uniform membranes are under the procedure mentioned above. For these, the procedure for manufacturing the membranes was controlled in order to reduce as many variables as possible. This included the use of the same substrate, substrates orientations, mechanism to control thickness, PDMS mixture and curing procedure. With the conditions established and process controlled, a set of 10 membranes were made and prepared for measurements. The preparation of the membrane consisted on cutting it in half which allowed taking measurements along the diameter and center of each membrane 2 at a time. Since it is a viscous liquid, once poured, the edges are thinner than at the center, this when using glass plates as molds but also happens when it is spin coated. This and the fact that the middle part of the circular membrane is the part used, the measurements were performed along its diameter. The laying process on the measurement plate was carefully performed in order not to introduce any variations in thickness at the points of measurements. Different laying conditions were tested resulting in no significant change on the measurements.

The thickness measurements where performed using a Wyko SP9900 surface profiling system. Figure 2.3 shows a top view and cross section profile of the membranes as well as a 3D representation of the membrane measuring area.

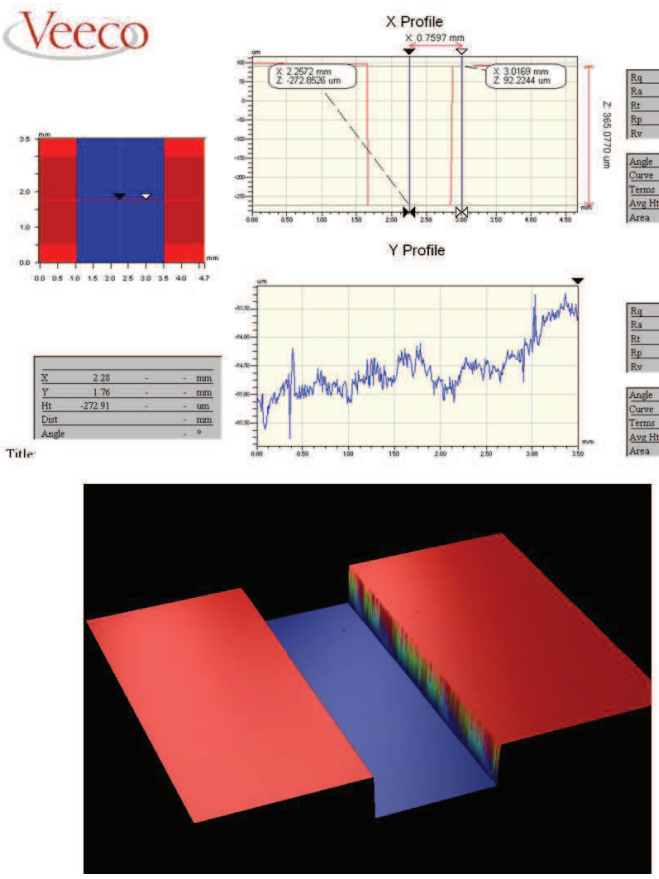

Figure 2.3: (Top)Cross section representation showing the user interface and information provided by the Veeco.(Bottom)3D representation of the membrane, the false color red indicated the top surface of both membranes and the blue at the bottom the substrate on which the membranes are resting.

Using the Vision software from Wyko, the thickness at 5 different points per membrane was obtained. Two sets of measurements were made using the same membranes with the difference that for Run #2 each membrane was removed from the plate and re-laid onto the glass plate and a small pressure was applied to where the measurements where taken. This was done in order to verify variations between both data sets. Table 2.2 shows the results of the values obtained in microns with the respective average per membrane and average per set, for the 10 membranes and both runs. A standard deviation of 5.70μm and 8.16μm was obtained for Run#1

and #2 respectively.

Table 2.2: Thickness measurements of 10 membranes prepared under same conditions using a Veeco interferometer

Membrane	**A**	**B**	**C**	**D**	**E**	**Average**
1	365.1521	362.1461	370.6307	390.0901	416.7596	380.9557
2	371.1078	368.1367	362.6866	359.6209	360.7433	364.4591
3	345.2462	350.8704	354.2947	354.9592	353.0431	351.6827
4	345.3969	352.5756	358.3222	364.7047	366.4138	357.4826
5	383.6268	368.3602	360.0699	368.624	377.7457	371.6853
6	361.0252	363.963	368.588	371.8118	370.2831	367.1342
7	359.3975	361.2013	362.2353	359.0856	354.0896	359.2019
8	359.2434	365.5236	370.699	374.6935	375.4683	369.1256
9	358.6236	359.4935	360.9292	362.9833	367.2614	361.8582
10	356.5545	358.2637	364.7291	368.7141	371.6205	363.9764
					Average	364.7562
					Stdev	8.157815

The smallest standard deviation obtained was $\sigma = \pm 5.7\mu m$ with an average of about $10.0\mu m$ and delta from the desire thickness of $34.75 \pm 10\mu m$. Stretched membranes wavefronts of these types of membranes are shown in the next section. This demonstrated no control on the thickness of how the membranes are made and the variation in the process. This experiment provided feedback on the repeatability and variations of making the membranes and provides data for FEM on how the membrane will stretch with those thickness variations. In order to improve repeatability, changes need to be made in which the thickness can be controlled as well as a more feasible way to measure thickness. The Veeco interferometers relies on the interference pattern from the top surface of the membrane and the bottom surface where the membrane sits, in this case the glass plate, which imply that the membrane has to be cut in order to perform a measurement.

Experiment 2: Confocal sensor

In order to perform the measurements in situ while the membrane is laying on top of any type of material that provides a change in index of refraction, or the membrane is suspended in air or even while it is stretched, a chromatic confocal sensor (CCS) was implemented on the process[27]. The chromatic confocal sensor was invented in 1995, and it is an accurate and reliable technique to perform non contact measurements for distance and thickness. With the CCS, multiple fast point measurements can be made on the membrane to verify the uniformity of the thickness in multiple directions and without modifying the membrane. These points are entered into Matlab to create a false color plot that represents thickness variations, seen in Figure 2.4(Left). For the second experiment, membranes were made using the same procedure as experiment 1 but then one variable was changed at a time while maintaining the rest constant in order to identify changes. Once membrane were made, it was cut to the dimensions that fit on the mechanical fixture and 25 equally space measurements were made. These points were used to generate the surface representation. These membranes were stretched and a relationship between thickness variations and aberrations was established. Figure2.4 shows samples of membrane thickness surface false color representation (left) and data from Zygo interferometer[32] (right) of that same membrane stretched prepared on the substrate. This data shows a relationship between the direction of the astigmatism (dominant aberration) and the direction of the thickness wedge on the membrane.

It is clearly shown in Figure 2.4 that the membranes are not uniformly symmetric. In order to correct for this non-uniformity, multiple changes where made on the membrane preparation process, from mixing and curing, substrates, improvement in thickness control, curing temperature recipe tailored for this membranes and the experiment was repeated. The implemented changes results can be seen in figure2.5, the left side shows the thickness measurements indicating the delta in thickness which

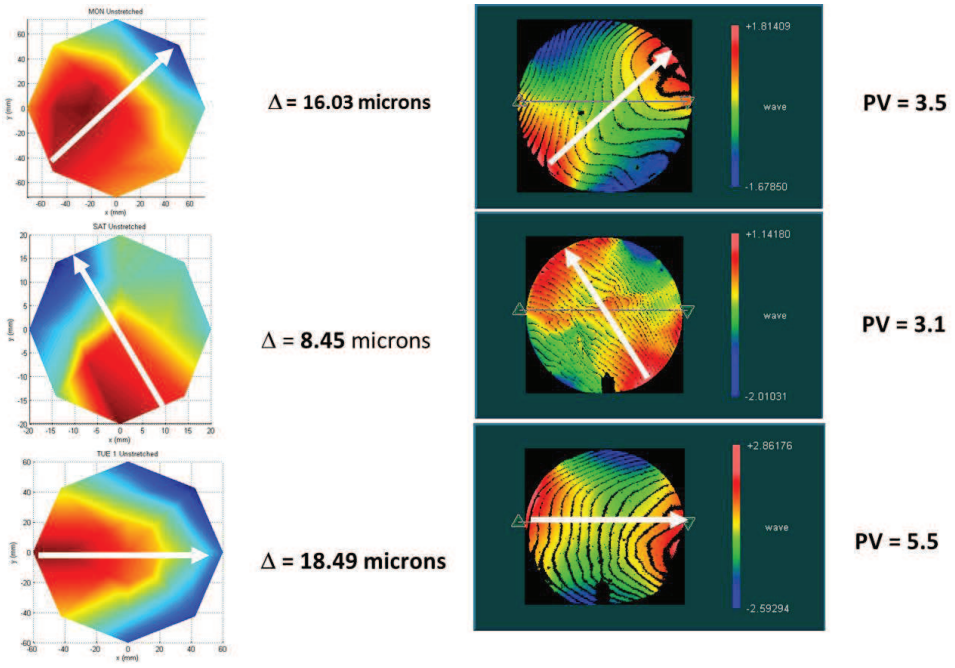

Figure 2.4: (Left) False color representation of thickness variations, interpolated from 25 point measurements using a confocal sensor. (Right) False color wavefront map from the Zygo interferometer with an overlay arrow indicating the direction of the astigmatism axis.

went from an average of $30\mu m$ to an average of about $2\mu m$ with the new procedure. For the case of the membrane shown in the figure the delta is in the order of $1.66\mu m$. The false color interferogram on the center shows the stretched membrane with the aberration that remains as power, shown by the concentric circles, which is expected, this power results from gravity acting on the membrane and it is symmetrical. The right figure shows the result when the power is removed with a resulting PV of 0.7 waves.

This demonstrated the improvement in thickness control as well as the aberration reduction, important characteristics for the APLS and APLD.

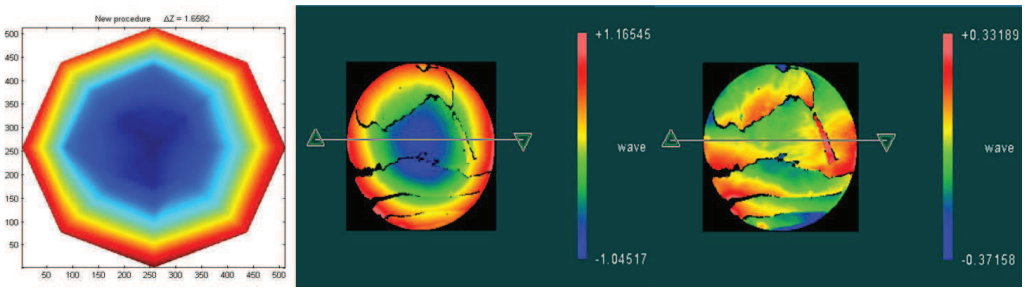

Figure 2.5: (Left)False color representation, resulting from 25 point thickness measurements performed on the membrane.(Center)False color representation of the full aperture(4 inches) interferogram when the membrane is stretched, focus is the main resulting aberration.(Right)Resulting wavefront after power is removed

2.2.3 Gas permeation

APL are normally fabricated with a short negative radius of curvature(ROC), meaning a concave surface, (150 mm or less) in order to increase the dynamic range at the system level, as well as allowing flexibilities in the design. One of the main limitations on how short the ROCs can be manufactured is the permeation of gases into the lens, since PDMS is permeable to gas if the differential in pressure between ambient and the inside of the lens large then air will permeate, therefore changing the prescription of the lens. The permeation of gases is due to gas moving through the PDMS membrane or due to weak bond between the PDMS and the supporting annular structure, glass, metal, or other. Commercial products limits their dynamic range in order to minimize this as well as implementing glass windows to seal the lens, adding windows increase complexity, aberrations and limits applications.

It is well know that PDMS is permeable to gases.[17] An RROC on the order of -100 mm or less, due to the difference in pressure with the ambient air pressure, results in air permeating through the membrane, which results in air bubbles inside the APL, as can be seen in Figure 2.6.

In order to design and manufacture a multi-chamber lens with a large dynamic

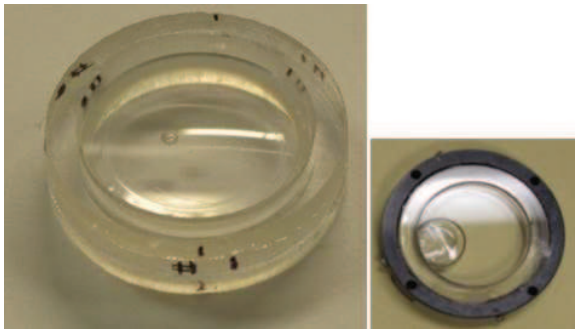

Figure 2.6: Air bubble inside a strong negative lenscore

range, ideally one of the surfaces will require a negative ROC, which is limited by permeation of gas through the membrane. The permeation of air by the boundary needs to be eliminated and the permeation by the membrane reduced in order to expand the dynamic range of the APL.

Due to the inherit characteristic of PDMS, one of the solution to minimize gas permeation was to make longer negative RROCs. The larger the negative RROC the less differential in pressure between inside the APL and ambient, minimizing gas permeation. After changes in the curing process and multiple APLS fabrications, it was noticed that for ROC values of -100 to -125 mm the permeation rate was reduced, but after about 2 months bubbles will be seen inside the lens. Some of the options explored at SNL, were flexible coatings which can present other complications during actuation, as well as introducing aberrations, and an increasing the thicknesses of the membrane which would imply and increase on required actuation force.

An effort was developed around this problem, which consisted in quantifying the permeation of PDMS in a representative way as used for APL fabrication and in making a membrane less permeable to atmospheric gas while maintaining similar opto-mechanical properties as PDMS. This effort resulted in membrane made out of Thiol-ene.

Thiol-nes:

A study was performed at SNL based on thiol-nes membrane while varying various components in its chemical composition[22][1][29]. First order properties of the material were qualitative verified such as membranes optical properties, elasticity and compatibility with the process. The formulations which comply with these basic characteristics were further studied by making sample tokens and using a thin film/fiber tooling in a Dynamic Mechanical Analyzer (DMA Q800), from TA Universal Analysis Equipment in which strain and stress curves, as well as studies under temperature sweeps, for storage modulus were obtained as shown in Figure 2.7.

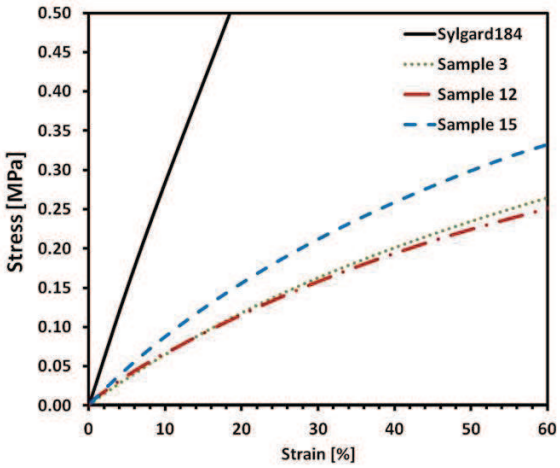

Figure 2.7: Strain-Stress curves for 3 of the main formulations of thiolenes in comparison with PDMS

Three formulations of thiol-nes membranes were selected to transition from token samples studies to membranes more representative of its final application used for APL fabrication. The main purpose was in order to performed comparative test on the opto-mechanical properties and permeability between all 3 samples using PDMS as the control. These formulations were the following:

- Formulation #3: Low young modulus, low permeation

- Formulation #12: High young modulus, low permeation
- Formulation #15: Low young modulus, low permeation

The formulation were label by numbers according to its composition.

Figure 2.8 shows the chemical structure of all the materials used for these 3 formulations. Using these 3 formulations and PDMS as the metric, membranes were prepared of the same shape and form as is performed with PDMS.

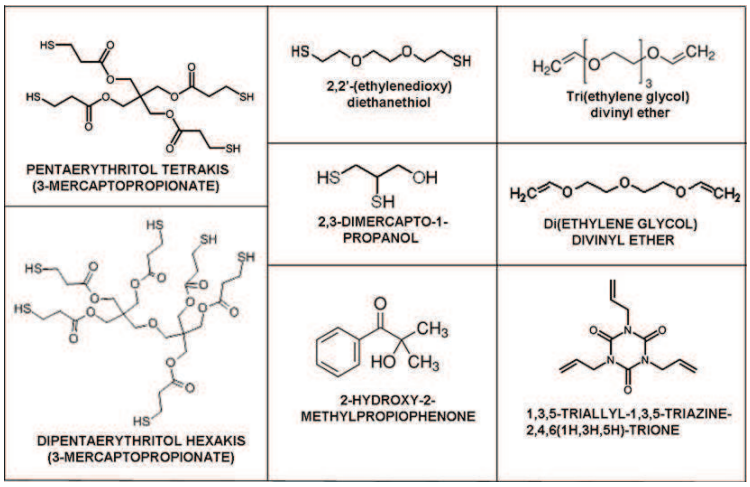

Figure 2.8: Chemicals Structures of the materials

Membranes Preparation:

Thiol-nes membranes are cured using a UV curing chamber from ReadyMax. The curing occurs in the first half second of exposure to UV and it tapers off as time increases, but is very dependent on variables such as intensity, distance, and exposure time of source. In order to produce membranes that can be used for the lens fabrication, the optimal curing process was determined. Curing Membranes of the desired thickness were manufactured between two 1 inch glass windows in diameter in which

the optimal curing time and conditions were identified. From this experiment the best conditions for curing thin membranes were:

- Distance from source: 9 inches
- Exposure time: total of 60 seconds exposures in increments of 10 seconds
- Intensity: 50% ($23.20 mW/cm^2$ measured through the glass plate)

Following the optimal curing recipe, membranes were manufactured of larger size (5inches in diameter) on 8 x 8 inches glass plates. This is shown in Figure 2.9.

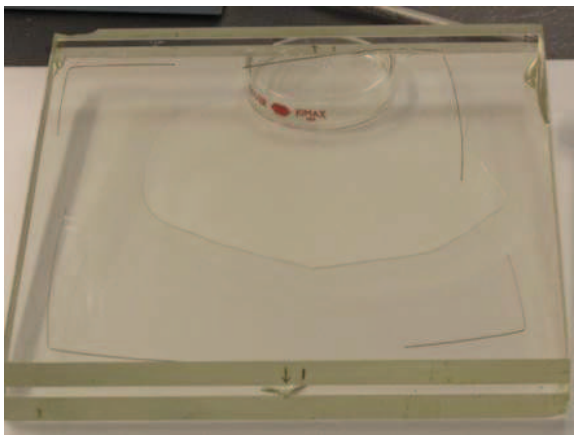

Figure 2.9: Thiol-ne membrane between glass plates

This size of membrane allows their use in the current fixtures for stretching and bonding to glass or metal rings.

Bonding to glass/metal rings

Bonding of PDMS and glass is done by treating the surfaces with a Corona treatment, in which the surface energy is increased–improving the wettability and adhesion properties of the material[6][12]. This is also possible due to the silica groups (SiO2)

present on both materials which is not the case with the thiol-nes, so an alternative method needed to be developed. As a first approach, UV adhesives from Norland Products were selected to bond the thiol-nes to the glass rings. Various UV adhesive from Norland were used and in the process it was discovered that once the membranes were stretched and exposed to UV. In order to cure the adhesive, the membranes would deform and appeared to lose its elastic properties.

Experiments were performed to identify if the cause of the deformation was the UV exposure, heat from the UV source, or the stress apply to it while stretching. Sample strips of thiol-nes were placed between clamps, a mark of a particular size was place on the membrane, followed by stretching the membrane a know distance, Figure 2.10. The membrane was returned to its original position and the mark was measure. A temperature sensor was place in contact with the membrane to monitor temperature changes. The next subsection will describe the experiments performed.

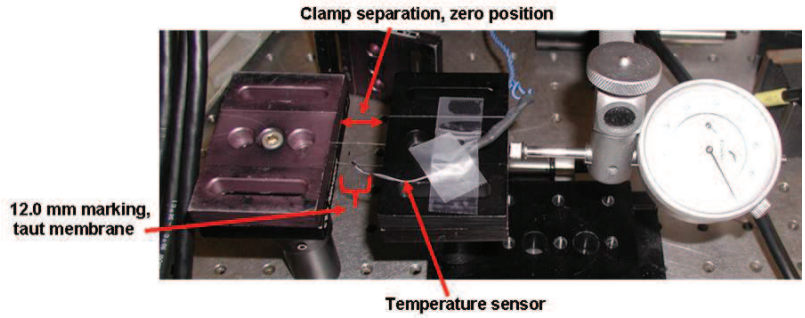

Figure 2.10: Experimental setup for testing thiol-ne degradation. The clamps hold the membrane, a temp sensor and a dial gauge to measure displacement.

Experiment #1: Mechanical Stretch

A strip of thiol-ne was marked, stretched and left under stress for 24 hours. Using the dial gauge the membrane was returned to its starting position, the mark was measured and it had returned to its original dimensions, no noticeable or measurable

deformation was observed.

Experiment #2: Heat exposure The procedure use in experiment #1 was followed with the difference of placing a heat gun 350 mm from the membrane. This distance is the same distance used when curing the bonds. The membrane was exposed for 90 seconds while temperature was monitored at the membrane, reaching $70°C$. There was no noticeable deformation of the membrane while stretched and the mark returned to its original dimensions. No noticeable or measurable deformation was observed.

Experiment #3: UV exposure The same procedure as previous cases was performed but with the UV lamp placed 350 mm from it. The membrane was exposed for 180 seconds while the temperature raised $0.5°C$. When the membrane was brought to its original position, sag was observed on the membrane and the mark has expanded 2.0 mm, as shown in Figure 2.11.

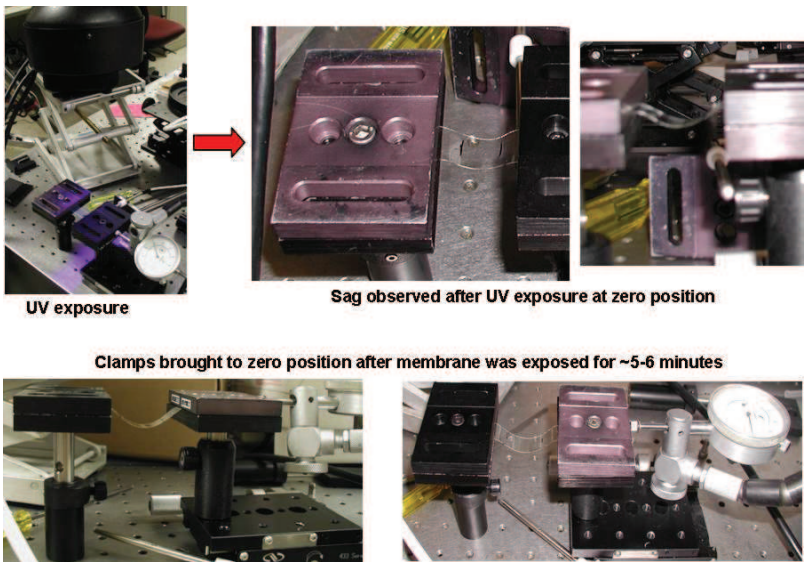

Figure 2.11: Observed membrane sag once membrane was exposed to UV for 180 seconds

It has not been determined with an analytical explanation the deformation of

the membranes under UV exposure. One hypothesis is that after the membrane had been cured on the UV oven it still had active radical groups. When the membrane was exposed to UV a second time these radical groups form new bonds, therefore changing the characteristics of the membrane and resulting in sag of the membrane when brought to its original position. This represents a problem while bonding the membranes while stretched in the assembly fixture. The previous UV adhesive cures in the order of 5 minutes. In the meantime, the UV adhesive was replaced by adhesives which contain a latent heat catalyst which can cure in 10 minutes at $125°C$ in an oven. This introduces other complications due to the need of applying heat while the membrane is stretched and on the assembly fixture. So, in order to perform the necessary comparison, the membranes were bonded un-stretched using the heat catalyst adhesives, as seen in Figure 2.12.

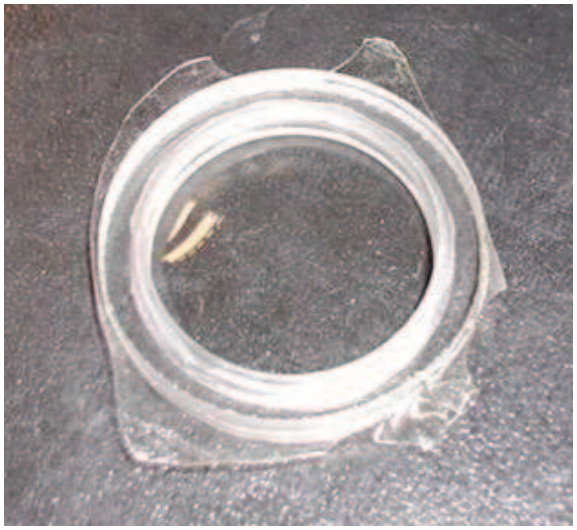

Figure 2.12: Thiol-ne membrane bonded un-stretched to glass using a heat catalyst adhesive

Bonds shown in Figure 2.12 were use to verify the mechanical properties as well as permeation test. Besides bonding to glass, bonding to metal is an important part when designing and fabricating a multiple chamber APLs. Bonding to metal,

will allow better flexibility in the volume control as well as reducing the overall dimensions of the APLs. Currently, there is a limit on how thin glass rings can be cut with out compromising the integrity of the APL, as well as the limit on the cutting mechanisms. Metal rings will allow a reduction in the thickness dimensions of the APL as well as better control of volume inside the core, which is key for passive athermalization of the APL.

Optical Properties

Membranes from each of the 3 formulation, were used to qualitatively and quantitatively verify optical transmissivity. Figure 2.13 show pictures of the first thiol-nes membranes fabricated for lens applications. Samples of the 3 formulations as well

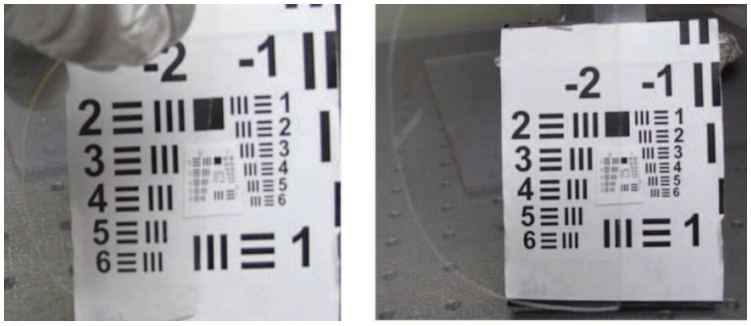

Figure 2.13: Thiol-ne membrane and PDMS in front of an Air Force resolution target chart

as PDMS were measured in an optical spectrophotometer from 300nm to 3200nm and the results are show in Figure 2.14. For a the optical region of 400-800nm the average transmission for PDMS is 94.15%, Formulation 3 is 91.38%, Formulation 12 is 90.37% and Formulation 15 is 91.03% an average difference of about 3.22%.

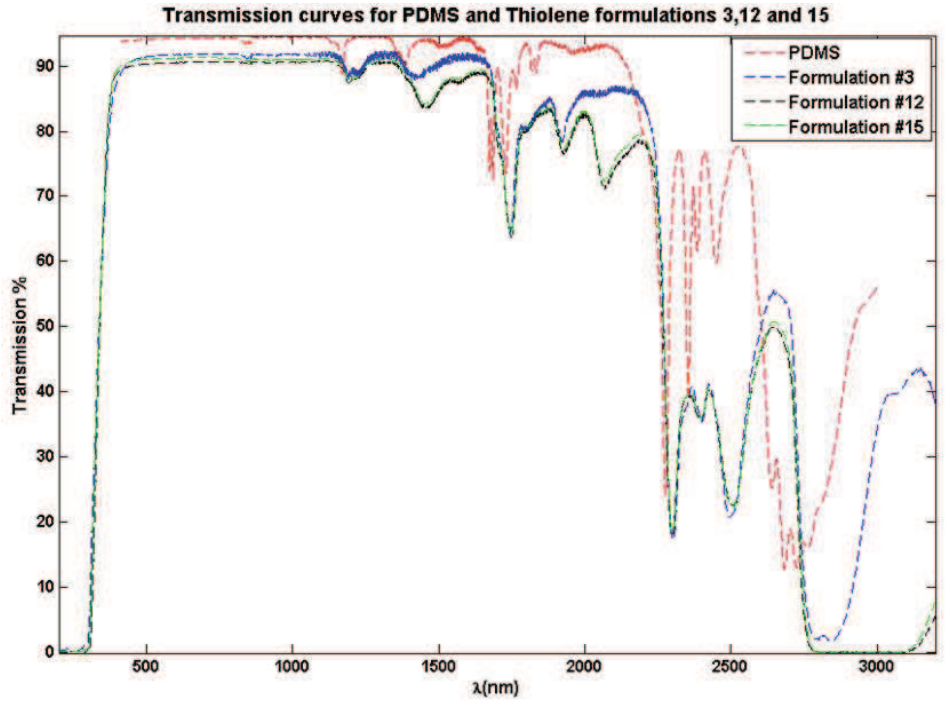

Figure 2.14: Optical transmission curves for 3 Thiol-nes formulations and PDMS.

Mechanical Properties

For the mechanical test of the membrane, the same procedure as for permeation was made; bonds were prepared of membrane with similar thickness un-stretched. A plunger, of the dimensions of the plunger use in the actuators was use in order to deflect the membrane from its resting position, using a force gauge and a translation stage Force vs Displacement was recorded. Figure 2.15 shows the setup and sketch of the quantities measured.

Table 2.3 shows the results for average Force vs Displacement, and respective thicknesses of the membranes for the 3 formulations and PDMS. Two measurements were made per membrane. These results demonstrated that Formulation #12 which in both cases broke at about 16 N and deflection from flat of 3.56 mm may the best candidate for fabricating the first doublet APL. In order to increase the force or

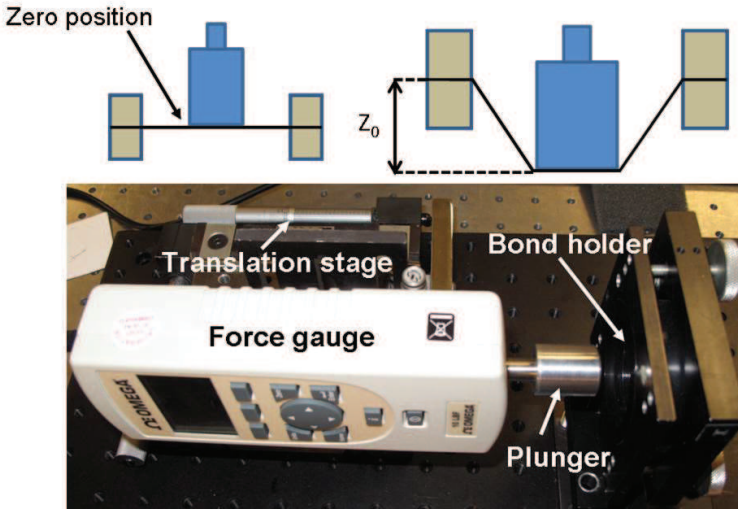

Figure 2.15: (Top) Sketch and (Bottom picture of Force vs. Displacement setup.

strength of this formulation the thickness of it can be increase therefore increasing strength.

Table 2.3: Thickness measurements of 10 membranes prepared under same conditions using a Veeco interferometer

x(inches)(Z_0)	Form 3 F(N)	Form 12 F(N)	Form 15 F(N)	PDMS F(N)
0	0	0	0	0
0.01	0.03	0.06	0.045	0.025
0.02	0.085	0.1725	0.11	0.075
0.03	0.17	0.39	0.235	0.21
0.04	0.335	0.74	0.46	0.465
0.05	0.5875	1.2825	0.785	0.915
0.06	0.9075	2.015	1.13	1.635
0.07	1.31	2.97	1.6	2.665
0.08	1.8975	4.32	2.235	3.99
0.09	2.69	6.055	3.1025	5.715
0.10	3.6125	8.085	4.0325	8.3
0.11	3.055	10.2675	5.0025	11.71
0.12	5.435	12.39	5.9325	16.045
0.13	5.545	14.38	6.795	19.535
0.14	6.055	16.33	7.6625	23.08
0.15	6.735	9.02	26.315	
0.16	7.39	9.9	29.615	
0.17	7.955		31.95	
0.18	8.4		35.115	

Permeation Test

The main parameter for the effort in developing these membranes is the reduction of the permeation of gases into the APLs. In order to perform permeation measurements on the membrane and on the bonds, the Materials Reliability Group at SNL designed custom hardware in order to test permeation of gases such as Helium and Nitrogen. Permeation tests were performed on all samples by preparing bonds of un-streched membranes. Since permeation is a function of sample thickness, bonds were prepared with membrane thicknesses as similar as possible. These can be seen listed in Table 2.4. The PDMS bonds were prepared using the corona treatment and the thiol-nes membranes using the heat catalyst adhesive.

Table 2.4: Thickness of thiol-nes and PMDSs bonds for permeation test

	Form 3	Form 12	Form 15	PDMS
Thickness(μm)	303.01	293.92	266.91	292.93

The measurements consisted of 3 main parts: testing of the bond for leaks using He followed by testing the membranes for He and N_2. For testing the bond a custom sealing flange manifold was assembled and He leak testing. The test ranged from 1 to 4 days at room temperature. Figure 2.16a shows the block diagram and Figure 2.16b the custom hardware for testing the bonds.

This test demonstrated that the bonds were sealed. A small He signature of about 3.0x10-8 atm-cc/sec was detected, but this is consistent with the He permeation through the materials. This test served the purposes of indicating that the samples could be used for permeation test, but most important it demonstrated that the heat catalyst adhesive used for bonding could be a solution for bonding the thiol-nes membranes to glass or metal.

For testing the membrane, a separate custom fixture was used, in which the

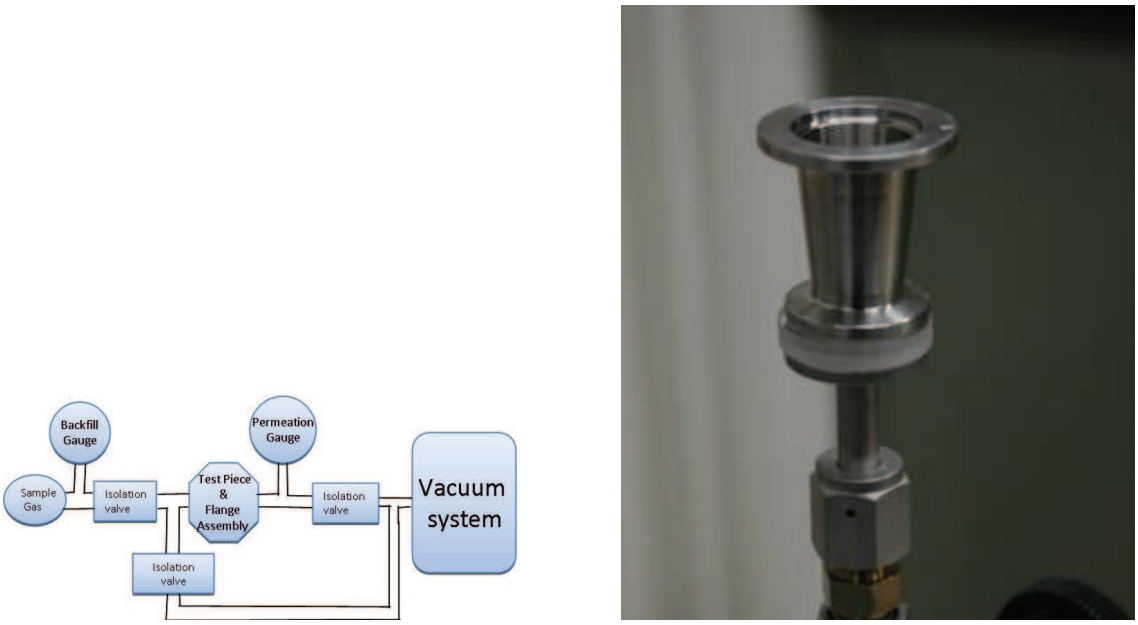

(a) (b)

Figure 2.16: Block diagram and custom hardware for the experiment

membrane is sandwiched between two Teflon disks with small holes of about 0.76 mm in diameter. The Teflon disks work as a support for the membranes since the delta in pressure would tear the membranes. Figure 2.17 shows the custom permeation hardware, the Teflon support parts and the manifold experimental setup.

The plot in Figure 2.18a shows the permeation of He through the membranes and Figure 2.18b shows the N_2 permeation.

The He permeation test shows Formulation #12 as the least permeable of all. Since most of the atmosphere is compose of N_2 this test is more representative of the operating conditions as well as the size of the gas molecule of N_2 are larger than He. The results indicated that Formulation 12 and 15 have similar permeation rates, which in order to identify a difference or obtain the permeation constant for these two membranes or any other one, a longer test would have to be made. Selecting 10 hours

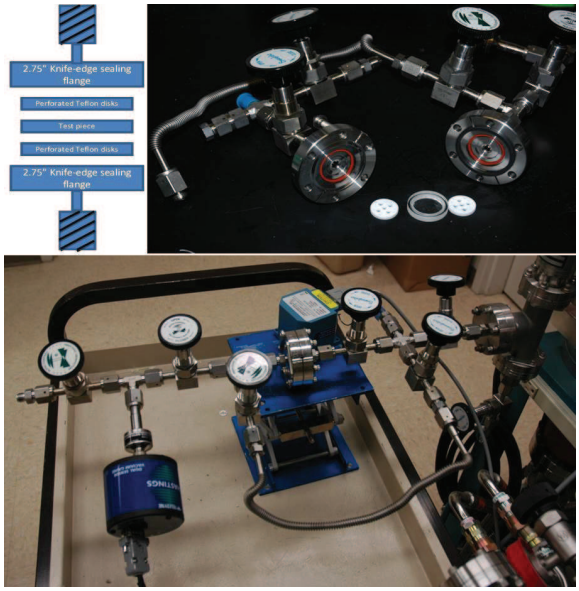

Figure 2.17: (Top Left) Diagram of test.(Top Right) Manifold Del-Seal for bond with membrane.(Bottom) Experimental setup.

as means of comparison, for Formulation #3 we got 17.12 $Torr$, Formulation #12 10.68 $Torr$, Formulation #15 10.25 $Torr$ and PDMS 178.6 $Torr$, which shows that PDMS is an order of magnitude more permeable than the thiol-ne membranes. From the permeation and Force vs Displacement results Formulation #12 was selected as the membrane to continue studying and development.

APL design with Thiol-nes

Formulation #12 was selected as the thiol-ene for manufacturing of the first APL. The first lens design was a split triplet, consisting of a glass lens and APL in which chromatic aberration was minimized. Figure 2.19a shows the layout of the $F/7.5$ and diffraction limited on axis triplet as well as the chromatic focal shift and spot size for the F,d,C lines of the visible spectrum obtained from the a ray tracing software, Zemax.

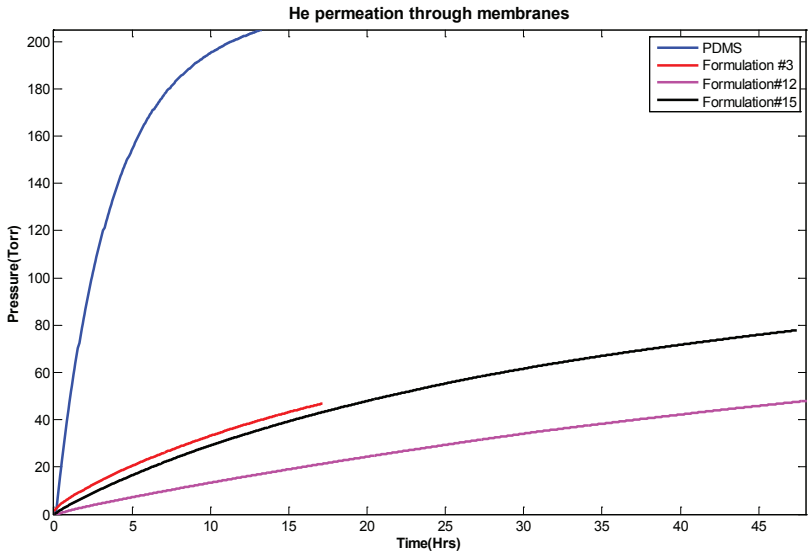

(a) He permeation through the membranes

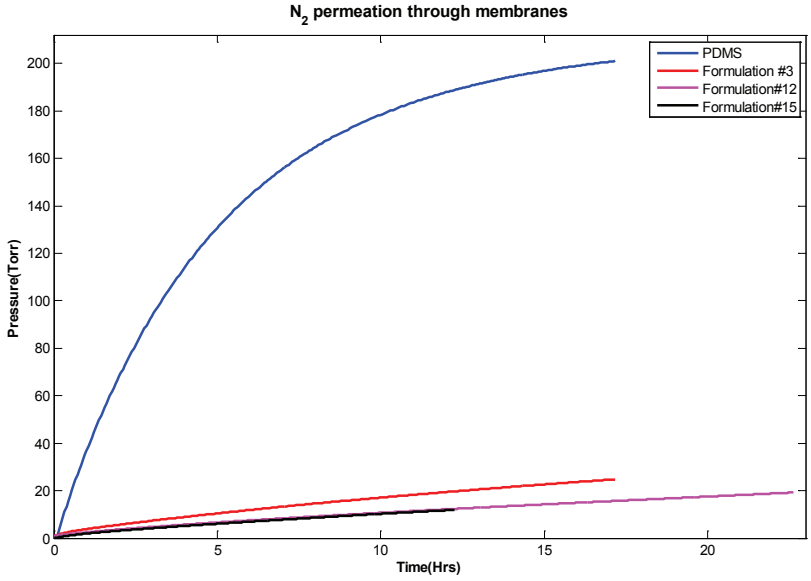

(b) N_2 permeation through the membranes

Figure 2.18: Permeation curves for He and N_2

As means of developing and identifying constraints during manufacturing, a PDMS and glass doublet was fabricated, shown in Figure 2.19. Following the PDMS

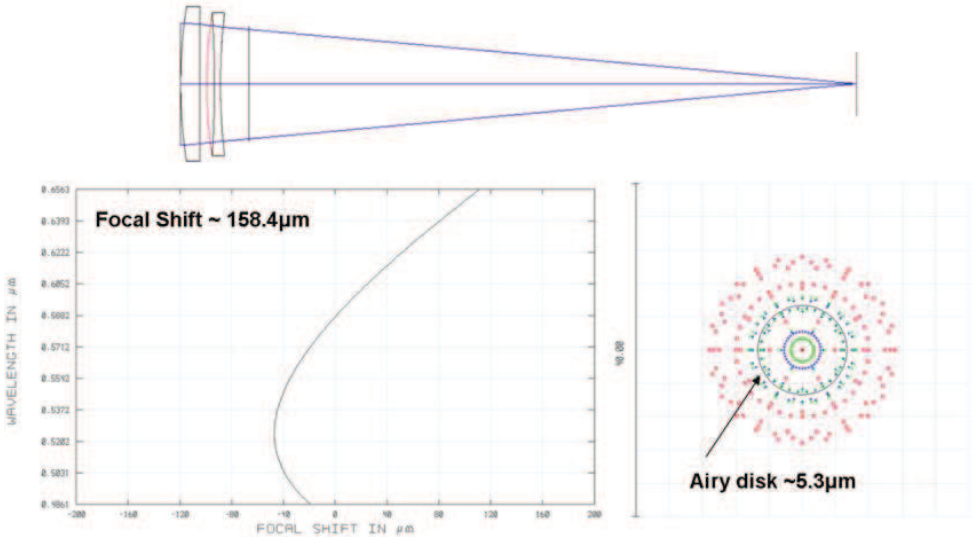

(a) Schematic layout of the APL, chromatic focal shift and spot size

DIMENSIONS IN MILLIMETERS

LEFT SURFACE	MATERIAL	MID SURFACE	MATERIAL	RIGHT SURFACE
R 56.4256 CX	GLASS: MODEL	R 151.612	GLASS: MODEL	R 79.6509 CC
$Ø_E$ 23.6	N_d = 1.300000	$Ø_E$ 23.6	N_d = 1.463000	$Ø_E$ 23.6
0	V_d = 108.00	0	V_d = 43.90	0

(b) Dimensions of APL

Figure 2.19: Design of proposed APLD fabricated with Thiol-ene membrane formulation #12

doublet manufacturing procedures and attempt was made on a thiol-ne membrane based doublet based on the design of Figure 2.20. The main goals were to identify a new fabrication procedure for these membranes, test the new bonding mechanism as well as verifying permeation by having short negative ROC. From the first attempt, key steps were learned in which modifications to the current building fixture were made in order to bond the thiol-enes using the heat catalyst adhesive.

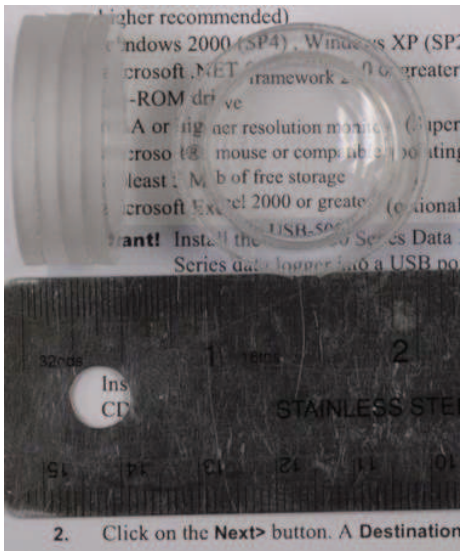

Figure 2.20: PDMS doublet manufactured in order to develop a manufacturing procedure.

A less permeable thiol-ene membrane was demonstrated as well as an optical design of an achromatic APL based on these membranes. Future efforts will focus on improving the bonding mechanism and fabrication process in order to build the design APL. Due to the problems with the bonding mechanism as well as the mechanical properties of thiol-ene, PDMS was used for the rest of the work performed in this dissertation. This limitations imposed a limit on how concave the membranes for the doublets or infrared lenses could be fabricated.

2.3 Bonding

The membranes are bond to the glass or other substrate by means of atmospheric corona discharge. When the surfaces are treated, this process activates the surface by cleaving existing bonds and leaving radicals and electrons thate are free to bond chemically to other surfaces. When using glass as the support structure Si-O-Si and

Si-O-C covalent bonds are created between the membrane and the ring. If a different material beside glass is used as the support structure, for example aluminum, which does not contain Si-O-C in the surface the process is more complicated. This process consist of chemically deposition of an adhesive or primer that contains SiO on the surface of the ring in order to be able to bond with PDMS. This enable PDMS to bond to other materials such as aluminum, titanium to mention a few.

Bonding is one of the key process for the lenscores, it enclosed the fluid and seals the core of the lens as well as join all the support components. Weak bond create bias in which air or the fluid can move through, resulting in a different prescription lens or a lens that can fail. Figure 2.21, shows a bond that have been submerged in a dye solution to identify weakness or paths for which air can be passing through. As can be seen on the picture, the dye entered the bonding area, meaning that a study need to be develop in order to identify the source of the bond weakness. From the study it was identify that once the treatment process was follow correctly and the parts where cleaned there were no failures. In order to improve the bonds, a semi clean room environment was established as well as new a cleaning and handling procedure of all materials require for making a bond. A 3 solvent cleaning process was used for the rings, which consisted of an ultrasonic clean in acetone followed by rinse with Methanol and Isoprophyl alcohol(IPA), dry with ultra-high purity nitrogen and then bake in an oven at $150°F$ for 15 minutes. The personnel used latex gloves and special tools where created to handles the rings, from the acetone bath to the end of the bond, the rings where never touch, only by the tooling and the bonds were made inside the clean room. This new procedure eliminates bond failures and permeation by 95 percent.

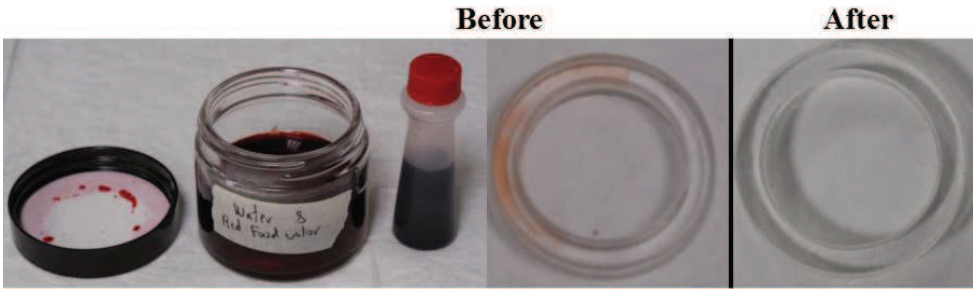

Figure 2.21: (Left)Red dye solution in which bond with membrane was submerged showing the marks of dye on the bonding area.(Right)Bond with membrane under new procedure after been submerged in the same red dye solution. No dye was seen on the bonding area.

2.4 Fluid permeation-absorption

Section 2.2 talks about permeation of air through the membrane and Section 2.3 talks about permeation of gases or leakage of fluid due to bond weakness but there is also permeation or absorption of fluid into the membrane depending on the fluid. PDMS is a porous material, meaning that gases and certain fluids can permeate through it. Low molecular weight fluids in the order of $100-200sCT$ would first be absorbed by the PDMS and further permeate through PDMS forming beads or micro bubbles on the outer surface of the membrane. These beading makes the lenscore hazy looking through it, and also change its curvature due to the change in fluid inside. This was most noticeable during high number of actuations (≈ 1000) and during temperature cycles. Research was performed in order to find fluids that have a high molecular weight, compatible with the fabrication process and at the same time meets the required optical properties. This is one of the most challenging problems since optical transparent fluids with the desire optical properties are limited, therefore presenting a limitation on the optical design of APL lenses.

Once a number of fluids were down selected based on the optical properties and the molecular weight, in order to test it, each fluid was exposed to the fabrication

process as well place on a fixture the mimics the lenscore but can be pressurized externally. The RROC of this was measure, then it was compress to a short ROC of about $45mm$ and left actuated for about 5 days. After the 5 days the RROC was re-measured in order to detect any change and the lens inspected under a microscope for beeding. A second test was to place the selected lens or lenses with the desire fluid under an accelerated test, which consisted of measuring RROC of the lens, place the lens in the actuator and actuate it from a negative ROC to short ROC about $10,000$ times. After the $10,000$ actuation the RROC was re-measured and change annotated. This test served multiples purposes, one in which it tested the bond structure, the membrane integrity (meaning if the membrane stress-strain would change over time and number of actuations) and fluid permeation under high number of actuations.

After this study a main Fluid A was selected for the singlets, with an index of refraction of 1.463 and Abbe number of 43.9. Using the Zygo interferometer no detectable change were measured on the lenscore before and after the compression and the high actuation test. This corroborated that the PDMS can sustain this high number of actuations as well as this type of fluid will not permeate through the membrane. An important note, is that multiple lenses with this particular fluid have also been tested and actuated at temperatures ranging from $-3°C$ to $50°C$ with no degradation on any of the components. Other fluids with similar molecular weight were place under the same testing conditions in order to identify the ones which presented different optical properties, such as index and Abbe number, as Fluid A so that they can be used for the doublet.

2.5 Support structure, rings

The support of the APLs are rings in which the membrane is bonded to it. These rings were made from glass plates of the desired thickness, by cutting them using a

waterjet process. The dimension are an outer diameter (OD) of 31.75 ± 0.02 mm, inner diameter (ID) of $23.77 \pm 0.02mm$ and a thickness of $2.70 \pm 0.02mm$ which could vary depending on the application. The ID and thickness of the rings are of extreme importance since this determines the amount of fluid volume for a particular lens therefore determining the resting radius of curvature. Any variations in these dimensions that are not taken into account will results in variations of the lens from its optical prescription. Besides support of the lenscore, the glass rings provides the bonding surface and the boundary conditions for the membranes. Any undulation, non-uniformities on the glass and pinch points[3] resulting from the support structure (due to cutting, glass chipped, metal cuts, etc) and bonding are transferred to the membrane. This translates to optical aberration or weakness on the membrane-bond interface. The quality of the support structure and the boundary edges are a very important parts of the manufacturing process. The original waterjet mechanism used to cut the rings, resulted in glass rings with defects such as surface uniformities, top and bottom diameter differences and lack of concentricity issues as shown on Figure 2.22a. As mentioned above the surface and the edge of the rings define the boundary conditions of the membrane, any defects are transferred to the membrane. Diameter difference, non-symmetric rings, introduces astigmatism during the manufacturing process. That difference in conjunction with lack of concentricity and chips or irregularities on the surface are the main sources of failures of the membranes during actuation and higher order aberrations. Misalignment make the membrane bond area non uniform, creating the failure point during actuation, Figure2.22b shows how the rings errors look and how they stack if lenscore is assemble.

This section investigate how the support rings cause the failures as well as are one of the contributors of aberrations. It also describe the mechanism used to correct the problems.

[3]Pinch points refers to compression points, or surface indentation that create high density fringe areas when measured with the interferometer

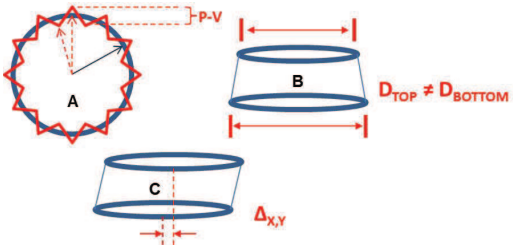

(a) Identified resulting defects from waterjet

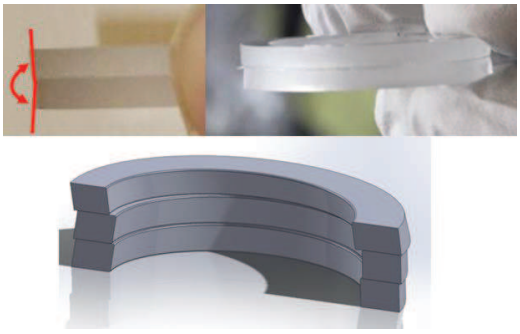

(b) Images of defects and CAD of how defects stack up

Figure 2.22: Defects resulting from waterjet cutting.

2.5.1 Identifying the problem

Various experimented where designed in order to identify breaking points and maximum deformation as well as force required for deforming the membrane, this latter of extreme importance since it will drive the actuation mechanism. One of the experiments clamped or bonded the membrane between the support rings and deformed using a ball bearing at the center with a force gauge attached to the deformation mechanism and that configuration was mounted on top of an x-y-z stage that allows to center the deformation mechanism but as well allows for fine control on the displacement. This setup allows the identification of the failure mechanism as well as force required to deform the membrane. The second setup, consisted of using the same configuration but with a plunger deformation mechanism similar to the one use to deform the membrane in the actuators, based on the results obtained on the first experiment, a physical change was made on the boundary conditions of the rings in order to increase the displacement or deformation of the membrane.

Failure during actuation

An experiment was designed in order to identify what was the failure mechanism while the lenscore is actuated. As mentioned above the support rings are cut by waterjet, follow by a sanding process in which the rough edges created by the cutting are removed or smoothed to form a small bevel about 45° between the flat bonding surface and the inner diameter of the ring. These rings are then clean and bonded using the procedure described in Section 2.3. Some of the hypothesis generated for the potential sources for the failures are the irregularities resulting from the cutting of the glass creating sharp edges that rip the membrane, the mechanism use for bonding weakens the membrane, the bonding of the membrane to the rings constrict the membrane in a way that shears it and the misalignment between boundary conditions due to irregularities in the rings.

An experiment was developed under certain representative condition in which some of the hypothesis could be explored, tested or eliminated. The experiment consisted of a membrane clamp between ring and as a further test, bonded to the support rings. This bond is then assembled in an optical mount in a configuration which contains the deformation mechanism in the shape of the plunger and the x-y-z stage, setup shown in Figure 2.23. The mechanical setup allow for quick change of the bonds without moving anything else on the setup. The contact between membrane and plunger was determined by visual and physically touching the membrane and plunger. That contact position was indicated as the starting position, and the micrometer on the stage was used to move a discrete position every 2 minutes and the position was recorded, this procedure was repeated until the point the membrane would break, following a visual inspection of the root of breakage.

First test consisted on clamping a stretch membrane between two rings and performing the experiment. The membrane was marked in a discrete position including

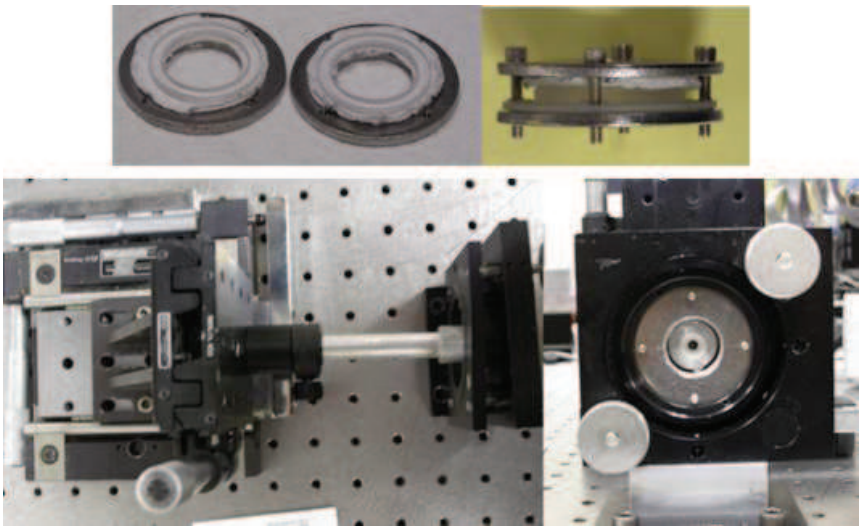

Figure 2.23: (Top) Bond clamped between modify washers. (Bottom) Setup of washer rings mounted on optical mount with tip/tilt and deformation plunger on translation x-y-z stage

the parts in contact with the glass in order to verify if it was sliding instead of stretching, results indicated no slipping or sliding. For case #1, the membrane was deformed about 7.6 mm from its flat position forming an angle of approximately 71.8°, from the picture in Figure 2.24(a) it is clear that it broke at the plunger diameter and not at the boundary where it was clamped with the rings. For case #2 the same rings were used but with the difference that the membrane was treated as it would be bonded, then stretched and clamped [4] between the rings. This membrane was deformed as in case #1 $7.6mm$ and 71.8° before it broke, the breaking of the membrane was exactly as with case #1, Figure 2.24(b). For case #3 the same rings where used but in this time the membrane was bonded to the rings and it only deformed to $2.3mm$ and formed and angle of 42.6°, and as seen in the Figure 2.24(c) the failure occurred at the bonding interface. It was determine that the failure is created once the membrane is constricted, bonded, to the rings, which could be a

[4]note: not bonded, just membrane treated, in order to verify if treatment weakened the membrane

result from non-symmetrical bonding of top and bottom surfaces of the membrane to the rings that when deformed creates that sharp angle which tears the membrane on the side that is more bonded towards the ID. The other option was that the deformation or bending point and the highest stress/strain point of membrane were collocated.

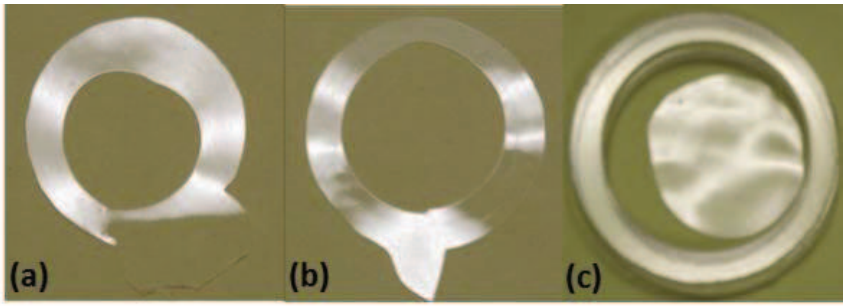

Figure 2.24: Membrane breaking points: (a) Membrane clamped only. (b) Corona treated and clamped only. (c)Corona treated and bonded to glass.

In order to minimize the effects from non-symmetrical rings, measurements of the complete inventory of rings were made in order to identify discrepancies in the ID as well as for paring rings with same IDs. Also new tooling that holds the rings were machined to higher tolerances and a concentricity study performed.

A modification of the experiment was made in which a shim was added to the ID of the rings, this makes the membrane bends on the shim top surface and away from the bonding area. Three extra tests were performed in which a shim were used, as shown in Figure 2.25. The results can be seen in Table 2.5 as well as an extra test performed without a shim for verification.

The shim improved the results, and demonstrated that by moving the largest deflection point away from the constrained bonding point the displacement was significantly improved. Lenscores with shims where made, Figure 2.26, resulting in no membrane failures at higher actuation.

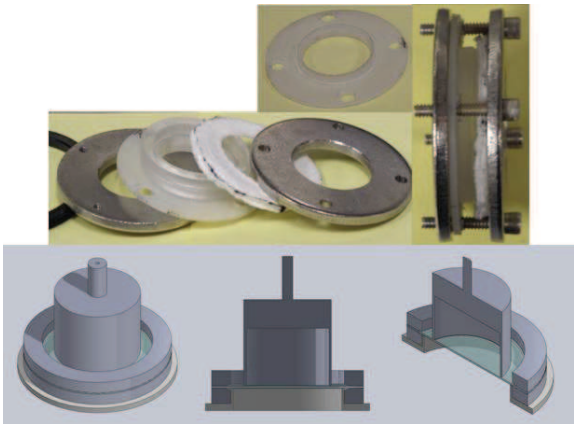

Figure 2.25: (Top) Washer setup with included shim for testing.(Bottom)CAD of setup.

Table 2.5: Results from adding a shim to the lenscore, last line a regular bond for comparison

Test #	Angle(°)	Displacement(mm)
1	64.87°	5.33
2	62.63°	4.83
3	63.20°	4.95
4	45.45°	2.54

This presented a solution but also introduced other problems. The problem

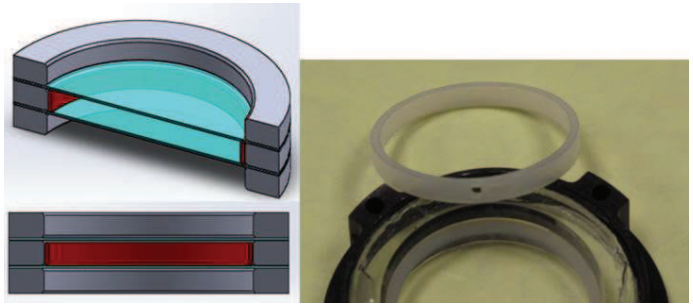

Figure 2.26: (Left)CAD of shim inside lenscore. (Right) Lenscore fabricated with shim inside.

arrived in the complexity of making the shims to meet optical tolerances as wells as alignment of it inside the core, but most impactful was that if the shim contained any non-uniformities on the surface that was in contact with the membrane, these would translate to wavefront aberrations. The shim is made and clean, once the first part of the bond is made the shim is aligned carefully in the center ring, this provides symmetrical deflection of the membranes. Once the shim is inside the lenscore the normal procedure for making a lenscore is continued. A key characteristic of the shim is the material it is made off, it cannot be made of metal because it will interact with a step in the process and it cannot be made of certain rubber or plastic type materials materials because it could contaminate the fluid. The shims were a solution but not a permanent one; most importantly it demonstrated that the idea and concept were correct. The point of maximum deflection and the bonding point needed to be separated. A concept was design in which the rings contain a bevel, the bevel consisted of a radius that tapers off towards the ID of the ring from the bonding point, allowing the membrane to be deformed gradually deflecting on the radius, Figure 2.27. The difficulty arises with machining that type of bevel and the repeatability of making such a bevel from ring to ring on glass. First investigation demonstrated that the cost of manufacturing this bevel on glass externally to SNL would be extremely expensive.

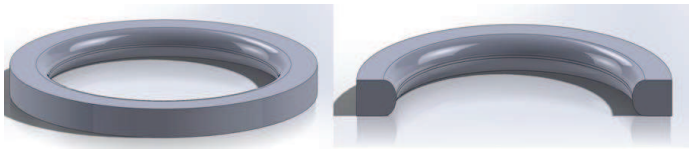

Figure 2.27: Conceptual ring with radial profile in the ID for membrane deflection.

In order to test the concept a straight bevel was machined on the glass rings, as shown in Figure 2.28.

The bevel was made using a desktop lathe and ceramic tooling to grind/polish

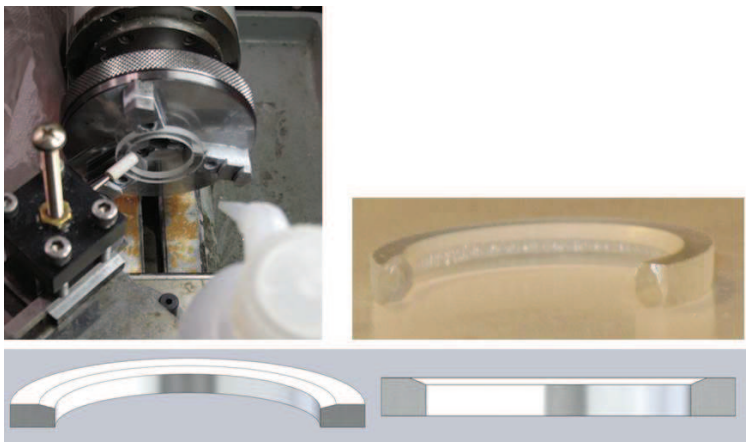

Figure 2.28: (Top) Straight bevel made on bench top lathe with cross section of result on glass ring. (Bottom) CAD of bevel.

the bevel at different angles. Three bevel degrees 18°, 15° and 12° where tested and compared to the original 45° bevel, which was made to eliminate the surface non-uniformities resulting from cutting the glass. The bonding surface area was kept constant in order to minimize differences between tests. The same experimental setup was used and the results are shown on Table 2.6.

Table 2.6: Overall results for a bonds with and without shims and the bevel results at 15°

Bevel Angle(°)	Displacement(mm)
45°	2.54
18°	3.81
15°	6.25
12°	5.46

From the results it can be notice that shallower angles produce better results, an indication that the radial bevel could be the best option. The fact that results from the 12 bevel did not produce higher displacement was understood, it was due to machining errors due to the shallow angle and tooling not design to be used on

cutting that type of bevel. Table 2.7 compares and average of all the results. The 15° bevel was selected and implemented for its simplicity to make in comparison with the other ones. A process step was developed and added, in which 3 tools of various diamond grits were designed and made that allowed symmetrically and consistently making the bevel on the rings as shown in Figure 2.29.

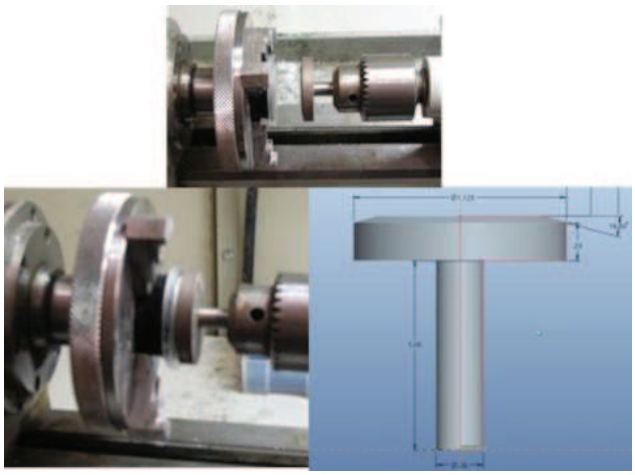

Figure 2.29: Beveling tool setup and CAD.

Another advantage of these procedure was the fact that the bevel was made using the ID of the glass ring as the reference, therefore as long as the bevel where made consistent, it resulted in concentric bevel which minimized variations in the lenscore support rings alignments, since all steps in the lenscore preparation process is referenced to the ID of the rings.

Table 2.7: Overall results for a bonds with and without shims and the bevel results at 15°

Metric	No-shim	Shim	Bevel 15°
Displacement(mm)	2.42	5.03	6.35

The same concept of the 15° was implemented to rings of different materials, such as Al or Ti rings. For these types of material the difference was that the bevel was

machined with the lathe and an extra bevel has to be made on the rings, due to metal residues and sharp edge left by the tooling on the transition between the bonding flat surface and bevel. In order to eliminate this, a curve bevel was introduce by using polishing compound and an optical glass lens which provided the curvature, after the ring was made it was polished against an optical lens, shown and describe in next section.

Rings and wavefront error

Another key characteristic of the support structure is that it can determine the resulting wavefront of the bond and therefore the lenscore by imparting its wavefront error to the membrane. For example if the support rings exhibit astigmatism, as shown in Figure 2.30, the resulting bond will contain astigmatism and the magnitude will also depends on the second support ring since the astigmatism would either cancel out or magnify depending on how the astigmatism in each of the rings is oriented. A second effects, are the pinch points in the membrane resulting from the residues on the transition between bonding surface and bevel as well as due to contaminants on the membrane or the rings reason by cleanliness is of extreme importance.

In order to minimize, thickness variation, concentricity and higher order effects due to the glass rings, optical flat glass substrate where used and the conventional waterjet was replaced with a microwaterjet and ultrasonic cutting. Microwaterjet was selected as the cutting mechanism since it was less expensive than the ultrasonic mill. The new optical flat glass substrate thickness tolerance was 2.70 mm ± 0.05. The microwaterjet have a linear positional accuracy in X and Y of $\pm 0.076mm$ and a repeatability $\pm 0.051mm$, with a water beam width of 0.42 which is the minimum cutting size, which help to reduce the issues mentioned above [5]. Even though mi-

[5]Conventional water jet techniques tolerances $\pm 0.254 - 0.762mm$

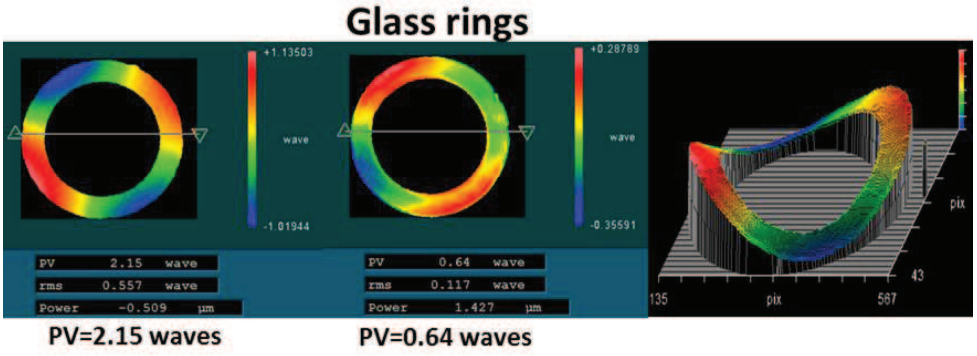

Figure 2.30: Zygo interferometric measurements showing astigmatism as the dominant aberration.

crowaterjet was an order magnitude improvement, there were still rings showing perfectly astigmatic shape, this is a result of the stresses imparted during the cutting. Rings that were cut in different sections of the plates will produce different magnitudes of astigmatism. For example the Figure 2.30 shows rings cut from the same glass plates, one ring have a PV of 2.15 waves while the middle one of just 0.64 waves, all this starting from a glass plate with no astigmatism. Further review showed that depending on how the plate is hold while cutting it, as well as if the cut is made at the center or at the edges, the stress of the cut will impart an astigmatic shape to the rings. No matter how the glass support is made, once the rings are cut, they will have astigmatism with different magnitudes.

Cost, yield and brittleness of glass prompted the search for new support rings. Less brittle material that could allow the reduction of overall size of the lenscore and different configurations. Also other materials like aluminum, stainless steel or titanium allow for in house fabrication. Even though other materials can reduce size, cost and reduce brittleness it introduce a bigger and more risky challenge, which is the bonding part. PDMS bonds to glass by forming a covalent bond due to the silicon and oxygen present in both, the lack of this components in other materials

present a big challenge.

In order to reduce cost, aluminum 6061 was selected as the support structure. This material is inexpensive and was machined in house, making it accessible and convenient.As mentioned above cutting annular rings of practically any material will result in astigmatism. This is a result of how the material is hold to cut and also materials stresses that are released once the part is cut. In order to use Al rings a process was developed that minimized the astigmatism that resulted from machining. This process made the rings thicker than the specifications in order to leave material for polishing. The materials used for polishing consisted on a granite slab, lambda by 10 or better 2 inch optics, 6 to 8 inches optically flat glass plates, 600 grit sand paper and fiber polishing papers. The process started by cleaning with solvents the rings and 2" flat window, follow by adhering the side of the ring opposite to the bonding surface to the 2" flat using a small amount of clear silicon grease and making sure the grease was evenly distributed, allowing for the application of some pressure on the part during polishing while maintaining the ring from sliding from the glass. No particles or air bubbles could be left between the glass and the rings, all excess grease needed to be balance out by pressing the two parts on a flat surface, any excess of grease or particles would be transfer to the surface been polished in the form of a bump on the surface, which would be extremely hard to remove once it was imparted on the ring, most of the time making the ring not useful. Using cutting oil and 3 square inches of 600 grit the part was sanded using a figure 8 motion, also rotating the paper to new areas when degradation was observe on it, followed by $5\mu m$ silicon carbide lapping sheet until a measurements could be obtained on the Zygo. Depending on the PV of the measurements, an assessment is made to go back and repeat the above process or continue working down on thinner lapping sheets, until about 1.5 to 2 waves where obtained. Once that was the case the parts where cleaned and rotated, and the process was started over on the bonding surface. When 1.5 to 2.0 waves where achieved, only 3 microns or less lapping paper was used and

the applied pressure on the part was reduced to the point on which the weight of the glass and part itself was used only, this allows to take the part from 1.5-2.0 waves to about 0.5 waves or less in most cases. Figure 2.31 shows the results obtained; notice that there are sections in which the bond area is minimal as indicated with the circle and there is a presence roll off. The roll off was introduced by the force applied on the part in combination with the grease and the lapping paper been dissipated and degraded.

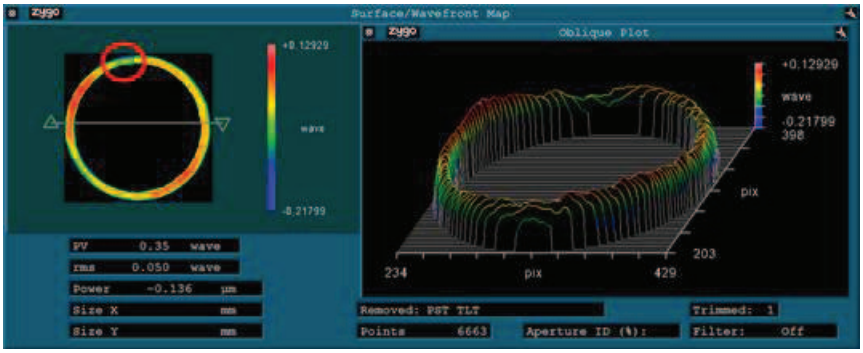

Figure 2.31: Best polished rings result obtained. Notice the small bonding area indicated with the circle. To get to this results it require constant monitoring of the wavefront, time wise took about 4 to 5 hours.

The process was repeatable but time consuming, as well if it was not follow step by step, the desire wavefront was achieved but a roll-off could be imparted on the bonding surface, reducing the surface area for bonding, Figure 2.32.

As the outer support structure, thinner rings are used to minimize the overall volume of the lenscore, these thin rings are extremely hard to polished and the best wavefront that could be obtain is between 0.9 to 1.2 waves, and this not very consistent. Figure 2.33 shows a thin ring and thick ring polished by using the above procedure. Once the rings are polished to the desire wavefront and making sure that astigmatism is minimized, the transition from flat to the bevel is polished as well in order to minimize sharp edges or areas which can create pinch points. This process

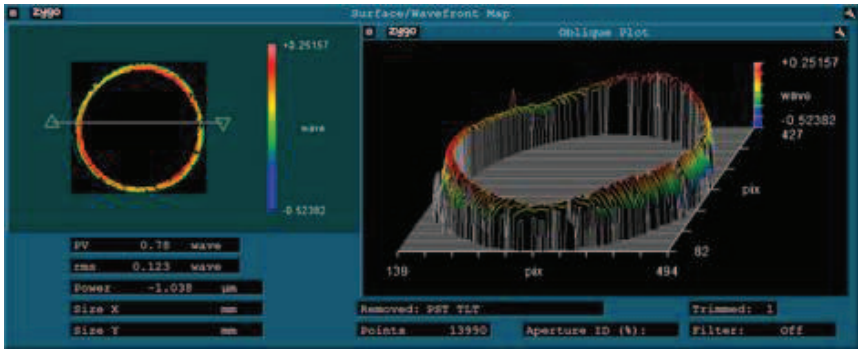

Figure 2.32: Wavefront error showing the roll off resulting from polishing.

is performed by applying 600 grit polishing compound to and optical glass lens of about 200 mm in curvature. The ring is place on the lens, which the part in contact is the bevel transition, and a rotation motion is performed with no force apply to it except for the weight of the ring, if force is apply, the ring is deformed and the process of polishing the flat surface has to be started. Figure 2.34 shows CADs and picture of the procedure.

Figure 2.33: Finished polished thin(Left) and thick(Right) Al rings showing the second bevel as lighter color indicated by arrow

This technique worked, it reduced or minimized the astigmatism as well as help improve the overall wavefront of the lenscore, but it is time consuming and is prone to the generation of error and parts waste, also there is not an easy way to polish the bevel part. Another issue is for example parallelism between top and bottom

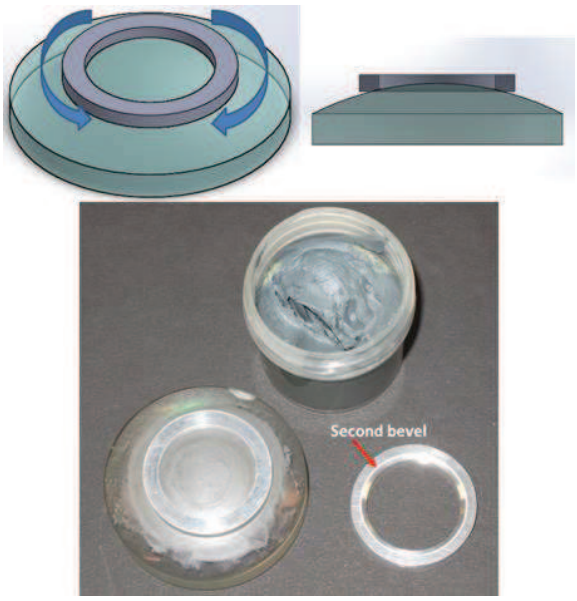

Figure 2.34: (Top) CAD of second bevel procedure. (Bottom) Picture of how double bevel is made and 600 grit polishing compound

surfaces of the rings which is extremely hard to minimize by conventional machining procedures used in the lab. Parallelism is important for alignment purposes, for examples of glass windows or lenses that are adhere to the APLs, lenscores inside the actuators as well as minimizing alignment between optical axis of system and APL. In order to solve these problems other techniques were implemented such as using a semiconductor substrate lapping machine as well as diamond turning the parts, this latter extremely costly. The lapping machine introduced other error and never got to the PV that was obtained by hand polishing. The first diamond turning(DT) attempt resulted in rings with about 8-10 waves of astigmatism which where imparted by how the parts were hold on the machine.

A second company for DT was identify and drawings of the parts were made in which high tolerances on parallelism between top and bottom flat surface where established as well as a PV of under a wave. The drawback of DT is that is an expensive process, is hard to reuse surfaces due to scratches resulting from cleaning

and this surface are mirror finish which in some cases or system can present problems with straight light reflection. This latter, can be solve by anodizing or power coating the rings surfaces that will not be DT prior to it, but it will increase cost as well, Figure 2.35a. Figure 2.35b show a thin and a thick DT ring as well as its wavefront error measured with the Zygo interferometer.

(a) Anodize rings. With the bonding process developed at SNL PDMS can be bonded to anodized surfaces.

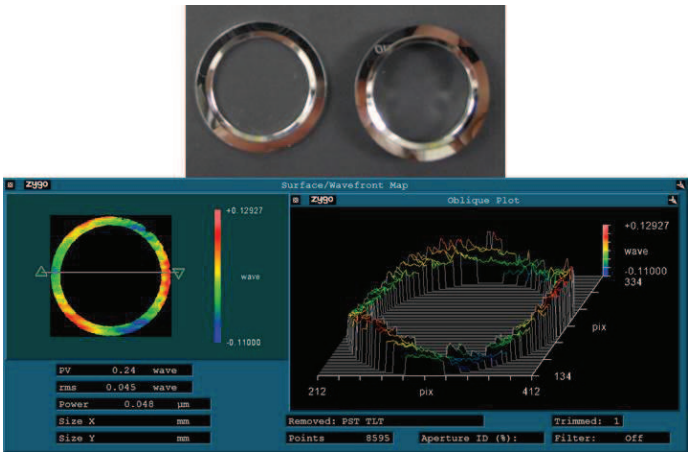

(b) Diamond turned rings

Figure 2.35: Different options for the support structure

Other options such as titanium, sapphire, silicon carbide and hard polymer were explored due to their hardness. Due to cost and on simplicity aluminum is mostly used, since rings made out of it can be made to the desire specs in our lab or any conventional lab.

2.6 Membrane Pre-tension

One of the most critical variable on the adaptive polymer lens process is the pre-tension imparted on the membrane. A membrane with a uniform thickness is stretch radially then bonded to the rings. Pre-tension is dependent on curing process, membrane thickness and variations on it, surface and uniformity on which the membrane is been stretch, how the membrane is handle and hold prior to stretching it, as well as prior and after knowledge of thickness. All this makes the pre-tension control the most complicated variable and also contributes greatly to the wavefront error of the APLs.

This section will focus on an experiment performed which help determine one of the sources of variation between APL made. It will also discuss briefly a mechanism implemented in order to control the pre-tension variable. Two important effects of membrane pre-tension are resultant coma as well as require force to actuate the APL. Coma is mostly dominant by the gravity effect on the fluid, so a more taut membrane would exhibit less coma than a loose membrane. High pre-tension membranes will also increase the required actuation force, therefore reducing the speed of actuation.

2.6.1 Pre-tension experiment:

The main goal of the experiment was to understand variations on tooling used to make the lenscores as well as identifying source of these variations. For a single membrane lens, it is not critical if there is a small variation on the membrane pre-tension because in theory the system can be designed or optimized around that, but when it comes to 2 or more membranes it is of extreme importance. Two manufacturing tooling are used in the laboratory to make lenscores, which will be refer as Fix#1 and Fix#2. These two fixtures were made from the same drawings but at 2 different machine shops. A set of 10 different lenscores RROCs were measured, as

seen on table the RROC were extremely different, when the lenscores where designed to have the same RROCs. Typically the fixtures are use in parallel meaning; a bond is made on Fix#1 and completed on Fix #2 or vice versa, but in other cases there was no tracking of the fixture used. One of the first thing performed was labeling each part of each fixture and maintaining each components with it respective fixture. Mechanical dimensions where made of each fixture which resulted on small variations in the order of 0.5mm or less on some of the parts.

Before the implementation of a confocal sensor for membrane thickness measurements, there was no means of verifying difference or variations in pre-tensions between the B1s or lenscore, except by measuring its Resting Radius of Curvature RROC once a full lenscore was made. So an inventory of existing double membrane lenscore was made and the results indicated a big discrepancy between RROC1 and RROC2, between 15 to 40 mm difference. This prompted the development of an experiment in which a B1 could be made and its performance studied. The experiment consisted of making membranes following an identical procedure to make B1 under the same conditions on each Fixture. The metric of this experiment was measuring force vs. displacement; if the bonds were repeatable the curves should be repeatable. The experiment consisted on a B1 mounted on the setup shown in Figure 2.36. This bond is then assembled in an optical mount in a configuration which contains the deformation mechanism in this case a plunger similar to the one used in the actuation mechanism. A digital force gauge was attached to the plunger and the setup mounted on a x-y-z stage, all this assembled in front of the Zygo interferometer, setup shown in Figure 2.36. Having the setup in front of the Zygo allows for optical alignment repeatability, by having the membrane and the plunger flat and parallel to each other, also it helps determining the precise displacement location of contact between the plunger and the membrane. That first contact was indicated as the starting position, the force readout from the gauge was recorded as well as the position read out from a micrometer on the translation stage.

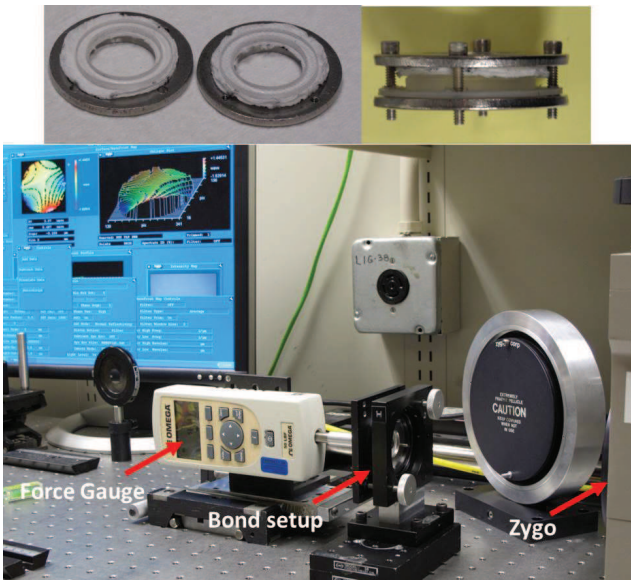

Figure 2.36: (Top) Bond holding fixture. (Bottom)Setup containing force gauge, plunger and bond holding fixture assembled in front of Zygo

The translation stage was move a discrete amount and the force was recorded. A maximum displacement was selected based on previous experiments, using the micrometer on the translation stage the plunger was move a discrete amount and force and displacement was recorded until the desire displacement was reached.

Plots of Force vs Displacement are shown in Figure 2.37. It was clearly seen from the data that there was a discrepancy between Fix#1 and Fix#2 as well as a major discrepancy between Fix#2 performance, meaning that just the difference in performance of both fixture can be a source of variations. This prompted other experiments to identify difference between the fixtures as well as on each fixtures as well.

An average force of 20.0 N was recorded which equated to a displacement of the membrane from flat of about 6.5 mm and this still did not broke the membrane. This displacement is more than what a typical lenscore will be displaced.

The above results demonstrated why Fix #1 would produce lenscore with RROCs closer to each other than Fix #2 would. A designed lens in Zemax would be out of prescription when manufactured with either one of the two fixtures or a combination of the two. In order to solve the problems, Fix #1 was kept as the control one and work was performed on Fix #2 while a new Fix was designed. Various modifications were made to Fix #2 from mechanical to process modifications directly on the fixture. The modifications provided the repeatability and the wavefront quality that was expected.

This experiment also prompted the idea of knowing the pre-tension of the membrane in situ, task which is extremely complicated. In order to by-pass pre-tension measurement, it was assumed that PDMS is incompressible. Assuming in-compressibility and a Poisson ratio of 0.5 for PDMS, the constant volume and geometry conditions can be apply, so knowing the initial and final thickness of the membrane, the pre-tension can be calculate using the following equation:

$$T_f = \frac{T_i}{(1+\epsilon)^2} \tag{2.1}$$

where T_f is the final thickness, T_i is the initial thickness and ϵ is the pre-tension or pre-strain applied to the membrane. So knowing the before and after thickness can provide a feedback in the repeatability off stretching a membrane and provide means to fully control that variable.

The problem arises on the assumption of the PDMS Poisson ratio of 0.5, most literature search seems to indicate 0.5 but some measurements values indicate between 0.46-0.48, meaning that PDMS is not perfectly incompressible as expected. If this is the case then equation 2.1 takes the following form,

$$T_f = \frac{T_i}{(1+\epsilon)^{\frac{2\nu}{1-\nu}}} \tag{2.2}$$

where ν is the Poisson's ratio, which if ν is 0.5 it reduces to equation 2.1. So technically if Poisson ratio is know or it is constant between batches of PDMS either of the above equation can be used to extract pre-tension.

The caveat on the above argument is the need to know accurately the Poisson ratio of PDMS, not a trivial thing to do, which would explain the lack of experimental data on this value in literature. Now in order to bypass this problem, it was decided that the key parameter was repeatability between membrane fabrication and making the first bond, meaning if the initial thickness is know as well as the final thickness, and the fabrication fixture allow for full control on the membrane stretching mechanism while thickness is monitor, the ratio between the membrane thickness can be used and the processes repeated. A calibration table can be use in order to make each of the membrane stretch as repeatable as possible.

Chapter 3 used the above argument in order to establish a relationship, between thickness ratio, pressure, volume of the lenscore cap and the radius of curvature.

2.7 Shape factor

From a systems level perspective glass singlets are not normally equiconcave or convex, in order to minimize aberrations and reduce size, these lenses are manufacture with a particular shape factor, meaning a difference in the ROC between front and back surfaces of the lens. Aberration in singlet's can not be eliminated but can be minimized by changing the lens shape factor, which result in a best form lens for an optical system, Figure 2.38. As in conventional systems by knowing the target

aberrations at the system level adaptive polymer lenses can be manufactured with a particular shape factor lowering the burden on the optical design. Besides manufacturing, a major challenge is to maintain the shape factor over the dynamic range of the lens. This is the first time that shape factor has been applied successfully to adaptive polymer lens for an optical system. Besides aberrations and system performance, understanding the behavior of an APL shape factor is of extreme importance for the doublet development. This section will not show how the shape factor is obtained it will only present the results obtained as well as the behavior of APL over the actuation dynamic range.

A shape factor study was performed during the dissertation work. This study consisted designing, building an APL with a particular shape factor and then actuated in order to verify how the shape factor changed under actuation. Table 2.8 show the results obtained for the same APL under both types of actuation. For the purpose of this dissertation the shape factor metric was selected as the ratio of the ROCs, between front and back ROCs during actuation.

Table 2.8: Shape factor results for 2 different configuration APLs

APL 1			**APL 2**		
ROC1(mm)	**ROC2(mm)**	**SF**	**ROC1(mm)**	**ROC2(mm)**	**SF**
27.79	54.13	0.51	35.10	23.72	0.68
38.61	83.03	0.46	41.10	26.80	0.65
141.55	344.93	0.41	82.17	49.53	0.60
	Average	0.46		**Average**	0.64
	Stdv	0.052		**Stdv**	0.037

This chapter demonstrated identification and control of the variables necessary to understand the APL singlets as well as developed critical studies and experiments necessary to fabricate an APL doublet(APLD). The next chapter will demonstrate the modeling, fabrication and work performed on APLD. It demonstrates the transition process from optical design to fabrication.

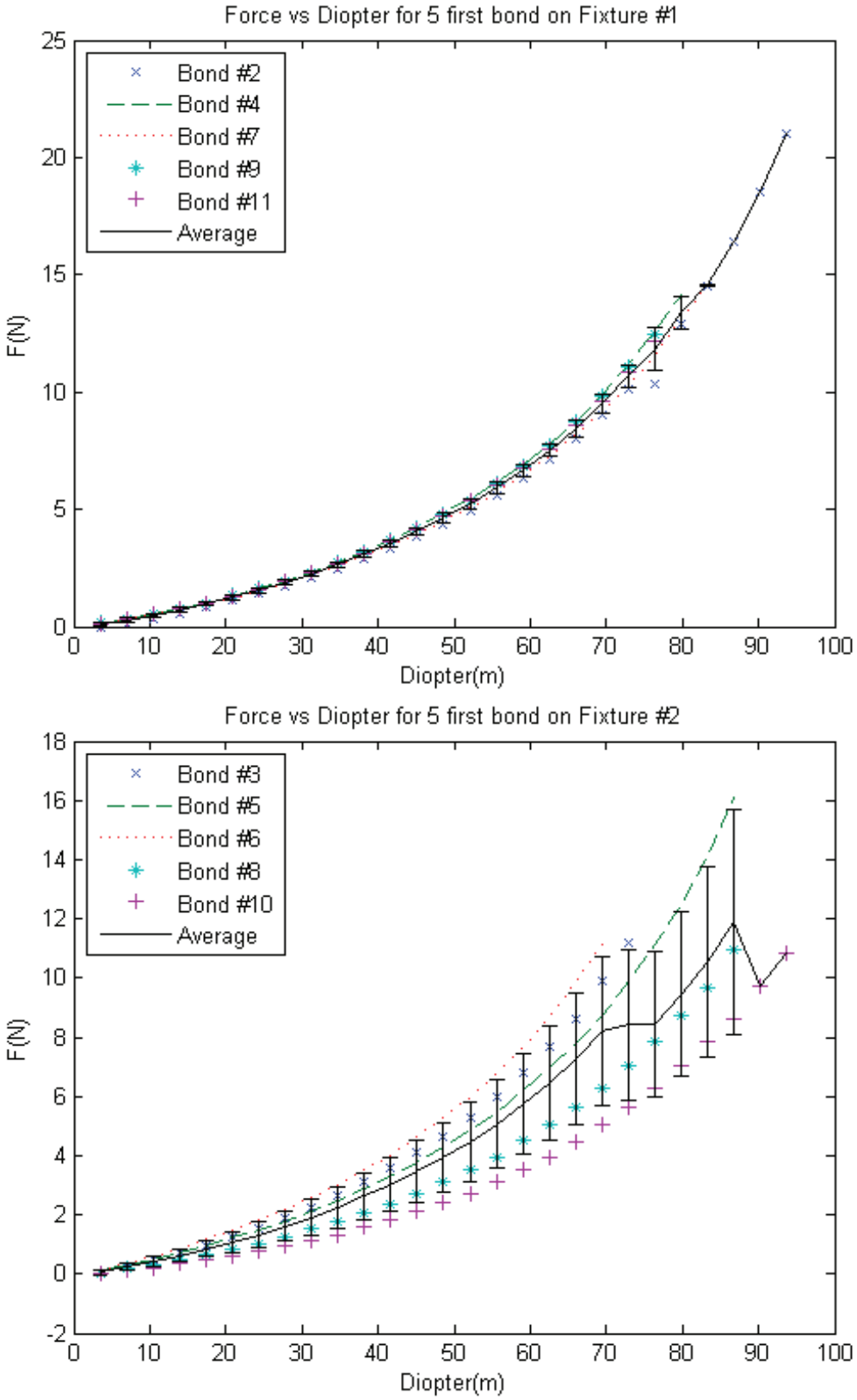

Figure 2.37: Force vs Displacement curves Fixture #1 top and Fixture bottom #2

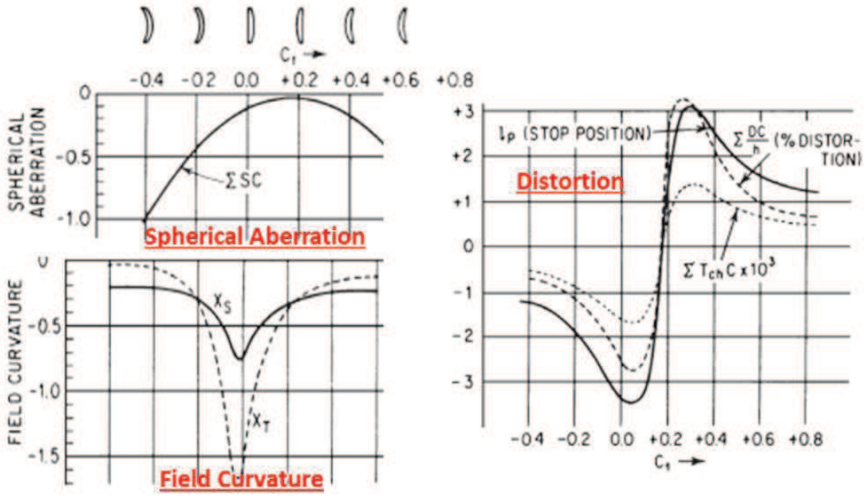

Figure 2.38: Shape factor of a lens and its impact on aberrations

Chapter 3

Adaptive Polymer Lens Doublet Development

3.1 Introduction

Chapter 2 consisted of understating and controlling the variables required to make APL singlets that can be used in imaging systems as replacements for glass elements. It also provided and implemented solutions to improve optical quality as well as fabrication feasibility of these lenses plus explore tools that are useful for fabricating the APL doublets, APLDs. Without the study performed in Chapter 2 it is almost impossible to start fabrication of a doublet or multiple chamber APLs because the level of complexity and the number of variables increase for every extra membrane and fluid that are added.

This chapter presents the experiments conducted to validate a low order FEM on the behavior properties of the APLs based on the parameters described in Chapter 2. It will also describe the optical and physical properties that are required to make the two main types of achromats, doublet variations, the fabrication challenges,

performance verifications as well as the results for an adaptive achromatic polymer lens.

3.1.1 Background:Achromatization

In imaging systems, chromatic aberration is very impactful. The images would look blurry and distorted, as shown and described in Chapter 1, Subsection 1.2.1. For example, Figure 3.1 shows a polychromatic light ray incident on a singlet and because the refractive index varies with wavelength the focal length of the lens varies as function of color. If a screen is place on either one of the three colors the other two would look blurry therefore reducing the resolution at those other wavelengths.

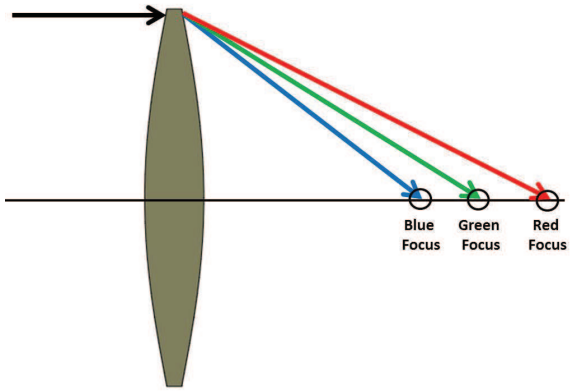

Figure 3.1: Dispersion of a singlet lens

In order to limit this effect an achromat can be used. A typical achromat glass lens consists of two types of glass with different indices of refraction and dispersion which correct chromatic aberrations by bringing two wavelengths to focus at the same plane (normally blue and red). There are two main constraints in the optical design of an achromat which are the following:

- Constraint #1: The power of the doublet is equal to the power of the singlet

$$\phi = \phi_1 + \phi_2 \tag{3.1}$$

- Constraint #2: The sum of the power of each element equals zero.

$$\frac{\phi_1}{\upsilon_1} + \frac{\phi_2}{\upsilon_2} = 0 \tag{3.2}$$

where ϕ is the optical power and υ is the dispersion coefficient, Abbe number[10].

Some of the main challenges of achromatization of APLs are from the materials perspective, maintaining achromatization over the multiple focal lengths and fabrication. From the materials perspective, there is limit on the amount of fluid that can be used for an achromat. Limitations such as Abbe number, index of refraction and permeability of fluid through the membrane, discussed in Chapter 2 are also factors.

As a first approach, from the fabrication perspective, the progression of an APL achromat from a conventional classical form will be the same. A design, model, and test APLD will be built for a particular fixed focal length, followed by a study on different actuation mechanisms. Now the fabrication and control of the design ROCs is extremely challenging due to the control, interaction and understanding of each membrane during the fabrication process. Multiple chamber lenses have been proposed in literature or have been attempted before, some using air chambers, other relying on the immiscible property of two fluids and others in a similar configuration as this research but with key physical differences[28]. Some of these key differences are the number of flexible membranes, most of previous work relies on two or just one membrane, most of these lenses with a diameter of about 2-5mm. Another key difference is that most of these lenses, each fluidic chamber volume is controlled independently, therefore the ROCs. The work on this dissertation uses a constant volume condition and the lens aperture is in the order of 19.3 mm, this presents a completely different challenge due to the physics, aberrations, gravity effects and

control/understanding of the intermediate flexible membrane. This dissertation research, relies on the interaction of 3 flexible membranes enclosing two different fluids.

3.1.2 APL Achromat

The APL achromat design consisted of selecting an effective focal length of 200 mm. One of the elements will have a positive power and high Abbe number and the second element with negative power and low Abbe number. The power required for the elements composing the achromatic doublet are given by:

$$\phi_a = \frac{V_a}{V_a - V_b}\phi \tag{3.3}$$

$$\phi_b = \frac{V_b}{V_b - V_a}\phi \tag{3.4}$$

where $V_{a,b}$ are the Abbe numbers of each fluid and ϕ the optical power of the doublet. From equation 3.4 the curvatures of the surfaces can be extracted and the APL manufactured. Now for this first design the first element was selected as positive equiconvex, resulting in lenses with the following resting ROC (RROC):

- $RROC_1 = 94.15$
- $RROC_2 = -94.15$
- $RROC_3 = -324.02$

The lens was designed in Zemax and the performance verified using the F,d and C lines of the visible spectrum, Figure 3.2. The F,d, and C lines are the Fraunhofer spectral lines of wavelengths 486.13nm, 587.56nm and 656.27nm respectively. The achromatic lens presented diffraction limited performance on axis in the visible spectrum.

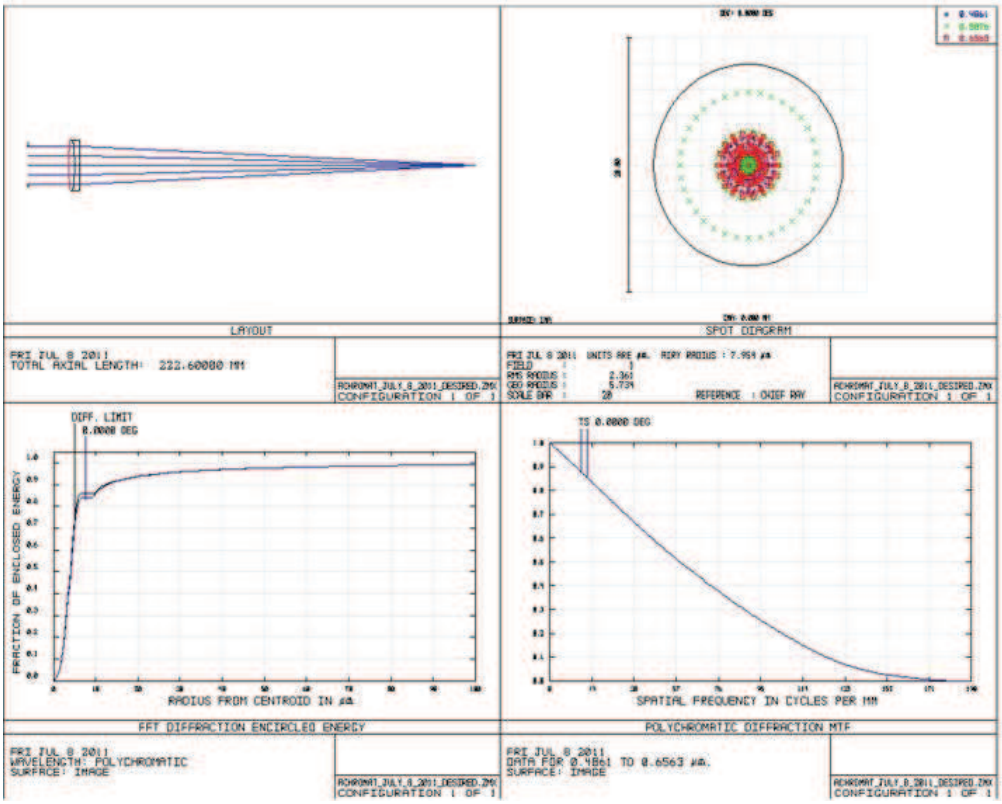

Figure 3.2: Zemax report Achromat

As mentioned about this first design relies on a equiconvex lens, this is challenging in the sense that a equiconvex APL can be fabricated but as a system when the third membrane is added there is balance of forces (internal pressures) which will modify the desire optical prescription. In order to fabricate this, there has to be an understanding on how that interactions takes place and how apriori the lens can be fabricated so the resulting APLD with the three membranes are as close to the design lens as possible.

A relationship is needed between design ROCs, variables in the manufacturing process, and polymer lenses which would enable ease in fabrication and provide an insight into achromatization in multiple wavelengths.

A study is presented that helped understand the relationship mentioned between ROC, volume, and pressure in Section 3.2. This section explores different types of models but the goal is to make the model as simple as possible due to the complexity in the fabrication. A model that will provide first order parameters to fabricate the APLD.

3.2 Membrane thickness ratio, Pressure and Volume

From Chapter 2, a uniform thickness membrane that minimized aberrations under tension was developed as well as means of producing a single membrane bonded between support rings with a low wavefront error. In order to use polymers in imaging or other applications in which wavefront error is of extreme importance, the wavefront errors need to be minimized. Typically a single membrane bonded to rings needs to be between 0.5 waves to 0.8 waves, which was a direct result from the work performed and described in Chapter 2. All the concepts used to develop a singlet are implemented in the study performed in this chapter for developing a doublet.

The next sections identifies the relationship between prescription variables an fabrication variables, Figure 3.3. These variables refer to design variables obtained from the optical design, ROC_1,ROC_2 and ROC_3 and fabrication or measurable variables such as volume, thickness and differential in pressures. This process, shown in Figure 3.4, will enable the design of a doublet and using the model developed, fabricate it, this by creating a relationship between design and fabrication variables. A FEM model was developed and verified experimentally which relates these variables and expand the model to multiple membranes and multiple focal lengths. An experimental testbed was built in order to verify the performance of the doublet

fabricated.

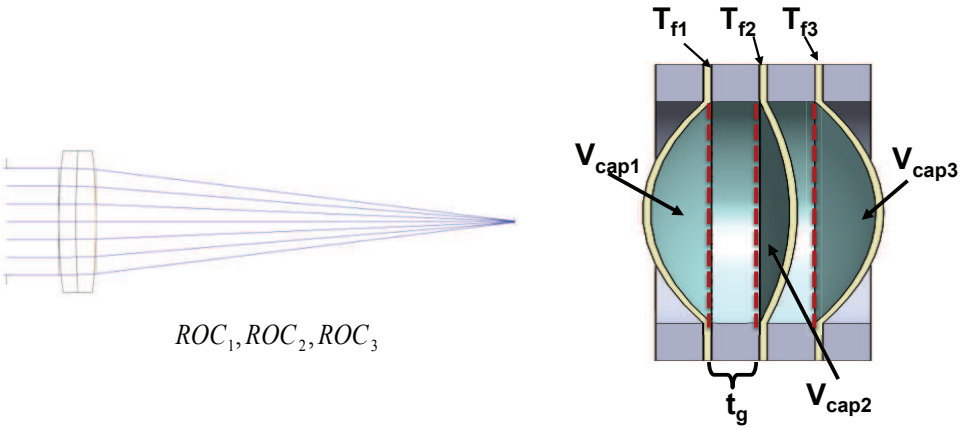

Figure 3.3: Relationship between design and fabrication variables

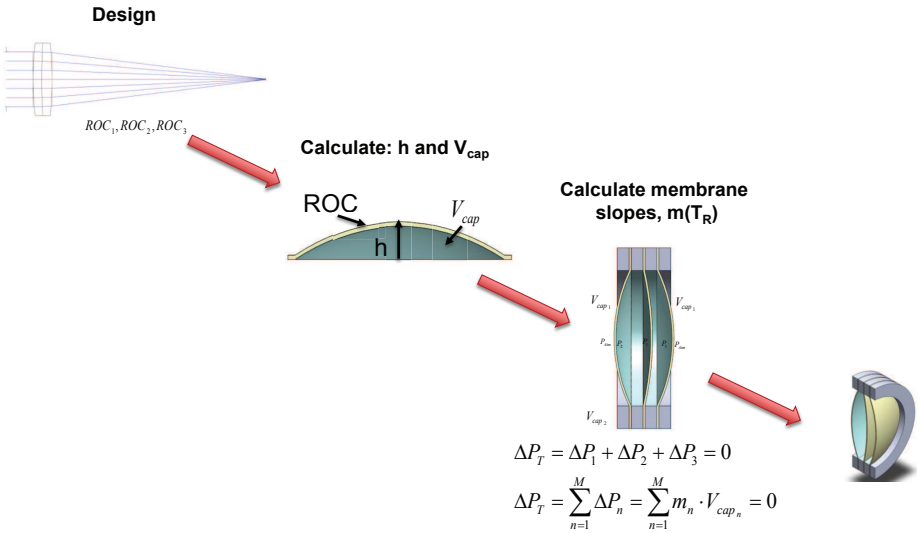

Figure 3.4: Design to fabrication process

3.2.1 Radius of curvature and Cap Volume relationship

The optical prescription generated from Zemax provides the ROCs for the APL doublet. From the given RROCs in Section 3.1.2, the sag of the lens can be calculate

using the following equation:

$$h = ROC - \sqrt{ROC^2 - r_g^2} \tag{3.5}$$

where r_g is the radius of the support ring. Assuming that the membrane is deformed spherically under actuation, the volume of the cap formed during deformation can be calculated by the following equation,

$$V_{cap} = \frac{\pi h}{6}\left(3 \cdot r_g^2 + h^2\right) \tag{3.6}$$

where h is from equation 3.5 and r_g is the radius of the ring. This is the equation for the volume of a spherical cap as indicated in the drawing shown in Figure 3.5. The above relationship demonstrated how ROCs from the optical prescription and the physical fabrication variable and volume, are related. For example, picking the equiconvex part of the achromat, $ROC_1 = ROC_2 = 94.15mm$ the volume of the spherical cap can be calculated using equation 3.6.

$$h = 94.15 - \sqrt{94.15^2 - 13.30^2} = 0.94mm \tag{3.7}$$

$$V_{cap} = \frac{\pi 0.94}{6}\left(3 \cdot 13.30^2 + 0.94^2\right) = 261.62mm^3 \tag{3.8}$$

The volume of the cylinder formed by the support ring is given, in this case for a ring of thickness (or cylinder height) $2.7mm$, by

$$V_{cyl} = \pi \cdot r_g^2 \cdot h_{cyl} \tag{3.9}$$

where h_{cyl} is the height of the cylinder, which for this example is $V_{cyl} = 1500.43mm^3$. Now it is important to notice that equation 3.9 describes a cylinder, from Chapter

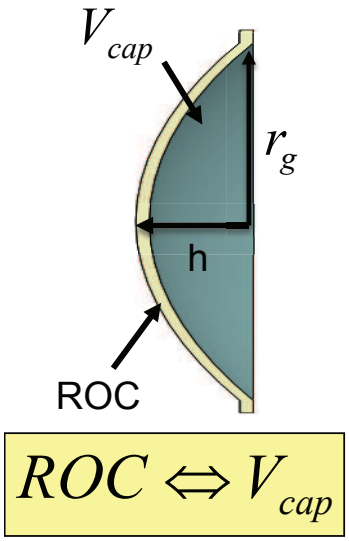

Figure 3.5: Diagram showing the relationship between volume of the cap, sag and ROC of a membrane.

2 subsection 2.5.1 it can be see that these rings are modified with a bevel in order to increase deflection. This implies that the cylinder contains extra volume due to the bevel. There are two procedures that can be used, one is the bevel is not taken into account or secondly it is. For the first case this presents an advantage since that would imply less volume which accounts for extra actuation in the opposite direction of the design ROCs. For the case the bevel is taken into account the ROCs are closer to the design ones. The modified equation takes into account the bevel is in the following form,

$$V_{cyl} = \pi \cdot r_g^2 \cdot h_{cyl} + 2 * (\frac{1}{2} * b * h_{bevel} * \pi * d) \tag{3.10}$$

where b is the base of the triangle formed by bevel, h_{bevel} is the height of it and the d is the diameter of the ring. Notice the factor of two on the right side of the equation, for a doublet or singlet based on two membranes that takes into account the bevel on both sides of the rings, for plano convex/concave singlets this will be one as

well as for doublets with glass substrate. The bevel can account for about $20.0mm^3$ for a single and for a double bevel about $40.0mm^3$. For example, an ROC of $150mm$ a ring of thickness $2.8mm$ and diameter of $23.77mm$, the volume of the cap is about $164.3mm^3$ which if the single bevel is taken into account that results in an ROC of $170.7mm$ and for the double bevel of $198.0mm$, or a range of $150mm \pm 40.0mm$.

From example above, for this positive equiconvex lens, the volume of the spherical cap is added to the volume of the cylinder and this is the volume of fluid that will be added during the fabrication of the lens core as seen in equation 3.11. Note that there is a multiplicative factor of two since the lenscore is equiconvex and it has two symmetrical caps.

$$V_{fluid} = V_{cyl} + 2 \cdot V_{cap} \tag{3.11}$$

Figure 3.6 shows the different configurations possible, for example, a single membrane lens core, only a single cap is added or subtracted depending on if the desired ROC is positive or negative. For a double membrane, added or subtracted twice to the volume of the cylinder, and for the doublet a similar procedure is used but knowing that a V_{cap} is shared between the two elements. For a positive equiconvex lens, the volume of the spherical cap is added twice. For a negative biconcave lens, the volume is subtracted twice from the volume of the cylinder.

The methodology described above allows for a way to understand the relationship of the ROCs and volume. There are also other steps performed when fabricating a lens, for example variations in thickness of the rings, bevels, etc.

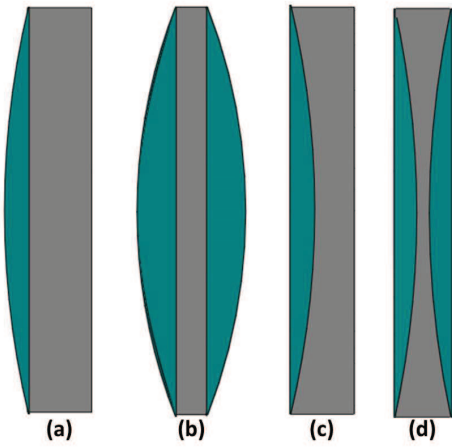

Figure 3.6: Cap configurations

3.3 Pressure, Volume of Cap and Thickness Relationship

The previous section identified the relationship between the ROCs obtained from the prescription to the volume of the cap and the volume of the fluid. This section identifies the relationship between the volume of the cap, the thickness of the membrane and the pressure, Figure 3.7, which are key variables in an actuated singlet or doublet APL.

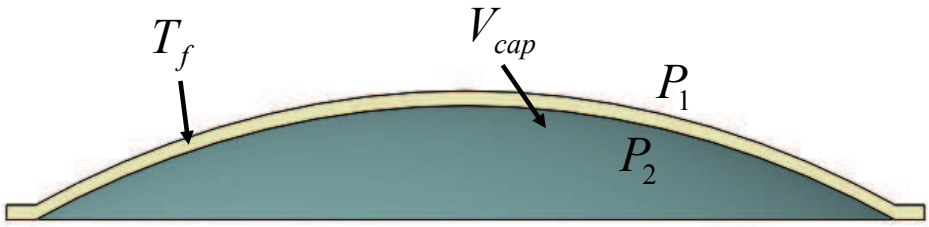

Figure 3.7: Differential in pressure, volume of cap and final thickness relationship.

There are multiple ways to actuate an APL, but two of the most common and

currently used techniques are by pumping fluid in and out of the chamber or by compressing the membranes which deforms the membrane, increasing or decreasing the pressure inside the chamber. There are practical reasons for these two techniques which are to minimize size, weight, and the minimization of moving parts which can present further problems depending on intended application. Pumping fluids in and out requires a bigger footprint and parts that can lead to leaks and further complications. So for tactical applications which is in the interest of SNL, this is not practical. SNL opted for the later option of applying compression to flexible membranes. One of the most important parts in developing a singlet and doublet polymer lens is to understand the physical, mechanical, and optical characteristic performances and have full knowledge and control of the variables involved. This is one of the main reasons that a lot of effort was placed on improving the singlets or two membrane APL. Also a lot of work was on knowing and correcting each of the problems introduced by materials and the manufacturing process.

In order to understand the performance of polymer lenses, an experiment was devised in which key metrics that are related to optical performance can be measured and used as inputs for the FEM for verification and further development of more complex lenses such as doublets. A relationship between measured quantities, fabrication variables, and optical performance metrics needed to be developed in order to create a FEM which will allow to make doublets or understand their performance and ease fabrication. Some of these quantities and variables are pressures, change in volume, radius of curvature, and thicknesses of the membranes. Based on the designed experiment, a FEA model was developed in order to verify and compare with experimental results.

This section will explore different models, but as mentioned before with the goal of developing a simple model as possible that will provide first order parameters and ease fabrication.

3.3.1 Pressure vs Volume and thickness modeling: Finite Element Model and Analysis

For this work two different FEMs were developed. The first FEM, using ANSYS, consisted on using the approximately initial thickness of the membrane, a percent on which the membrane was stretched and the mechanical properties of PDMS to determine a relationship between pressure, volume and percent of stretch. This high fidelity FEM produced important results which help in the improvements of APL singlets, but the feedback loop between model and experiment was long due to the complexity of measuring the percent of stretch of the membrane as well as the lack of control in fabrication variables. The latter reason, prompted experiments and research on measuring techniques which would allow a more direct link between model and measured or fabrication variables.

The second FEM, using Solidwork Simulation, narrowed the gap between measured and model variables. This FEM was developed based on the measured quantities. The model consists of creating a membrane based on measured thickness when it is made and measured, know as initial thickness(T_i) and after a stress/strain is applied to it by stretching it, know as final thickness(T_f), therefore bypassing the percent stretch variable which is complicated to measure. Then the model applies a deformation consisting on a constant pressure which is equivalent to how the lens core behaves. In order to develop a model, the mechanical properties of PDMS membrane, shown in Chapter 2, Table 2.1, were input into Solidworks Simulation.

In order to produce the correct size and stress/strain, the model was divided in multiple steps. For example, the final diameter of the membrane is determined by the multiple rings support structure and bevel on it, for this case 26.6 mm was the diameter of the bevel. So in order to simulate the appropriate stress/strain condition on the membrane, a membrane is created with the initial thickness as measured with

the confocal sensor and a diameter smaller than the desire end state, so that once deformed it will have the desired stress/strain as a polymer lens would. As mentioned before the initial thickness was selected for the modeling and the experiment was $330\mu m$.

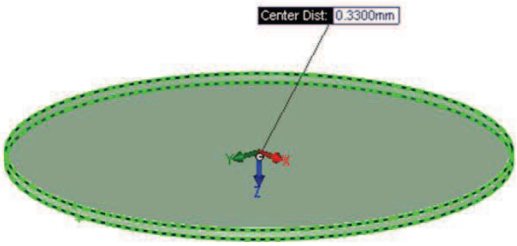

(a) Shows the membrane created with an initial diameter of 17.6 mm.

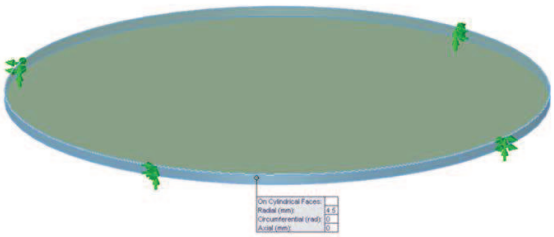

(b) Shows the boundary conditions applied to the membrane for displacement that would result in the desired strain/stress on the membrane.

Figure 3.8: Created membrane for FEM study.

The final diameter(D_f) of the membrane is known, so from the desired radial displacement (r_d), the initial diameter(D_i) can be calculate and used in the FEM, using $D_i = D_f - 2 \cdot r_d$. For example to introduce the desired stress/strain on the membrane, which is produced by stretching the membrane from the initial 17.6 mm to its final 26.6 mm, a reference geometry cylindrical boundary condition fixture is applied to the cylinder side face and a radial displacement of 4.5mm is applied to it, Figure 3.8b. This boundary condition fixes the edge but allows radial translation

and rotation in the desired direction, outward, therefore stretching the membrane. This will stretch the membrane by 4.5mm radially therefore imparting a stress/strain onto it.

Due to the ratio between the diameter and the thickness of the membrane, a mesh control has to be applied. Since the membrane initial thickness is small in comparison with the diameter and a translation is applied to the cylinder faces, reaction forces are developed and localized stress concentrations are likely to appear affecting the results. In order to minimize this, there are two techniques, one is to use shells, the other is a mesh control. Cases were process using both the shell and the mesh approach, resulting in close performance, therefore the mesh control was selected since it simplified the set up. A mesh control consists of applying a smaller mesh in certain regions. For this case finer mesh was applied to the cylinder face, which is the thickness, and a coarse mesh to the faces of the cylinder, which is the top and bottom. This also helps in the convergence of the FEA as well improve accuracy in the resulting stress/strain calculations. Using the initial and final thicknesses measured experimentally, a range of radial displacements was introduced in the model for calibration purposes. Table 3.1 shows the initial and final diameter, radial displacement and final thicknesses.

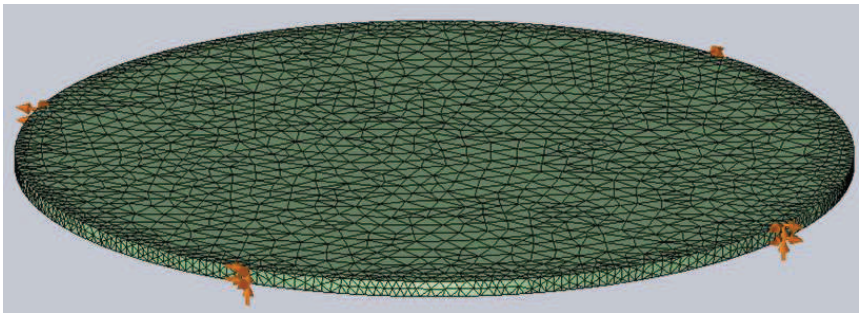

Figure 3.9: Mesh used on the membrane

From empirical data, the thickness ratio of interest are known, which were reproduced on the model using the values obtained in Table 3.1. Figure 3.10 show three

Radial displacement	D_i	D_f	T_i	T_f
1.5	23.6	26.6	0.330	0.261
1.8	23.0	26.6	0.330	0.248
1.9	22.8	26.6	0.330	0.244
2.0	22.6	26.6	0.330	0.240
2.5	21.6	26.6	0.330	0.220
2.9	20.8	26.6	0.330	0.203
3.0	20.6	26.6	0.330	0.200
3.5	19.6	26.6	0.330	0.180
3.6	19.4	26.6	0.330	0.182
3.8	19.0	26.6	0.330	0.170
4.0	18.6	26.6	0.330	0.160
4.5	17.6	26.6	0.330	0.144

Table 3.1: Initial displacement and thickness membrane with applied radial displacement in FEA and resulting final thickness calibration

images of an example: left shows the displacement change of the membrane, from initial to final diameter. Center and right its respective stress and strain magnitudes introduced during the stretch at the membrane final diameter.

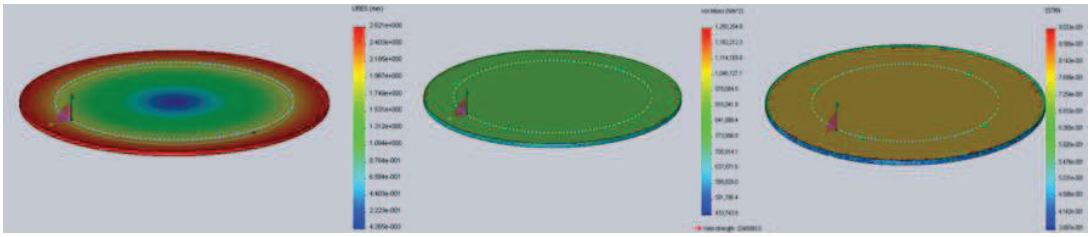

Figure 3.10: FEM results of a uniform thickness membrane

Once thickness calibration was performed, the FEM model was modified in a way in which the external load of constant pressure is applied to the membrane. So the model is divided in two steps: step one introduces the stress and strain as

shown in previous figures and step 2 introduces the external load, as shown in Figure 3.11. This external load is applied constant and uniform to the surface. Reference geometry conditions are applied to the membrane and the load is applied with a time curve given in Figure 3.11. This time curve allow the process to be separated on the respective two steps, the stretching of the membrane follow by the pressure load applied.

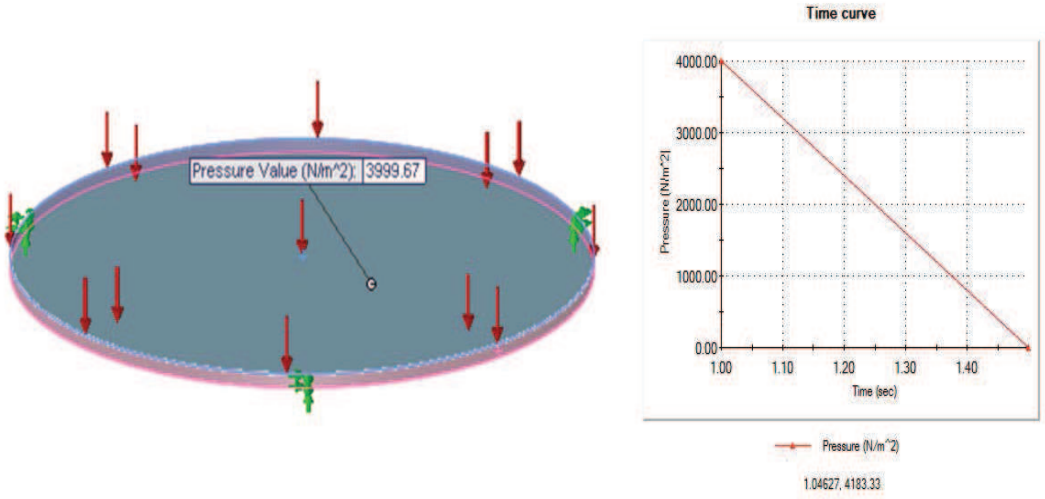

Figure 3.11: Applied Load conditions and time curve for applied force.

Once all the boundary conditions and external loads are correctly indicated, the code is run obtaining the results shown in Figures 3.12. As shown in the figure the membrane had been stretched follow by a deformation due to the pressure applied to it.

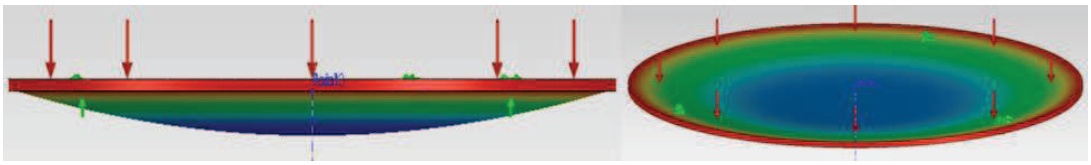

Figure 3.12: Deformed membrane by constant pressure load

Once the deformed membrane is modeled, further analysis provides the sag and curvature with applied pressure. This related pressure to volume of the cap, as well as radius of curvature all relate to initial and final thickness. As a next step the FEM was ran for a pressure range from 0 to 60 torr for each initial and final thickness combination, which was based on empirical data, for a starting thickness of $330\mu m$ and final thicknesses ranging from 185 to $255\mu m$. From the model we can extract the parameters that can be measured experimentally, such as pressure, volume, and thickness and compare the model to experimental results.

3.3.2 Design of experiments

Various experiments were developed based on the ANSYS model and on the later Solidworks FEM. The advantage of the Solidworks model over ANSYS, was that most of the work performed in Chapter 2 was completed therefore there was a more direct correlation between measured and model variables.

An experiment was developed in which membrane thickness (initial and final) is known very accurately, pressure inside, volume change, radius of curvature, and wavefront could be measured simultaneously. This experiment allows to understand the performance of the polymer lens in a similar configuration that would be used in systems. Various configurations of the experiment where made until a setup was identified as the one that produce the results in terms of wavefront error in front of the Zygo interferometer.

Setup #1, shown in Figure 3.20a, which was design to compare the ANSYS results, consisted of using glass bond, which were placed on a fixture filled with water which contained a pressure gauge on one end and a precision calibrated syringe on the other end which allowed for changing the volume inside therefore deforming the membrane and increasing or decreasing the pressure inside accordingly to which

direction the fluid was moved. In order to minimize errors, all the air is removed from the system, a process which could take half a day to a full day. As can be seen in Figure 3.20a (left) the glass bond would sit on an O-ring which then uses a washer on the top to compress the glass against the O-ring to create a seal and eliminate fluid leakage while compression is added. This setup added complications because it relied on the screws which deformed the rings when tightened, increasing aberrations, and the O-ring presented the problem of deformation when at higher pressure inside the core. The results from these experiments are shown in Section 3.3.3, and indicated that there was a cubic relationship between pressure vs volume. This contradicted the FEM ANSYS results which indicated that the relationship should be quadratic instead of cubic. At the time this experiment was performed, there was no way to measure the membrane in situ, the thickness average obtained from the Wyko measurements were used on the ANSYS FEM.

Figure 3.14 shows the actual setup in front the Zygo and the interference pattern on the science camera which clearly shows the astigmatism produced by the screws. Adjusting the screws demonstrated the change of the astigmatism axis.

The contradicting results and the aberrations seen on the Zygo due to this setup indicated that the experimental configuration was introducing other effects to the membrane deformation. This led to a design of a second pressure vs volume fixture, shown in Figure 3.20b.This fixture improved the O-ring configuration and eliminated the four discrete screws used on the previous fixture which deformed the ring therefore creating aberrations. This fixture has the advantage that the bond could be placed in and a ring used to hold the bond down which in theory provided uniform force on top or on the bottom of the ring, therefore minimizing aberrations. Problems arose with the locking ring if it was to be used on the top ring, even when polished it still introduced aberrations. If the locking ring was to be used on the bottom ring, that implied that a different size bottom ring had to be made of aluminum or cut if using

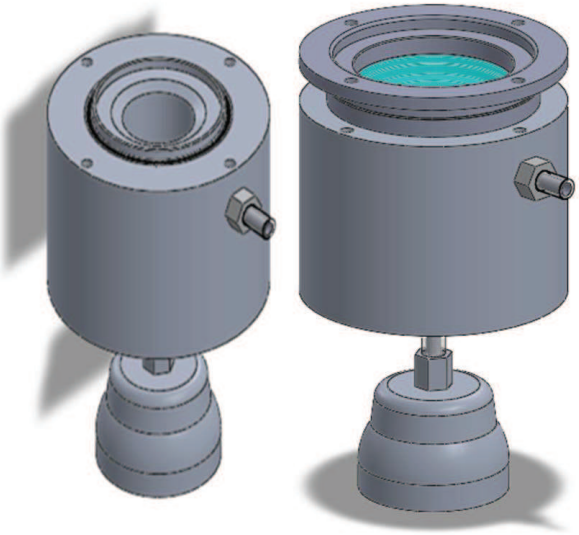

(a) Fixture 1, which used screws to hold down the B1 and seal the fluid in place.

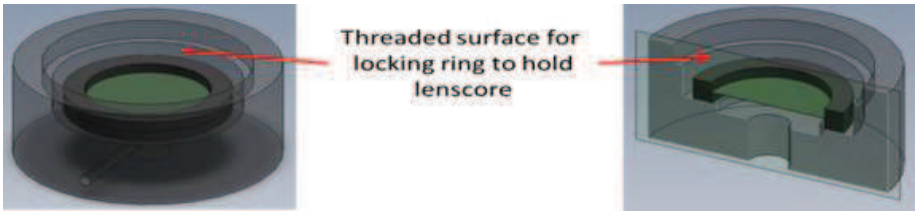

(b) Fixture 2, or modified version of fixture 1 that used a flat locking ring that will press B1 in place.

Figure 3.13: First two fixtures used to measure pressure vs volume as a function of thickness ratio.

glass making this setup complicated, time consuming and more expensive.

A third design was made, shown in Figure 3.16. This setup was design with the Solidworks Simulation FEM in mind, since it would allow a direct comparison between model and experiment. This setup, made of aluminum was an exact representation of an actual bond and allows for the reuse of the parts as well as verifying directly the performance of the rings. Aluminum rings made with the new process and two bevels in the lab could be tested in the same conditions as would be used in

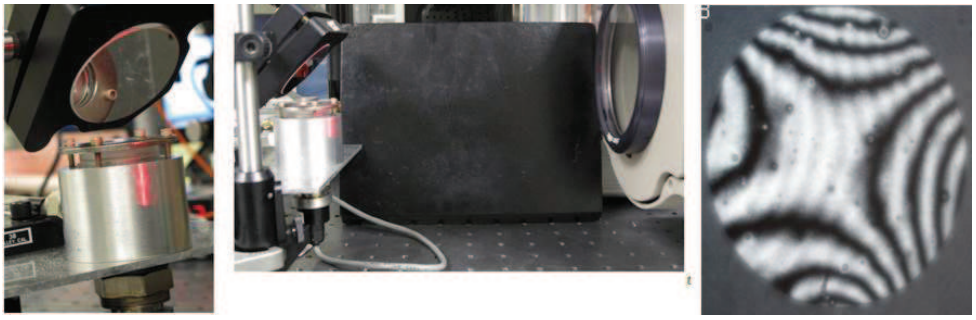

Figure 3.14: (Left)Shows the B1 hold by 4 screws and the washer, with incident laser from the Zygo interferometer.(Middle)Setup in front of Zygo.(Right)Analog image of the full aperture of the membrane obtained from the Zygo. Astigmatisms can be clearly seem on the image, depending on how the screws were modified the magnitude and direction of it could be alter.

the APL presenting a big advantage over the other configurations. So, by using this setup, multiple variables and process steps can be tested and direct measurements

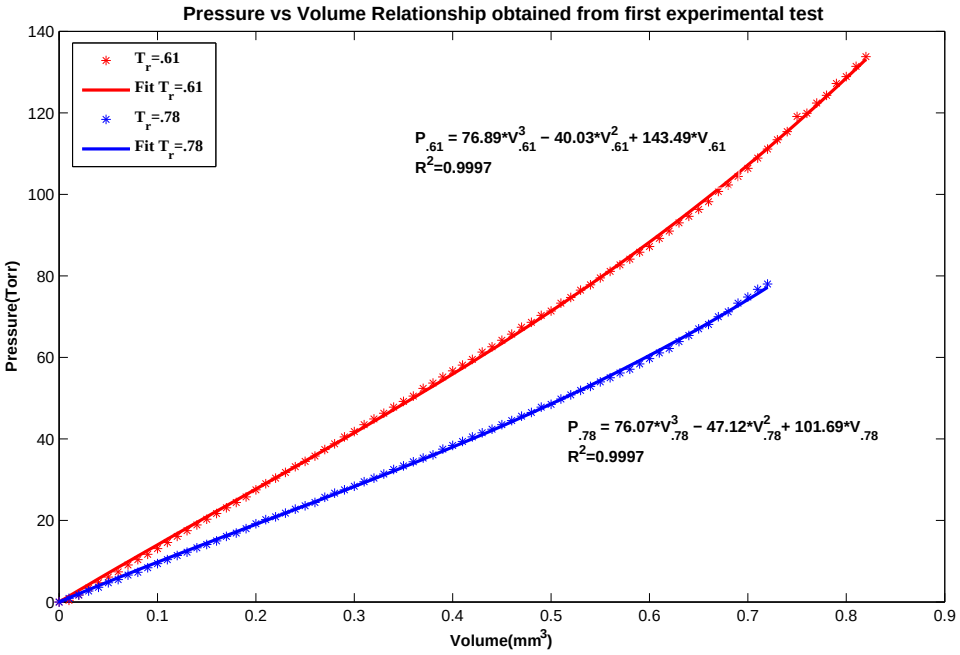

Figure 3.15: Cubic results obtained from using Fixture 1

of pressure vs volume measurements could be made.

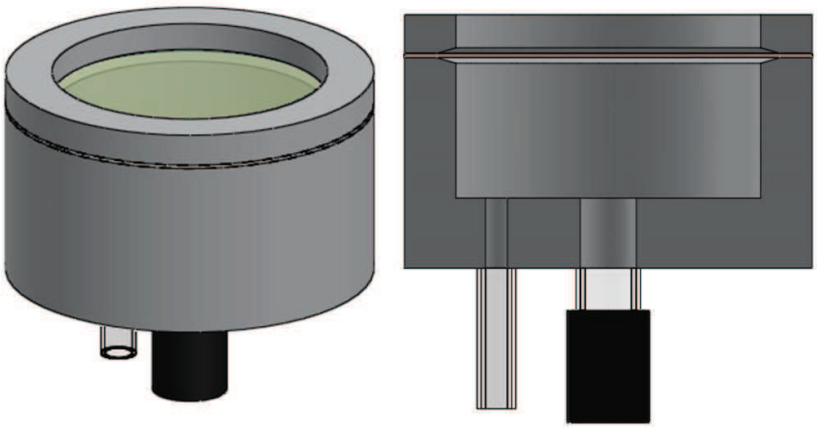

Figure 3.16: Fixture made on the same configuration as with the APLs.

3.3.3 Results

The first model created in ANSYS suggested that the relationship between pressure vs volume was quadratic as can be seen in Figure 3.20a which did not match the first results from Fixture 1 as shown in Figure 3.20b. But as mentioned before the idea or main goal is to develop a simple model that can help in the fabrication. In order to do this a linear approach was tried. The linear model simplified complexities that resulted from the higher model at the time of extracting the fabrication parameters.

As described in the previous section the results from the first experiment indicated that the relationship between pressure and volume is cubic as seen in Figure 3.20b. This generated the discrepancy with the ANSYS results but also a cubic relationship complicated the end results, which is, to extract the fabrication variables and the membranes interactions.

It is extremely important to note that for the ANSYS results, the T_r is based on approximate measurements of the thickness of the membranes, reason is at the time

the model was made there was no means of knowing the initial or final thickness of the membrane in situ, this is when the data obtained from the Wyko interferometer was used to upgrade the model. A similar caution applies for the data taking with setup 1, all the work from Chapter 2 had not been completed, so variation in thickness of the membrane were present as well.

Now from the design of fixture 3, the Solidworks FEM was ran for three distinct thickness ratio membranes, of $T_R = 0.77, 0.65$ and 0.57 utilizing a constant pressure range from $P = 0 - 60$ Torr per case. The thickness ratios were carefully obtained by measuring the thickness with a confocal sensor. Figure 3.18 shows the results obtained from Solidworks FEM 3.20a for a linear fit and 3.20b for a quadratic fit. This demonstrated the errors introduced by Fixture 1 and how the form of the ANSYS matched the SW FEM. To compare the model quantitatively there are many updates that needs to be done on the ANSYS size, reason there is not a direct comparison or details about the model here.

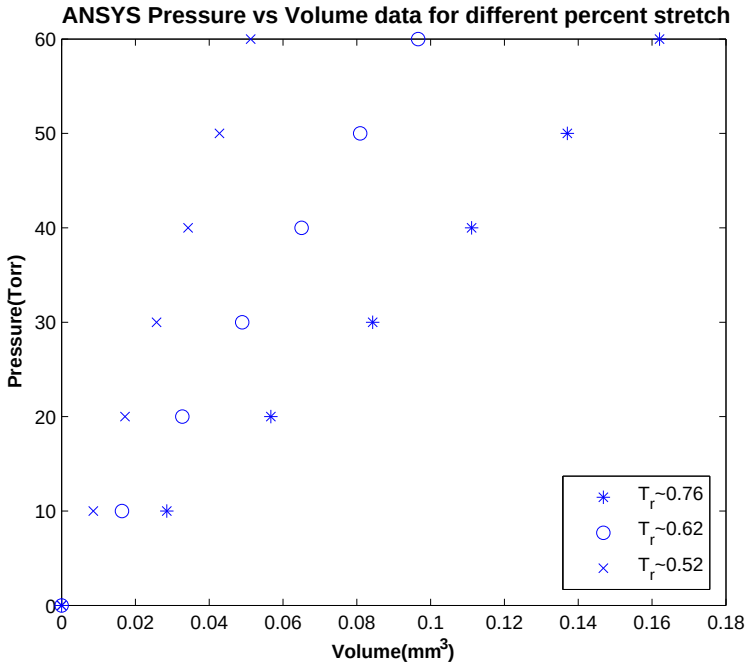

(a) ANSYS results

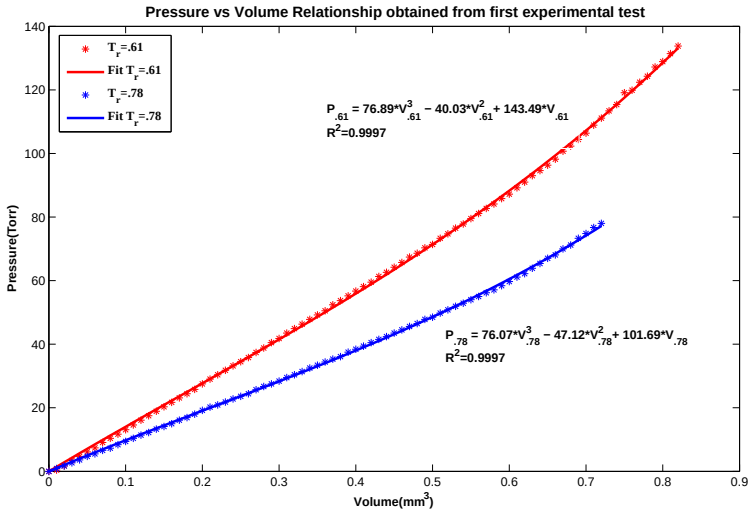

(b) Experimental results from Fixture 1

Figure 3.17: Shows the results obtained from ANSYS. These results indicate a quadratic relationship between pressure and volume. Fit are not shown on the ANSYS data due to a scaling offset on that model.(b)Experimental results obtained from Fixture 1 showing a cubic relationship between pressure and volume.

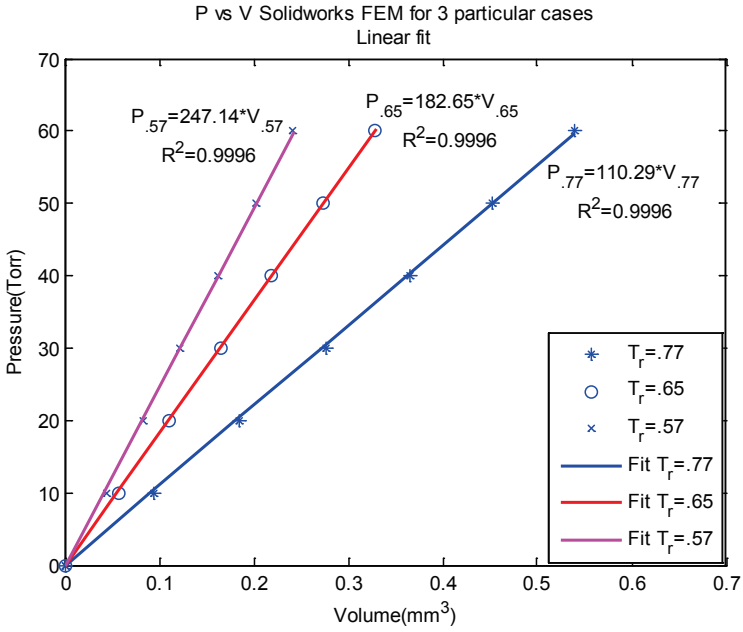

(a) SW FEM results with linear fit.

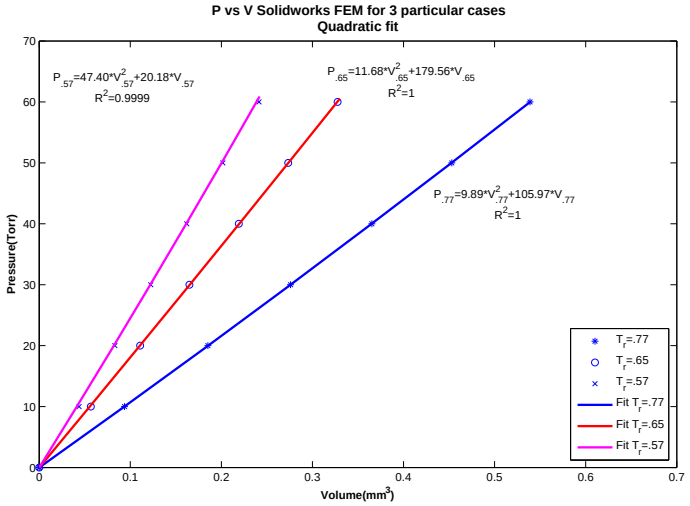

(b) SW FEM results with quadratic fit

Figure 3.18: Shows the pressure vs volume results obtained from the SW FEM, and the respective linear and quadratic fit with the corresponding R^2 fit coefficient.

Following the SW FEM results experiments were conducted using Fixture 3 and similar thickness ratio,T_r, as used in the FEM were tried. The experimental result obtained from the following thickness ratios $T_R = 0.77, 0.63$ and 0.52 are shown in Figure 3.19 (a) for the linear fit and (b) for the quadratic fit.

The case of $T_R = 0.77$ was selected from both SW FEM and the experimental data since it matched the thickness ratio and is shown in Figure 3.20. These comparisons show how close the model is to our experimental results. The model can be matched to the results, but the goal was to replicate the model. The reason why the thickness ratio is not exactly as with the model had to do with the physical hard stops used when the membrane is stretched to get the final thickness. The thickness of the membrane is monitored continuously in situ by using the confocal sensor, but the stops are discrete locations. These locations are a physical limitation of the mechanical fixtures currently used and in order to eliminate this a lot of effort went into developing new fixture which eliminate the discrete stretching points while monitoring the thickness. This is of great advantage due to the fact that a singlet or a doublet can be fabricated more precisely, for example for a equaconvex lens, giving the particular T_r of the first membrane, the automated fine control fixture would allow the second membrane T_r to match the first membrane. For a doublet knowing the prescription and T_rs desired the lenscore can be fabricated more accurately.

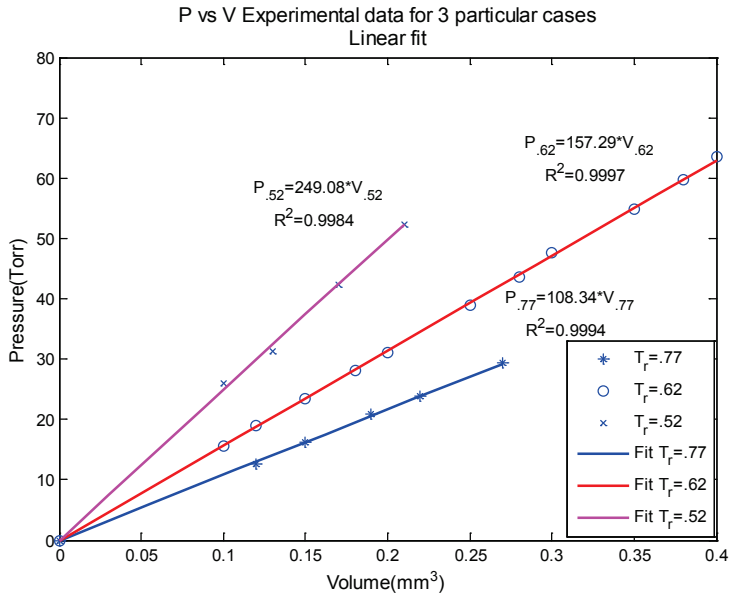

(a) Results for different T_r with the linear fit

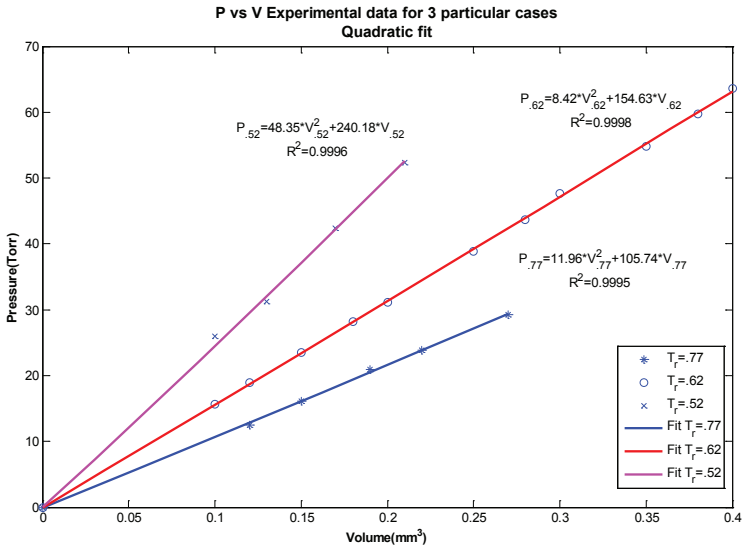

(b) Results for different T_r with the quadratic fit

Figure 3.19: Experimental data for different T_r similar to the ones used on the SW FEM.

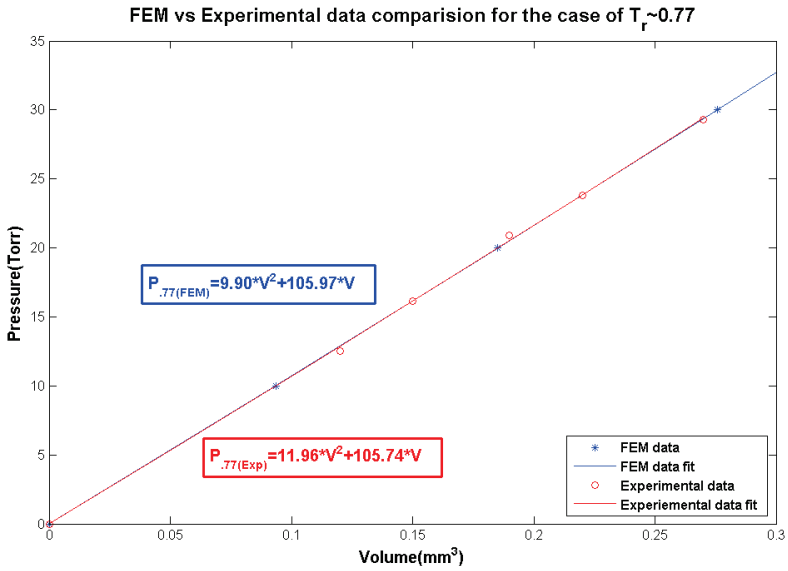

(a) SW FEM and experimental result with linear fit

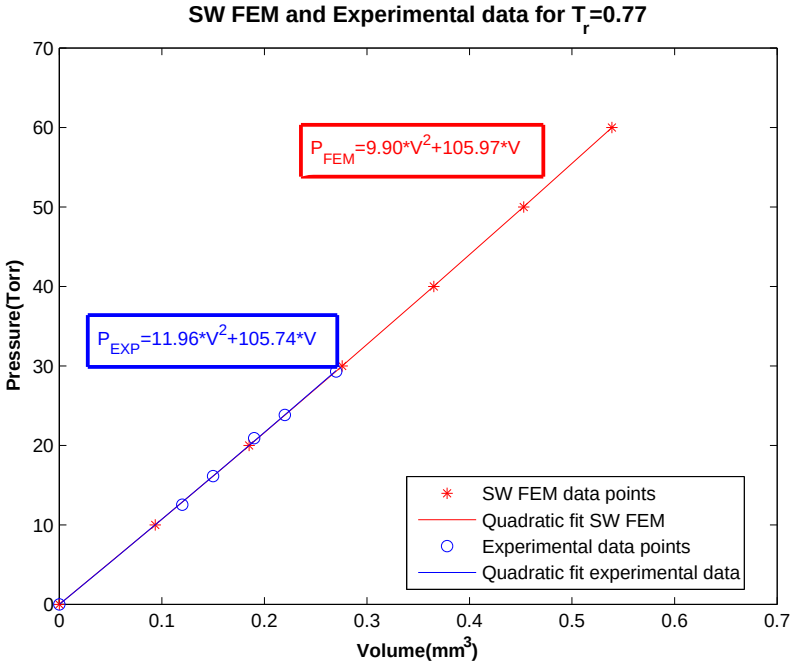

(b) SW FEM and experimental result with quadratic fit

Figure 3.20: SW FEM and Experimental data T_r=0.77 with respective fits.

Shown in the previous sections are the results from the last experimental fixture and how they match the SW FEM model. It can also be seen that the expected functional form seen on ANSYS was obtained using SW FEM. As mentioned at the beginning of this section a linear model would be simpler to extract the information necessary for the fabrication.

3.4 Model approximation and fabrication parameters

From the models and empirical results there are two approximations that can provide the desired fabrication parameters for the APLD. Table 3.2 shows the linear and quadratic fit obtained from the FEM model and Table 3.3 shows the same fits for the experimental data.

T_R	Quadratic	R^2	Linear	R^2
0.77	$P_{0.77} = 9.89 * V^2 + 105.97 * V$	1.0	$P_{0.77} = 110.29 * V$	0.9996
0.65	$P_{0.65} = 11.68 * V^2 + 179.56 * V$	1.0	$P_{0.65} = 182.65 * V$	0.9996
0.57	$P_{0.57} = 47.40 * V^2 + 20.18 * V$	0.9999	$P_{0.57} = 247.14 * V$	0.9996

Table 3.2: FEM model fit obtained.

T_R	Quadratic	R^2	Linear	R^2
0.77	$P_{0.77} = 11.96 * V^2 + 105.74 * V$	0.9995	$P_{0.77} = 108.34 * V$	0.9994
0.62	$P_{0.62} = 8.42 * V^2 + 154.63 * V$	0.9998	$P_{0.62} = 157.29 * V$	0.9997
0.52	$P_{0.52} = 48.35 * V^2 + 240.18 * V$	0.9996	$P_{0.52} = 249.08 * V$	0.9984

Table 3.3: Experimental fits obtained.

3.4.1 Linear approximation results

From the results presented on the previous section, a linear approximation is utilized to narrow fabrication parameters for the achromat.

From the optical prescription from Zemax for a single surface, an ROC is obtained. Given that, ROC, the procedure in section 3.2.1 can be used to obtain the sag of the surface and from the sag the volume of the spherical cap. The liner approximation between pressure and volume is given by the following equation:

$$\Delta P = m \cdot V_{cap} \tag{3.12}$$

where m is the slope of the line and is a function of the thickness of the membrane. Now there is a relationship of m with respect to the T_r which after further experimental work it was determined of the following form:

$$m = a \cdot T_r \tag{3.13}$$

where a is a coefficient obtained from empirical data for known T_r. From empirical data shown in Figure and knowing m from the calculations above, the T_r for that membrane can be obtained as well as the coefficient a by using,

$$m = -499.48 * T_r + 484.22 \tag{3.14}$$

$$T_r = \frac{(484.22 - m)}{499.48} \tag{3.15}$$

and $T_r = T_i/T_f$.

For example, given an optical prescription for a singlet as $ROC_1 = 260.16mm$ and $ROC_2 = 132.73$, and selecting a starting $T_r = 0.62$ for the first membrane a description of the second membrane can be obtained, by following the above procedure.

First calculate the sag and volume of the cap for the given ROC which results in:

- $h_1 = 0.34$ and $h_2 = 0.67$
- $V_{cap1} = 0.094$ and $V_{cap2} = 0.185$

and it is know that the relationship between pressure and volume for $T_r = 0.62$ is given by equation 3.12 for a $m_1 = 157.29$,

$$\Delta P = 157.29 * V_{cap1} \tag{3.16}$$

Also it is know that the summation of all pressure of that particular singlet is 0, given by:

$$\Delta P_T = \Delta P_1 + \Delta P_2 = 0 \tag{3.17}$$

$$0 = m_1 \cdot V_{cap1} + m_2 \cdot V_{cap2} \tag{3.18}$$

Using equation 3.16 and substituting the results obtained for each of the volume of the caps into equation 3.18 the calculated value for m_2 is 111.78. From this value obtained and usinging the empirical relationship between slope and T_r given by equation 3.15 the value of T_r for that second membrane results in a thickness ratio of 0.81.

Given the optical prescription of a singlet, it can be fabricated first with membrane thickness ratio of 0.62 and a second membrane with a thickness ratio of 0.81.

To summarize, given the ROC from the optical design, a T_r is selected, the below procedure is followed and with the relation of pressure vs volume for that membrane a description of the behavior of that singlet is obtained.

- Calculate sag, h, given by $h = ROC - \sqrt{ROC^2 - r_g^2}$
- Calculate volume of the spherical cap, V_{cap}, $V_{cap} = \frac{\pi h}{6}\left(3 \cdot r_g^2 + h^2\right)$
- Use T_r to calculate the slope for that particular membrane
- From the slope obtained and the volume of the cap calculated the differential in pressure of that membrane with ambient or another fluid can be calculated

For the doublet case, two of the T_r are selected and the third is calculated using the procedure described above. The challenge is identifying and knowing the range of T_r that are appropriate in order to obtain the desired optical performance of the lens as well as to minimize optical aberrations. This range will not be discussed in the dissertation.

This demonstrates how to go from prescription to fabrication of the achromat. Next section will demonstrate how to go from a single focal length to more than one focal length while maintaining achromatization.

3.4.2 Multiple focal length APLD

A major difference between the work presented in this dissertation and other work performed on polymer lens research is the constant volume conditions. There are other companies and research groups performing constant volume conditions lenses but not for doublets or multiple chamber lenses. All work performed pass a single chamber, is done with independent control of each fluidic chamber, meaning fluid

is pumped in and out of that chamber or air chambers which separate the flexible surfaces with flat glass, so this implies full control of the fluid inside [28][18]. For the work performed in this dissertation and due to the application, there is not fluid moving in and out of the chambers, therefore the challenge of constant volume condition. Figure summarize how the constant volume condition is define, how the net differential pressure of a lens is equal to zero. Once the T_r is calculated the m_n

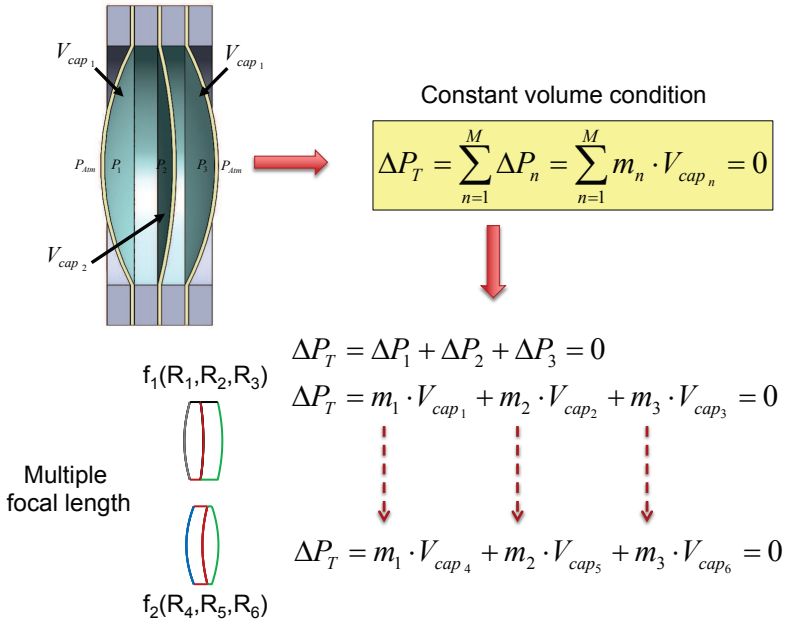

Figure 3.21: Diagram showing the relationship between constant volume condition and multiple focal lengths APLD.

are fixed, this determine the doublets under a constant volume condition. Now for multiple focal lengths, a numerical algorithm was created in which using the solution obtained, a change in volume of the cap is created and since the volume of the APLD is constant, a solution is calculated for the other two caps. The doublet is design base on correction for chromatic, spherical aberration or other. So using the design, once that next solution is determine, it is input into design and performance verify. If this solution satisfied the metrics that is label as a second focal lengths solution,

if not, the algorithm calculates another solution and the iterations continues. This process is shown in Figure 3.22. Once the solutions for multiple focal lengths are calculated the performance of the doublet is verified on the experimental testbed which is presented on the next section.

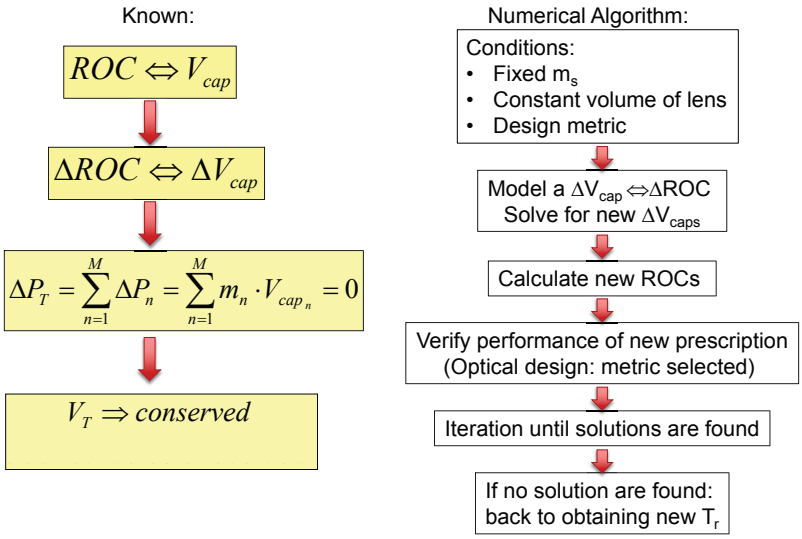

Figure 3.22: Flow chart representation of variables known and numerical model to obtain multiple focal length solutions.

3.5 Achromat fabrication

The fabrication of a doublet in this case and achromat, consist of various steps. The first step is the selection of the two fluids. The second step is to use those fluids in a Matlab code to determine the ROCs and following that the ROCs are input into Zemax to verify performance of the doublet, which for this case the metric of interest is the focal shift, between blue, green and red wavelength. That second step can be changed and allow the user to go straight to Zemax to obtain the desired ROCs.

Once the ROCs are identified, they are used as input in a second Matlab code

based on the results obtained from the linear approximation model described in Subsection 3.4.1. This code will explore a fabrication variable solution space bounded by the user. The key solution of this code is to provide the thickness ratio for the third unknown membrane.

For example, an achromat doublet is desire to have a focal length of $250mm$. This focal length and parameters from list 3.5 are inputted into the Matlab script and a number of solutions which can be set by the user are produce. For this particular case the user is interested in exploring solutions for T_r for the intermediate membrane.

- Fluid 1: $n_1 = 1.44$ and $V_1 = 62.2$ (Crown)
- Fluid 2: $n_1 = 1.58$ and $V_1 = 29.0$ (Flint)
- Achromat focal length: 250 mm
- ROC1 solution exploration space: 70 mm to 150 mm
- Cylinder dimensions: thickness of 2.8 mm and interior diameter of 23.77 mm
- Selected thickness ratios: $T_{r1} = 0.62$ and $T_{r3} = 0.62$

The output of the code is shown in Table 3.4, provide guidelines on narrowing down the fabrication of the doublet. From that list the user can select the doublet starting desired ROCs based on known fabrication constraints.

The list provides not only the thickness ratio and final thickness but also the cap volume based on the calculated ROCs. From this the user can select one of the rows and verify performance of the achromat in Zemax. For this case the last row was selected and the performance results are shown in Figure 3.23

Using the above results the achromat is fabricated in a similar procedure as is done with the singlets with the main difference that extreme care is taken on making the initial and final thickness as close to the design and as well as with the volume.

Table 3.4: Output fabrication parameters from code, the two columns on the right show the T_r and the T_f

fl	ROC1	ROC2	ROC3	Vcap1	Vcap2	Vcap3	Tr	Tf
250	92.22	-162.61	-9539.42	268.35	151.47	2.58	0.42	137.58
250	97.78	-147.80	-1387.10	252.90	166.72	17.72	0.53	173.33
250	103.33	-136.69	-786.92	239.15	180.36	31.23	0.61	200.12
250	108.89	-128.05	-566.72	226.82	192.61	43.37	0.67	220.94
250	114.44	-121.13	-452.42	215.71	203.70	54.34	0.72	237.59
250	120.00	-115.48	-382.43	205.64	213.76	64.29	0.76	251.20

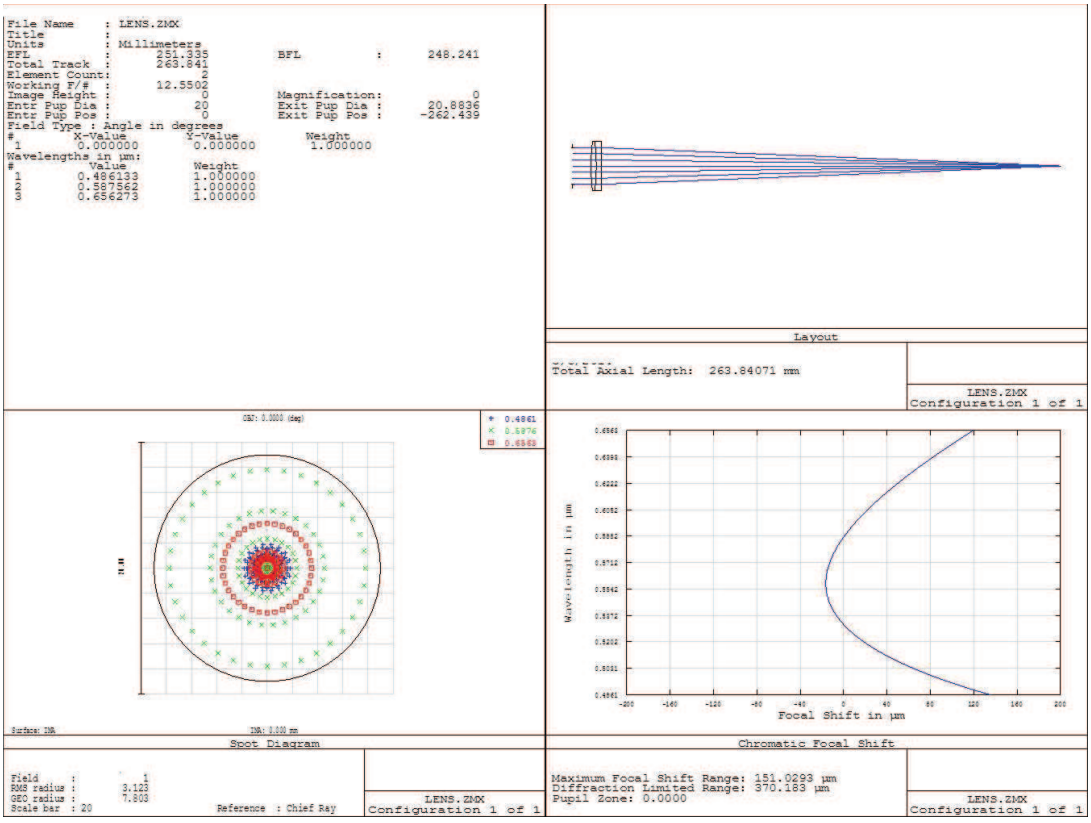

Figure 3.23: Zemax results from prescription selected from the list.(Top Right)Prescription information. (Top Left)2D layout.(Bottom Right)Spot diagram.(Bottom Left)Chromatic focal shift, $\Delta fl = .151mm$ for the F, d and C lines.

3.6 APLD testing

In order to test the achromat, an experimental setup was designed, the APLD is driven to a particular focal length in which incident collimated light is focus on a target, in this case a charge couple device (CCD). This CCD is placed on a accurate translation stage which can be moved towards and away from the lens and a centroid or best focus algorithm is used determine best focus. In Zemax as mentioned in the previous section, the design is based on the F, d and C lines, but for the experimental case three laser sources were selected. The concept is to measure best focus of the lens for 632nm, 532nm and 405nm with the accurate translation stage, measure for each case the back focal length and compare those results with Zemax. Once the model is close with the experimental results, performance can be verified for the desired spectral lines. Once again the metric is the chromatic focal shift. Figure 3.24 shows a sketch and the optical setup built for testing the doublet lens for achromatization. Glass singlets of 3 different focal length, 200mm, 500mm and 750mm were tested on the same setup and compared in Zemax.

3.6.1 Achromat results

Multiple achromats were designed and built in order to test different configurations based on fabrication variables, specifically which of the membranes was considered the unknown. All lenses were tested using the setup described in the previous section, under the same conditions and using the Zygo interferometer to measure accurately ROC_1 and ROC_3 or the outer ROCs of the APLD. The middle ROC or ROC_2 can not be measured easily using the interferometer due to the small delta in index of refraction between fluids. This ROC can be extracted from the volume of fluid, calculated using the doublets equation or by an optimization in Zemax using the measured back focal length of the APLD. Figure 3.25 shows the point spread function

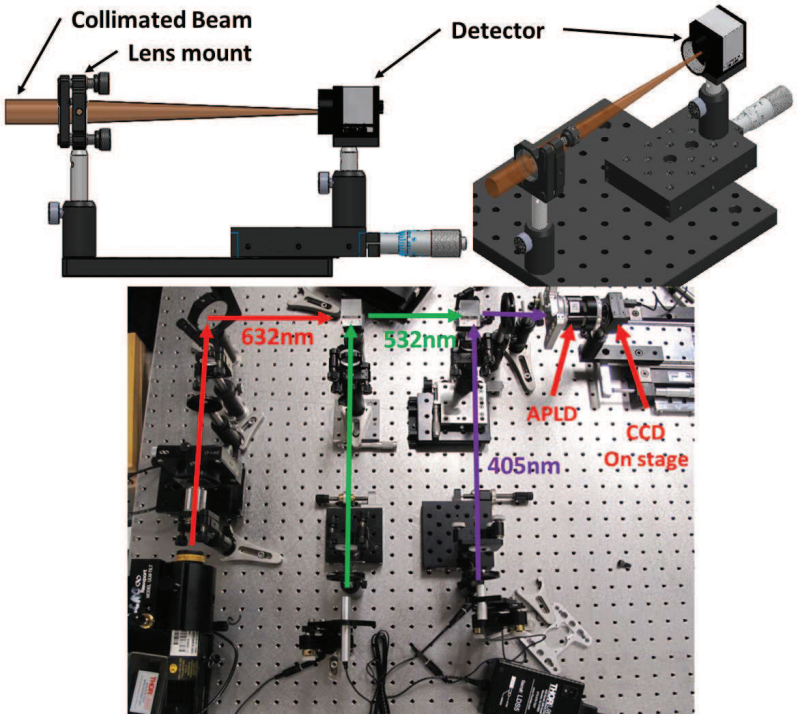

Figure 3.24: (TOP)Sketch of achromat test setup.(Bottom)Optical table setup, showing collimated HeNe laser(632nm), green laser(532nm) and blue laser(405nm) with aperture stop common for 3 laser, APLD and CCD on a translation stage.

of each of the setup wavelengths as recorded on the CCD.

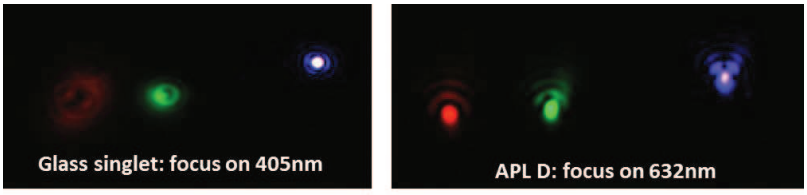

Figure 3.25: (Right)PSFs for the three wavelengths of the setup for a glass singlet of $fl = 500mm$ focus at blue 405nm.(Left)PSFs for the three wavelengths of the setup for a APLD of fl=600mm focus at 632nm.

As mentioned previously the main metric use for these lenses is the focal shift. The focal shift is the measurements of the delta in focal length of two wavelengths for this case, the smallest the better the correction of that achromat for those two

wavelengths. Figure 3.26 shows one of the fabricated achromatic doublets. This particular lens as can be seen in the picture is a positive lens.

Figure 3.26: Achromatic doublet fabricated

The procedure to measure a doublet consisted, of first measuring the radius of curvatures with the interferometer. The lens was aligned on the optical path of the three co-aligned beams, while one of the laser was on, best focus position was identified and the separation from the back of the lens to the camera CCD measured. From that distance the back focal length was calculated and the procedure was repeated for the other 2 wavelengths. Following that, the delta on focus position was calculated between the three wavelengths, more importantly between blue and red(B-R) and green and red(G-R). Table 3.5 shows the data obtained from two of the constructed doublet. As a reference, a commercial achromat doublet of focal length 750 mm, test under the same 3 wavelength will result in a focal shift of 3.2 mm, and it is a fixed focal length. Table 3.6 shows different glass singlets test under the same conditions as the APLD.

A APLS made using Fluid 1 was measured on the same optical setup. For a back focal length of $fl \approx 650mm$ the focal shift for B-R was in the order of $15.26mm$ and for G-R of about $10.46mm$. This same APL at a back focal length of $fl \approx$

Table 3.5: Focal shift results for two achromatic APLDs obtained from measurements from the test bed and calculated from Zemax.

		ROCs		Measured		Zemax	
Doublet #1	**ROC1**	**ROC2**	**ROC3**	**B-R**	**G-R**	**B-R**	**G-R**
RROC	85.15	-172.16	-104.24	3.9	1.5	3.77	1.1
	64.73	109.67	-75.36	2.79	0.71	3.7	1.03
	70.05	140.32	-79.45	3.2	1.09	3.94	1.09
	53.6	79.86	-61.91	2.81	0.228	3.1	0.859
Doublet #2	**ROC1**	**ROC2**	**ROC3**	**B-R**	**G-R**	**B-R**	**G-R**
RROC	177.76	-242.04	-184.36	8.55	0.27	6.91	1.98
	113.5	179.6	-114.35	6.2	1.17	3.21	0.97
	84.25	175.61	-83.57	4.47	1.24	2.3	0.7
	65.21	86.62	-63.83	2.84	0.81	3.54	0.98
	60.03	41.5	-51.49	2.46	0.76	3.22	0.88

Table 3.6: Focal shift results for glass singlets obtained from measurements from the test bed and calculated from Zemax.

				Measured		Zemax	
Singlet	**fl**	**ROC1**	**ROC2**	**B-R**	**GR**	**B-R**	**G-R**
KPX106	200	103.36	INF	6.24	2.49	5.68	1.61
KPX624	500	259.36	INF	17.27	7.54	14.3	4.06
KPX630	750	387.21	INF	28.93	13.76	21.46	6.33

$230mm$ resulted in B-R of $6.60mm$ and G-R of about $2.67mm$. The average focal shift achieved by the APLD is of 0.87 mm for the G-R band, this presented an improvement or chromatic correction in the order of 67.56% over an APLS, 65.22% in comparison with a glass singlet of $fl = 200mm$ and 93.7% with a glass singlet of $fl = 750mm$.

Achromatization has been achieved in a constant volume conditions for an adaptive polymer lens doublet. Besides the advantage of rapid focal length change of APL and shape factor implementation a step forward had been achieved with APL, achromatization under constant volume condition.

Chapter 4

APLs for DVO and infrared applications

This chapters present the results of implementing APLs and the knowledge acquire in the previous chapters in systems for variable magnification or field of view (FOV) applications. It also shows the development of APL for longer wavelengths more importantly in the short-wavelength (SWIR) and mid-wave infrared (MWIR) mostly for tactical applications in which systems lack variable FOV capabilities.

4.1 Direct View Optics(DVO) Visible Systems

4.1.1 RAZAR

Rapid adaptive zoom rifle scope(RAZAR), shown in Figure 4.1, consist of the implementation of two ro more APLS or APLD to produce variable magnification DVOs with push of a button at a fraction of a second.

Figure 4.1: Adaptive polymer rapid adaptive zoom rifle scope.

Figure 4.2 shows images taking through RAZAR at three different FOV, 3.50°,1.75° and 1.17° respectively. This systems was test on a live fire event with the United States Special Forces, Figure 4.3.

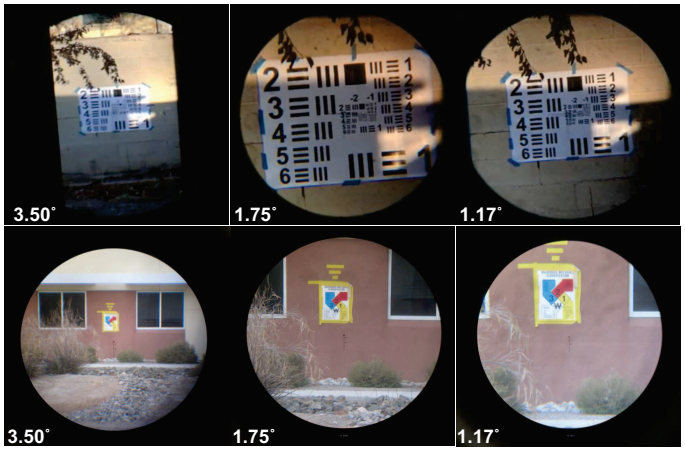

Figure 4.2: Images taken through the DVO system RAZAR of two different scenes at three FOVs.

Due to the application, a process was developed which enable the fabrication of these lenses for military applications. These APL can withstand high g-forces (≈1500-2000 g), experienced during a live fire. This is one of the main reason behind the motivation of using stronger materials as the support structure instead of glass.

Figure 4.3: Live fire event of RAZAR with the US Special Forces

4.1.2 Push button zoom binoculars

SNL in collaboration with the Kansas City Plant National Nuclear Facility is building upon RAZAR to develop a push button rapid adaptive zoom binocular. Following the same concept of RAZAR, the APL binoculars consist of a two APLs in series for each eye with a 6-12x zoom, as seen in Figure 4.4.

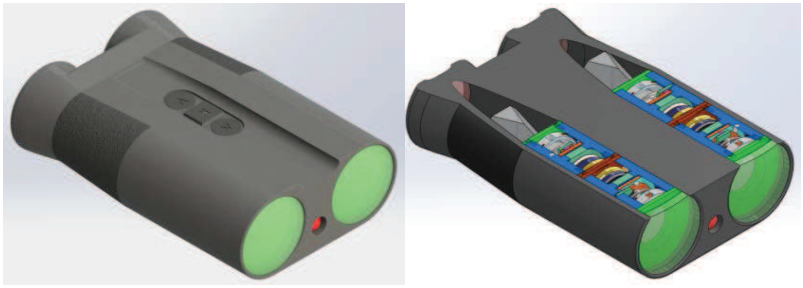

Figure 4.4: APL push button binoculars

4.2 Infrared PALs

Current tactical infrared systems, or night vision devices (NVD) lack variable FOV capabilities, this limiting the operators and making him choose between situational awareness, wide FOV, or target identification, narrow FOV. This limitation is mainly due to size and weight of these devices, which currently is in the order of ten pounds. Adding a conventional zoom system, requires mechanical components in order to move glass along the optical track therefore increasing the size and weight. By introducing APLs, the size and weight is either reduce or comparable to current systems but with the added capabilities of variable push button FOV.

4.3 Introduction to SWIR

Advances in short wavelength infrared (SWIR) sensors, lasers and light emitting diodes (LED) are allowing the use of SWIR systems in many tactical environments where limited size, weight and power (SWaP), and out-of-band performance (λ >1.0 um) are desired. Short range, tactical unmanned aerial systems (UAS) and small-arms, weapon-mounted systems are benefiting from these advances in SWIR. The option for active pointing/illumination is often coupled to both of these applications. But there have not been parallel advances in the optical components that these systems rely upon.

This part of the dissertation present the results obtained by using adaptive polymer lens designed for variable magnification in the SWIR. It also demonstrates how the APL developed for the SWIR can be implemented in an illuminator or as a designator for push button control of beam divergence or target area illumination when active illumination is required. Figure 4.5 shows the concept of an illuminator parallel to an imaging system and their overlapping fields, which could be matched

or customized by the operator.

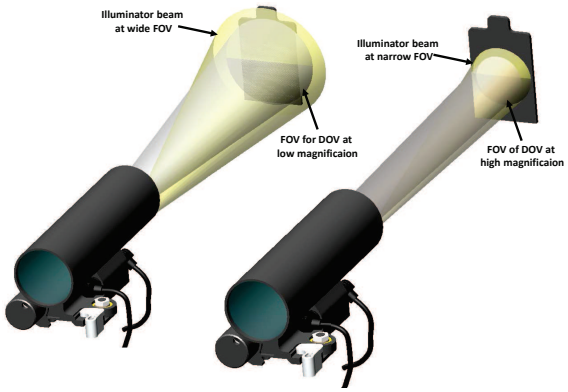

Figure 4.5: Conceptual representation of a variable FOV imaging system with a variable divergence illuminator in parallel.

4.3.1 Experiment and results

The main challenges in the fabrication of SWIR APLs are material compatibility and optical transmission within the desire application band, for this case $0.90 - 1.50\mu m$ band. For this work the fluid used contains an index of refraction of 1.45 and Abbe number of 39.5. The first task was to characterize the transmission of the fluid and the membrane on the band of interest. Figure 4.6 shows the transmission curves at the appropriate thickness used for the APLs. From the transmission results, the process described in previous chapters was used and two APLs were fabricated.

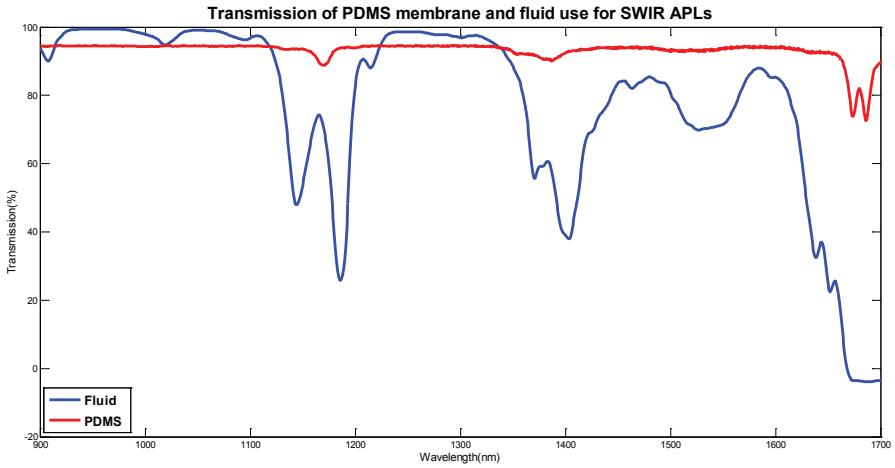

Figure 4.6: Transmission curve for the fluid used and the PDMS from $0.90 - 1.50\mu m$ and at the representative thickness used in APLs.

Variable FOV SWIR

A methodology was develop in which an afocal system could be design, built and placed in front of most fixed power DVO to increase its performance. This system, shown in Figure 4.7, was placed in front of a fixed field of view lens of 50 mm focal length, F/1.4 SWIR M42x1 from Edmund Optics and a Sensor Unlimited Mini-SWIR Camera model SU640HSX, 640x512 pixel format, 25μm pitch. The afocal zoom module was programmed and optimized for three distinct magnification states. Figure 4.8 shows images taken of three different scenes at three "zoom" states (field of view), corresponding to 1.17°, 1.75° and 3.5° times the base FOV, at distances of 50, 100 and 250 meters respectively. Figure 4.9 show results from the system at the three distinct FOVs of an Air Force resolution target at 15 meters. At that same distance, 15 meters, Figure 4.10 shows facial images at 1.75° and 3.5° FOV respectively. This demonstrates that SWIR APL based systems can be used in applications involving facial recognition.

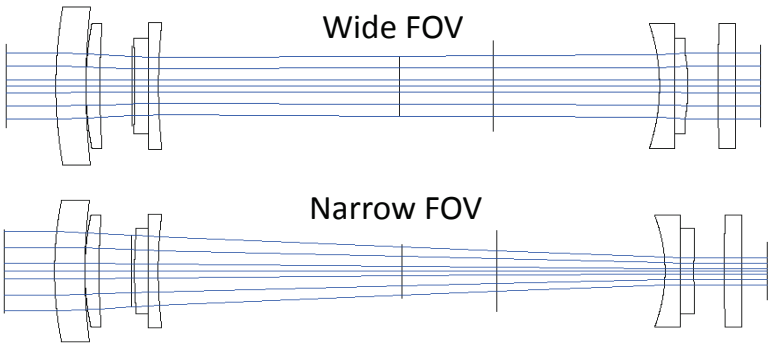

Figure 4.7: Afocal system designed showing two of the three preset states, (top) wide FOV and (bottom) narrow FOV.

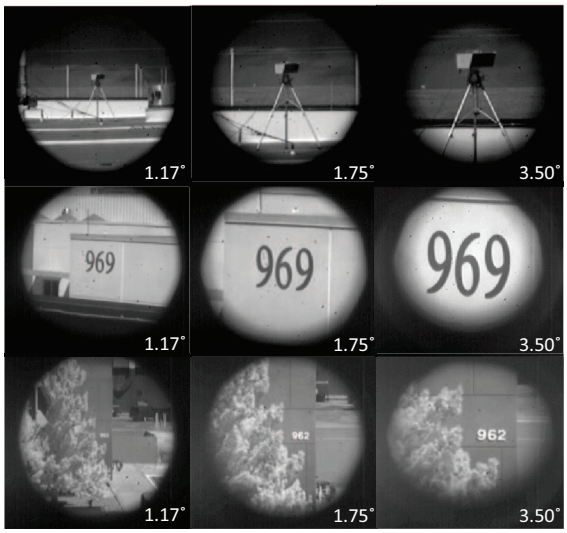

Figure 4.8: (TOP ROW)Images taken at $50m$, (MIDDLE ROW) $100m$ and (BOTTOM ROW) $250m$ for all three states of the zoom module.

Figure 4.9: Images at the three different states of an Air Force resolution target at 15 meters.

Figure 4.10: Facial images taken at two of states at 15 meters.

4.3.2 Variable FOV SWIR illuminator

A lower resolution camera from Sensor Unlimited, 320x240 and with a 40 μm pitch, was used to demonstrate the concept of variable push button divergence for illuminators, in which the SWIR camera was pointed at a target and the divergence of a 1550nm laser diode was controlled using an APL. Figure 4.11 shows the results for the illuminator concept. The top row of the images was obtained using a narrow field of view lens and the bottom row with a wide field of view lens.

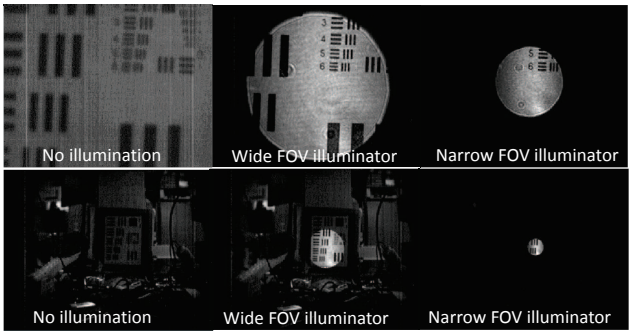

Figure 4.11: Illuminator concept, showing how the divergence can be controlled with the APL. Top row shows the results using a narrow FOV lens and the bottom row with a wide FOV lens on the camera.

4.3.3 Variable FOV SWIR designator

A proof of concept was built in which the variable FOV of the camera was combined with a variable FOV of a designator. A designator is a laser with a fixed divergence used to mark a target at a distance. Depending on the distances, diffraction and atmospheric conditions it is desirable to have control of the divergence of that laser, so that the desired energy is place on the target. With the use of a single APL lens, the operator can have control of that divergence. We used 1064 nm source with a single APL to demonstrate the concept. This APL allowed us to control

the divergence of the beam on target by simply pushing a button. This test was combined with the configuration described in subsection **??**. Figure 4.12shows the experimental setup used and Figure 4.13 shows the concept for two preset FOV states on the imaging system and as well as two divergence states on the laser pointer. It is important to note that the poor quality of the beam is due to the laser pointer used to prove the concept.

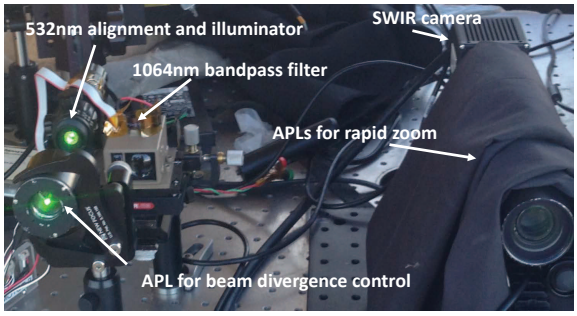

Figure 4.12: Experimental setup used for FOVs control

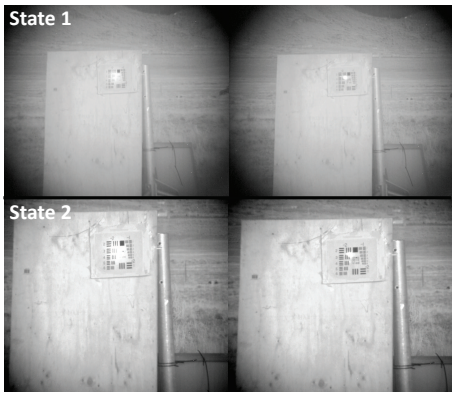

Figure 4.13: Proof of concept for push button FOV and divergence of a laser beam on target

This work demonstrated that APLs can be used for variable magnification application in the SWIR reducing SWaP of conventional optics and providing the user or system a rapid adaptive optical zoom capabilities. It was also demonstrated how

these APLs can be used in other applications for example but not limited to illuminators and designators.

4.4 Introduction to MWIR

Defense and military applications are driving the development of state of the art focal plane arrays, read out integrated circuits and cooling mechanisms for tactical systems. But there has not been a concomitant advance in variable magnification optics for these bands, mainly because of size/weight/power (SWaP) restrictions.

The majority of mid-wavelength infrared (MWIR) tactical systems function as in-line night vision devices (NVD), meaning the system is mounted in front of a direct view optic (DVO), as shown in Figure 4.14. These in-line sights are always fixed power (no optical zoom), forcing a compromise between situational awareness (wide field of view) and target identification (narrow field of view). Variable magnification is needed.

Figure 4.14: Operator demonstrating "in-line" configuration of DVO and NVD (Image courtesy of DRS Technologies)

The dissertation presents the work on developing APLs for the MWIR. It presents the main challenges, as well as the first results of a variable FOV system based on APLs in the MWIR.

4.4.1 Material challenges in the MWIR

The main challenge for MWIR APLs are material compatibility and optical transmission within the $3-5\mu m$ band. The fluid must not be absorbed into the polydimethylsiloxane (PDMS) membrane, changing its mechanical and optical properties.

An extensive search of fluids was performed that lacked C-H bonds, which absorb strongly in the MWIR, with the hopes of identifying a fluid with a high transmission at the wavelengths of interest ($3.4 - 4.8\mu m$) that is easily available.

A systematic approach was used when choosing a potential fluid to be used in the APLs. Using a standard IR functional group absorption chart, materials containing those functional groups that absorb from the $3-5\mu m$ wavelength range were avoided, i.e. alcohols, amines, aliphatic carbons, aldehydes, nitriles, alkynes, etc[9]. This greatly reduced the pool of compounds from which to choose. A polymeric material is desirable for use as the liquid in the lens core because a large size would inhibit diffusion through the membrane material. Furthermore, the polymer fluid must be chemically compatible with the membrane material, as to not compromise its integrity.

Most organic polymers are aliphatic, but a perfluorinated version would avoid the C-H absorption associated with aliphatic chains. Perfluorinated polymers and small molecules were investigated using transmission Fourier transform infrared spectroscopy (FTIR) both between two CaF_2 plates as well as through a variable path length cell, setup shown in Figure 4.15. Thin film measurements gave evidence that many of these materials would work, with transmission being greater than 90% over the critical wavelengths. Moving to longer path lengths (mm), a large absorbance was observed around $3.7 - 3.9\mu m$ ($2500 - 2700cm^{-1}$). This result can be attributed to the overtones from the excitation of the ground state (v0) of the C-F stretch to its second ex- cited state (v2). This is in agreement with the frequency

of this absorbance being found at twice the v1 excited state absorption frequency ($1200 - 1350\ cm^{-1}$)[9]. Perfluoropolyethers, (PFPEs) and polychlorotrifluoroethylene (PCTFE) formulations also exhibit similar absorbance behaviors. Eliminating

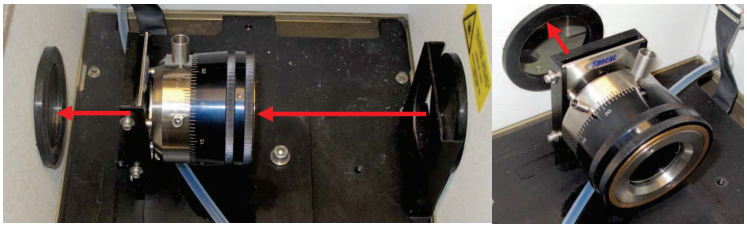

Figure 4.15: Variable path length cell used to measure transmission of fluids using an FTIR.

fluorinated compounds, inorganic polymers were investigated. The most common inorganic polymers are either siloxane or silane based[15]. Removing carbon from the backbone of the polymer either completely removes or greatly reduces the occurrence of the C-H absorption stretch, depending on the composition of the side chains of the polymer. Of the inorganic polymers, polysiloxanes are the most widely studied, and thus the most widely available. Numerous polysiloxane-based polymers were obtained and their transmission properties were examined. These studied fluids also resulted in the same strong absorbance at $3.7 - 3.9\mu m$.

A transmission curve was finally obtained for Fluid #6, which is a silicon base polymer, from $3.0 - 3.2\mu m$ and then from $3.6 - 5.0\mu m$, with maximum transmission centered around $4.1\mu m$. Though not completely transparent over the critical range, it did provide with an initial, viable, route for the construction of a polymer-based lens that would transmit in the MWIR. The absorbance coefficient for this fluid was then calculated using the variable path length cell, and plotted versus wavelength.

4.4.2 Experimental results and variable magnification APL system

Transmission measurements

Transmission measurements were performed using and FTIR and the variable path length setup shown in Figure 4.15 for the fluids and for a single membrane between support rings. Figure 4.16 shows the transmission curve for PDMS and also a shaded region which indicates that atmospheric absorption between $4.2 - 4.4\mu m$ dominates when imaging [20]. This is of importance when selecting a fluid, this area of transmission of the fluid can be discarded. Figure 4.17 shows the transmission curves for the fluids used in this research. Fluids 1-3 are perfluorinated compounds, fluid 4 is a PCTFE-based fluid and fluid 5 is a fully halogenated small molecule.

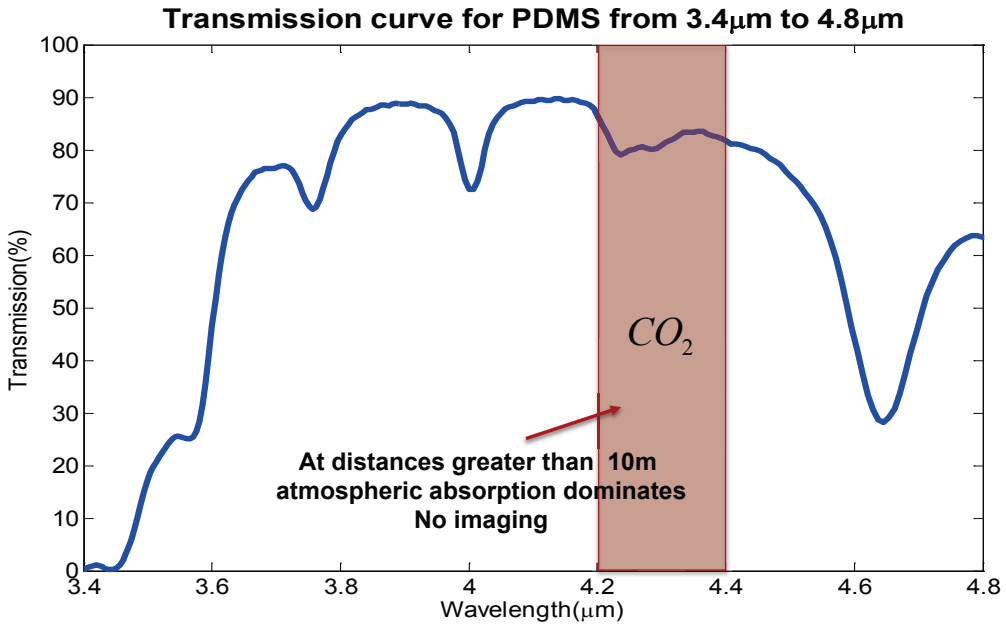

Figure 4.16: Transmission curve of PDMS membrane bonded to support rings

Fluid #6 presented the best transmission in the infrared spectrum, Figure 4.18

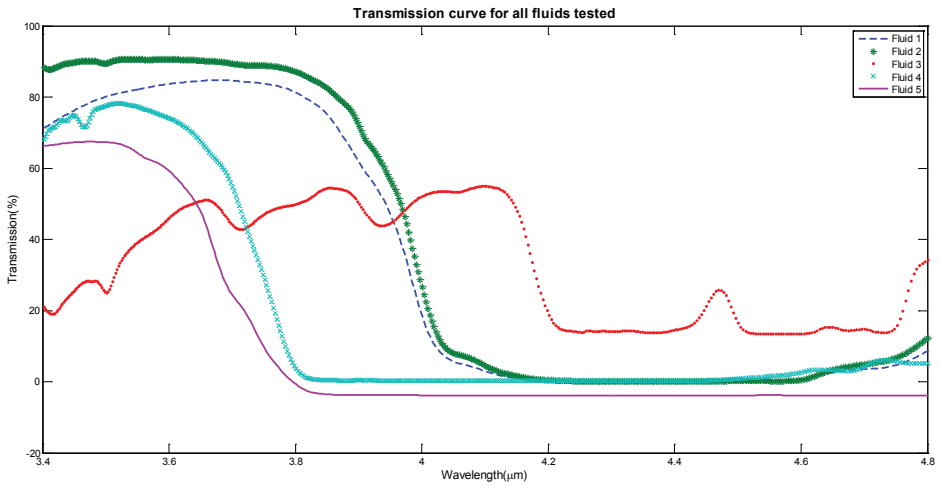

Figure 4.17: Transmission curves for all fluids under study from $3.4\mu m - 4.8\mu m$

shows the transmission curve results at different thickness, used to calculate the absorption coefficient shown on the right side axis.

4.4.3 Variable magnification results

Zemax was used to design the adaptive zoom system based on APLs using Fluid #6. The optical design was for $1 - 3^{\circ}$ full field of view, on an image plane diagonal of $9.6mm$, producing a true 3X change in the optical magnification of objects located $5m$ away from the system. One of the objects was an aluminum plate with circular apertures $6mm$ diameter and the second one a $50.050.0mm$, United State Air Force resolution target.

The FPA used was a Zafiro 640 Micro from DRS Technologies. This is a low power(5W at room temperature) cooled compact 640×480 pixel resolution $12\mu m$ pitch HgCdTe FPA with a spectral response of $3.4\mu m - 4.8\mu m$. Figure 4.19 shows optical breadboard, with the two APLs in front of the Zafiro system.

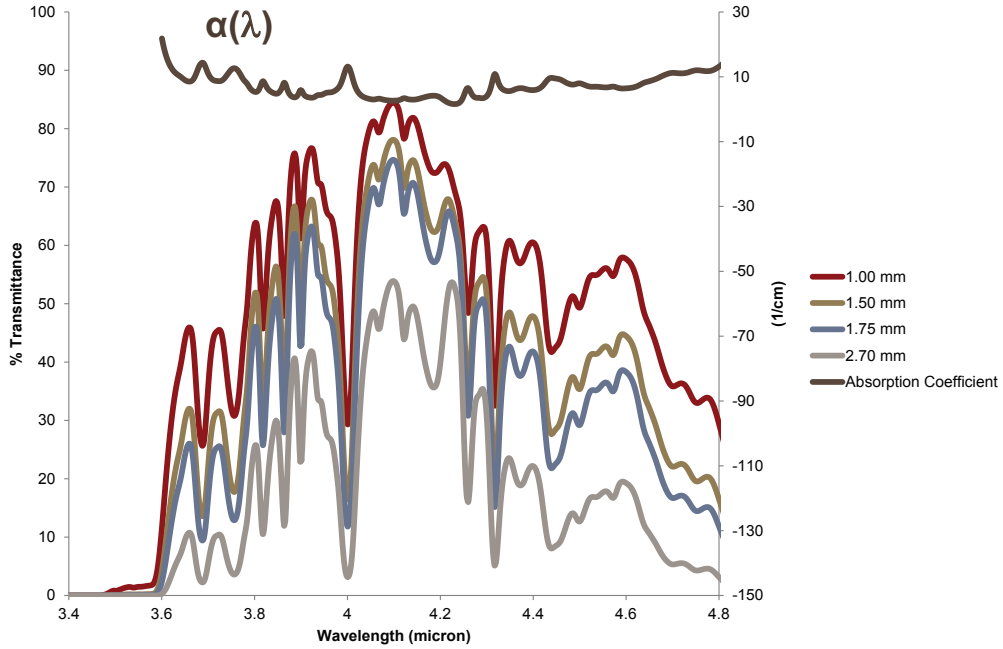

Figure 4.18: Transmission curves for Fluid 6 at different path lengths, 2.7 mm is a close representation of APL thickness. Also shown is the calculated absorption coefficient$(1/cm)$ versus wavelength.

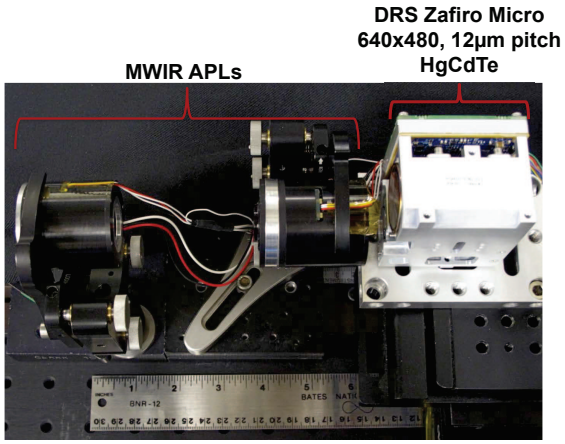

Figure 4.19: Breadboard built, showing the two APLs and the MWIR focal plane array

Figure 4.20 and Figure 4.21 show the optical magnification obtained by the 3X zoom system consisting of 2 APLs. The aluminum circular mask and the AF resolution target were kept at room temperature, about 23.5°, and an object at a temperature of 50°C was placed in the background to improve contrast. The ΔT(min to max) was thus 26.5°C.

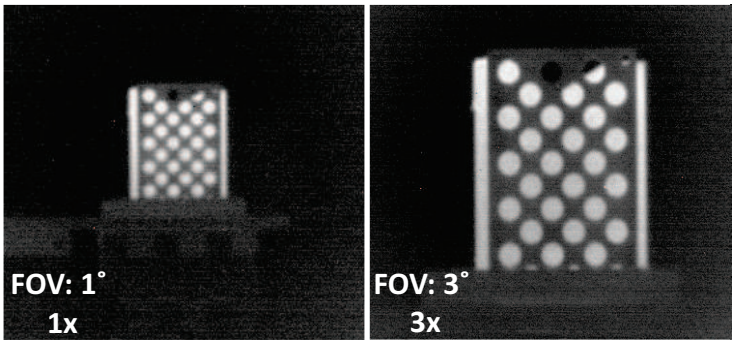

Figure 4.20: Aluminum mask with an object in the back at a higher temperature.(Left) 1x magnification and (Right) 3x magnification

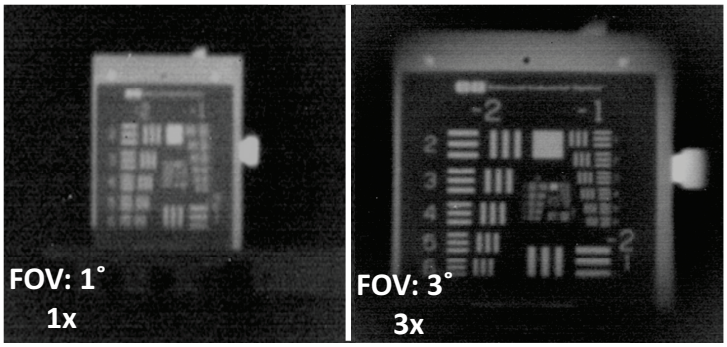

Figure 4.21: United States Air Force resolution target with an object in the back at a higher temperature.(Left) 1x magnification and (Right) 3x magnification

For the first time, variable focal length lenses were developed and a optical zoom system demonstrated in the MWIR. The main challenge was, and remains, the development and selection of the appropriate fluid to support both membrane com-

patibility and optical transmission. The current optical transmission is in the order of 35% and the goal is to achieve above 70% transmission. As a comparison, fixed power tactical MWIR systems weight in the order of 10 lb with a length of 9.5". For the system built using APLs, the components only weight 1.40 lb and the over all length was 8.2", this while providing the capability of push button variably FOV.

Chapter 5

Conclusion

This dissertation presented the results for an adaptive achromatic doublet based on constant volume condition. In the process of achieving an achromat, work was performed on singlets as well as doublets which use glass lenses as convex/concave as one of its surfaces. The concept of shape factor, which was very important for the doublets, was explored and demonstrated for the first time on adaptive lenses. Various fabrication problems such as bond failures, actuation limits and wavefront errors due to mechanical tolerances were eliminated or reduced. A FEM was developed that help understand the behavior of the membranes under stress as well as the lens cores under a constant pressure. This was key in order to reduce the aberrations on the lens cores. The dominant aberration, astigmatism, was reduced by understanding the sources of it. Current membranes bonded to support rings can achieve a flat wavefront of about 0.50 waves(peak to valley) at 632nm which translate into lens cores of about 1.5 waves (peak to valley) over the full actuation dynamic range, with coma (due to gravity) being the dominant aberration. The developed model was use to ease the fabrication process, by identifying a relationship between design and fabrication variables. It was also demonstrated how the model and the process could be use to the use of APLs for the infrared.

5.1 Improvements

It had been demonstrated that APL singlets can be used for direct view optics, but there is still improvements to be made. One of the main drawbacks on these type of fluidic lenses, is temperature, the APL changes prescription due to the CTE and $\frac{dn}{dt}$ of the fluid which are orders of magnitude larger than with glass or plastic optics. Sandia National Labs had demonstrated active compensation of its lenses and systems but also passive compensation at the lens level[3]. Due to space constraints on current systems passive was demonstrated but not implemented at a system level. Passive athermalization is key for successfully expanding the applications of APLs.

With respect to the aberrations, astigmatism was reduced and could be reduced even more, by improving the tolerances hold on all surfaces involved in the APL fabrication process. Now coma, is mostly or entirely due to gravity but it can also be reduce, as long as the operational orientation of the final system is known a priori. The membrane can be tailored in order to minimize coma but also to reduce other aberrations that my be present.

For doublets and achromats, a higher fidelity FEM model should be developed based on the results of this dissertation. Current fabrication fixtures need to be improved in order to have better control on the final thickness of the lens. In collaboration with Boulder Non-Linear Systems[1] and as a result of the process depicted in this dissertation a fabrication fixture was designed and built, which reduced the human factor. This fixture promise to improve the reliability and repeatability of APL and could be a key for developing better doublets. Currently this fixture is being calibrated. Another area of key importance for the doublet is understanding and having the capability to measure the intermediate surface. Some of the things that can be implemented are:

[1] http://bnonlinear.com/

- flexible coatings one the middle surface which increase reflection
- material deposition that could generate an electrical signal due to deflection (strain/stress), something that works similar to a strain gauge. For example SNL explored and performed compatibility tests on using graphene on the APL membranes.
- using a similar concept as in chromatic confocal sensors
- a fixture that will allow the user to know very accurately the pressure and volume inside each chamber while the system is under actuation and both of outer surfaces are measured with an optical interferometer

The above techniques can help improve the achromat performance. Once the FEM and the experimental results are validated, a more accurate measurement of the focal shift can be made using monochromator.

This dissertation has demonstrated that an achromatic doublet based on adaptive polymer lens under constant volume conditions can be fabricated and optical performance verify with respect to the design. Future work will implement these achromatic lenses on a system and verify its performance as well as exploring lateral chromatic aberrations and the possibility of using the doublet to correct other aberrations.

5.2 Applications and Infraed APLs

This work demonstrated the research performed and on going on applications of APLs. The use of APL in a direct view optic application at a higher technical readiness level have been demonstrated with the RAZAR, [2] and work is been performed to expand this to tactical binoculars.

Work at longer wavelengths was presented, more specific for rapid variable field of view, laser illuminator and designators in the SWIR and rapid variable field of view for MWIR sensors[23][24]. It was demonstrated the advantage, such as reduction in size and weight as well as improve of performance of using APLs for tactical applications in the SWIR and MWIR, in which to this date is not existing. Further work have to be made on the materials development for improving the performance of MWIR APLs in order for this lenses to achieve the technical rediness level of VIS-NIR-SWIR APLs. The same procedure used for the SWIR and MWIR APLs development should be used to explore the use of these lenses in hyperspectral applications and verify performance in the longwave infrared (LWIR).

5.3 Accomplishments

The following is a list of the contributions or accomplishment resulting from the work performed in this dissertation.

1. First APL for tactical military direct view optics (DVO) applications: APLs were developed an incorporated in a DVO system for small arms systems.
2. First APL doublet under constant volume condition for imaging applications.
3. First APL for SWIR tactical applications: push button variable magnification and divergence control.
4. First APL for MWIR tactical applications: push button variable magnification.

References

[1] B. J. Anderson, J. P. Bruhn, M. I. White, J. R. Brown, J. M. Hochrein, E. R.F Beckel, F. Santiago, and Brett Bagwell. Development and characterization of low permeation optical membranes for variable focal length rifle scope lenses. 41st polymeric materials adhesives and composited(polymac) conference, Sandia National Laboratories, P.O. Box 5800, Albuquerque, NM., 87185, April 2012.

[2] B.E. Bagwell and F. Santiago. Rd100: Razar adaptive zoom rifle scope. RD100, 2014.

[3] M.S. Baker, B.J. Anderson, G. Soehnel, B. Bagwell, and F. Santiago. Polymer adaptive lens athermalization. Sandia Report SAND10, Sandia National Laboratories, P.O. Box 5800, Albuquerque, NM., 87185, 2011.

[4] G. Beadie, M. L. Sandrock, M. J. Wiggins, R. S. Lepkowicz, J. S. Shirk, M. Ponting, Y. Yang, T. Kazmierczak, A. Hiltner, and E. Baer. Tunable polymer lens. *Optical Society of America*, 16(4), Aug 2008.

[5] B. Berge and J. Peseux. Variable focal lens controlled by an external voltage: an application of electro-wetting. *Eur. Phys. J*, E3:159–163, 2000.

[6] S. Bhattacharya, A. Datta, J. M. Berg, and S. Gangopadhyay. Studies on surface wettability of poly(dimethyl) siloxane (pdms) and glass under oxygen-plasma treatment and correlation with bond strength. *Journal of Microelectromechanical Systems*, 14(3):590–597, Jun 2005.

[7] M. Born and E. wolf. *Principles of optics*. Cambridge University Press, Cambridge, UK, 1999.

[8] Y. Chen, H. Xianyu, J. Sun, P. Kula, R. Dabrowski, S. Tripathi, R. Twieg, and S. Wu. Low absorption liquid crystal for mid-wave infrared applications. *Optics Express*, 19(11), May 2011.

[9] N.B. Colthup. Adaptive polymer lens for mid-wavelength infrared tactical applications. *Journal of the Optical Society of America B*, (40):397, 1950.

[10] J. M. Geary. *Introduction to lens design with practical Zemax examples*. Willmann-Bell, Inc, Virginia, USA, 2011.

[11] M. L. George. *Lean Six Sigma, Combining Six Sigma Quality with Lean Speed*. McGraw-Hill, US, 2007.

[12] K. Haubert, T. Drier, and D. Beebe. Pdms bonding by means of a portable, low-cost corona system. *Lab on a Chip*, 6(12):1548–1549, Oct 2006.

[13] S. Kuiper and B.H.W. Hendriks. Variable-focus liquid lens for miniature cameras. *Applied Physics Letters*, 85:1128–1130, 2004.

[14] P. Kurowski. *Engineering analysis with SolidWorks Simulation 2012*. Schroff Development Corporation, Kansas, USA, 2012.

[15] J.E. Mark, H.R. Allcock, and R. West. *Inorganic Polymers (2nd Edition ed.)*. Oxford University Press, New York, USA, 2005.

[16] T. Martinez, D.V. Wick, D.M. Payne, J.T. Baker, and S.R. Restaino. Non-mechanical zoom system. *Proc. SPIE*, 5234:375–378, 2004.

[17] T. C. Merkel, V. I. Bondar, K. Nagai, B. D. Freeman, and I. Pinnau. Gas absorption, diffusion, and permeation in poly(dimethylsiloxane). *Polymer Science, Polymer Physics*, 38(3):415–434, Feb 2000.

[18] A. Miks, J. Novak, and P. Novak. Chromatic aberrations of thin refractive variable-focus lens. *Optics Communications*, 285:2506–2509, 2012.

[19] H. Ren and S. Wu. *Introduction to adaptive lens*. John Wiley and Sons, New Jersey, USA, 2012.

[20] A. Richards and G. Johnson. Low absorption liquid crystal for mid-wave infrared applications. *Proc. SPIE*, 5782:10, Mar 2005.

[21] Y. Liu S. Xu, H. Ren, and S. Wu. A novel adaptive mechanical-wetting lens for visible and near infrared imaging. *Optics Express*, 18(12), June 2010.

[22] F. Santiago, B. J. Anderson, and Brett Bagwell. Development of thiol-ene membranes for picatinny adaptive lens(pal). Jssap final report, Picatinny Arsenal, NJ, Picatinny Arsenal, Joint Service Small Arms Program Office, October 2011.

[23] F. Santiago, V. Pinon III, B. Bagwell, and S. Krishna. Adaptive polymer lens for mid-wavelength infrared tactical applications. *Optical Society of America*, 2014.

[24] F. Santiago, V. Pinon III, B. Bagwell, and S. Krishna. Adaptive polymer lens for rapid zoom shortwave infrared(swir) imaging applications. *Optical Engineering Letters*, 2014.

[25] M. Scaggs and G. Haas. Thermal lensing compensation objective for high power lasers. *Haas Lasers Technologies*.

[26] W.J. Smith. *Modern Optical Engineering*. McGraw-Hill, New York, USA, 2000.

[27] STIL. http://www.stilsa.com/en/exem/measure-example/thickness-measurements.htm.

[28] P. Waibel, D. Mader, P. Liebetraut, H. Zappe, and A. Seifert. Chromatic aberration control for tunable all-silicone membrane microlenses. *Optical Society of America*, 19(19), Sep 2011.

[29] M. I. White, F. Santiago, B. Bagwell, E. R. Beckel, J. P. Bruhn, B. J. Anderson, J. R. Brown, , and J. M. Hochrein. Characterization of gas permeation through optical membrane for variable focal length rifle scope lenses. 41st polymeric materials adhesives and composited(polymac) conference, Sandia National Laboratories, P.O. Box 5800, Albuquerque, NM., 87185, April 2012.

[30] D.V. Wick, T. Martinez, D.M. Payne, W.C. Sweatt, and S.R. Restaino. Active optical zoom system. *Proc. SPIE*, 5798:151–157, 2005.

[31] D.A. Woodward. Improvement in fluid lenses. *Letters Patent*, 109(60), 1866.

[32] Zygo. Verifire^{TM} series: Interferometer systems, Aug 2012.